Dynamic Range Implications for the Effectiveness of Semi-Active Tuned Mass Dampers

by

Cory W. Lindh

SUBMITTED TO THE DEPARTMENT OF CIVIL AND ENVIRONMENTAL ENGINEERING IN PARTIAL FULFILLMENT OF THE REQUIREMENTS FOR THE DEGREE OF

MASTER OF SCIENCE IN CIVIL AND ENVIRONMENTAL ENGINEERING AT THE MASSACHUSETTS INSTITUTE OF TECHNOLOGY

FEBRUARY 2010

Signature of Author:

Department of Civil and Environmental Engineering
January 29, 2010

Certified by:

Jerome J. Connor
Professor of Civil and Environmental Engineering
Thesis Supervisor

Accepted by:

Daniele Veneziano
Chairman, Departmental Committee for Graduate Students

Dynamic Range Implications for the Effectiveness of Semi-Active Tuned Mass Dampers

by

Cory W. Lindh

Submitted to the Department of Civil and Environmental Engineering
on January 29, 2010 in partial fulfillment of the requirements for the
degree of Master of Science in Civil and Environmental Engineering
at the Massachusetts Institute of Technology.

ABSTRACT

The response of tall buildings subjected to dynamic wind loads has been widely studied. For excitations approaching the resonant frequencies of the structure, ensuring serviceability is a significant concern. One traditional solution is the implementation of a tuned mass damper (TMD), which acts as a passive damping device in the region of the tuned frequency. However, TMDs exhibit a limited bandwidth and often require a significant mass. Active systems, such as the active mass driver, have been utilized to improve the effectiveness of the TMD concept, but these systems require significant power and bring the inherent risk of instability. Hybrid semi-active schemes with variable damping devices have been proposed. They are stable, require low power, and are controllable, thus providing a broader range of applicability. The concept of a semi-active tuned mass damper (STMD) has been investigated, but the influence of the dynamic range of the semi-active damping device has not been documented. This analysis assesses the effectiveness of STMD systems using a variable-orifice damper and a magnetorheological damper with varying dynamic ranges. Results demonstrate a performance dependence on the dynamic range and also elucidate the superiority of non-linear damping devices. It is shown that the prescribed TMD mass may be reduced by a factor of two when semi-active control is implemented, thereby making the STMD an attractive and feasible option when space and weight concerns govern design.

Thesis Supervisor: Jerome J. Connor
Title: Professor of Civil and Environmental Engineering

Contents

Chapter 1

Mitigating dynamic response of tall buildings under wind excitation

Large civil structures are exposed to dynamic loading from a variety of sources, including earthquakes, high winds, and reciprocating machinery. Satisfactory design must ensure structural integrity and occupant safety under the most adverse conditions, the severity of which varies widely based on building location and structural purpose. This study focuses on the specific case of tall, flexible buildings, which are particularly susceptible to wind-induced vibrations and may require more significant control measures to satisfy performance requirements.

1.1 Motivation

Recent decades have marked a trend towards the design and construction of very tall buildings. Advancements in analysis, coupled with an increased use of lighter building materials and a decrease in heavy claddings, have led to structures that are not only taller but also more flexible. Consequently, most modern towers are especially prone to oscillations under persistent winds, which can lead to swaying motions of several feet on the top floors [12, 39].

In many cases, these large deflections may not threaten the integrity of the structure, but the steady rocking can cause considerable discomfort and even illness to

building occupants. If persistent, the dynamic response under severe winds may render the top floors completely uninhabitable. Studies by Chang and Hansen investigated the effects of this motion on the human body, creating benchmarks for the perception of and physiological response to various increments of lateral acceleration [12, 17]. Additionally, Ruderman noted that the psychological effects of observable lateral displacements can be a key factor in human comfort, emphasizing the need to limit both quantities – displacements and accelerations – in tall buildings [12].

The maximum amplitudes of these responses are ultimately dictated by the ability of the structure to dissipate energy; the more significant the energy dissipation, the smaller the vibrations. All structures naturally release some energy through mechanisms such as internal stressing, rubbing, and plastic deformations. In large modern structures, however, the total damping may amount to as little as 1% of critical, making them very vulnerable to dynamic effects such as resonance [20]. As a result, additional measures are generally necessary to meet servicability standards. Since eliminating the excitation source is impractical, this necessitates implementing a control scheme to enhance the effective damping of the structure.

1.2 Methods of control

Numerous techniques have been tried to produce better control against wind excitation, and these fall into three broad categories: passive control, which provides additional damping with no additional energy; active control, which uses feedback and an external energy source to provide optimized actuator forces in real-time; and semi-active control, which relies on feedback and low-energy devices to provide optimized reactive forces in real-time. Each of these will be further introduced in this section.

1.2.1 Passive control

The most mechanically simple set of control schemes is encompassed in the passive control categorization, which has thus far been the most accepted for civil engineering

applications.

Definition

Housner et al. [20] and Spencer [55] have both provided comprehensive overviews on structural control, including succinct definitions for the various types of control implemented in structures. They define a passive control system as any that does not require an external power source. All forces imparted by passive control devices develop as direct responses to the motion of the structure. Hence, the energy of both the device and the primary system can never be increased by the control scheme.

The main goal of these systems is to efficiently dissipate vibrational energy, and the various methods of accomplishing this can be categorized in two ways. The first method involves converting kinetic energy directly to heat, such as through the yielding of metals, the deformation of viscoelastic solids and fluids, or the implementation of friction sliders. The second method entails transferring energy among two or more of the vibrational modes of the building, generally achieved by installing a supplemental oscillator that absorbs the vibrations of the primary structure [20].

Implementation for wind-excited structures

Both categories of passive control have been carried out in a variety of ways in the design of tall buildings subjected to dynamic wind loading. The first method, relying on direct conversion of kinetic energy to heat, has been most successfully accomplished through the addition of auxiliary dampers to the primary frame of the structure. These damping devices may be viscous, viscoelastic, or plastic, and are generally distributed throughout the building in a manner that optimizes their energy dissipation. This technique was most notably implemented in the original World Trade Centers in New York City but has also been implemented in several buildings in Seattle and throughout California [20, 37].

The second method of passive control increases effective damping indirectly by modifying the vibrational modes of the structure. In general, the response of structures under wind loading is dominated by the first mode of vibration. Hence, by

adding an oscillatory control device that vibrates out of phase with the structure during resonance conditions, it is possible to use it as a "counterweight" against the fundamental mode, thereby decreasing the overall response of the primary structure. Current passive devices that take advantage of this property include the tuned mass damper (TMD), tuned liquid damper (TLD), and the tuned liquid column damper (TLCD).

Tuned mass dampers, discussed in full in chapter 2, are the most frequently used supplemental oscillators in buildings. Consisting of a mass, spring, and damping element, the TMD is attached to the frame of a structure on one of its uppermost stories. There it is allowed to move out of phase with the rocking building by sliding on low-friction bearings or a thin film of oil, and energy is absorbed through the affixed damper [33, 37]. TMDs have been used throughout the world, but examples in America include the Citicorp Center in New York City and the John Hancock Building in Boston.

Tuned liquid dampers and tuned liquid column dampers utilize oscillations of fluids instead of a mobile mass. TLDs are essentially large sloshing tanks, theoretically as simple as a swimming pool, the dimensions of which determine their oscillatory properties. Energy is absorbed through the viscous motion of the fluid and through wave breaking. Notable examples of TLDs in practice include the Shin Yokohama Prince Hotel and a steel-frame tower at the Nagasaki airport, both located in Japan [20]. Tuned liquid column dampers are based on the same concept but rely on the motion of liquid in a U-shaped container with an orifice in the middle. The amount of energy dissipation is contingent upon the inherent heat-loss characteristics and the velocity of the fluid as it passes through this opening. Two $50,000$ gallon TLCDs have been installed in the One Wall Centre in Vancouver [26, 60].

Advantages and limitations

Passive control is the most widely-used method of mitigating structural response under wind loading, but it comes with limitations. While reliable and relatively straightforward to design, passive control systems are generally only good for limited

bandwidths of dynamic input. As a result, they are vulnerable to the effects of off-tuning, de-tuning, or resonances of secondary modes. It is primarily due to these limitations that more elaborate active and semi-active control techniques have been coming into practice.

1.2.2 Active control

Active control is a relatively recent subfield of structural engineering; it promises improved response to passive systems at the cost of energy and more complex systems.

Definition

Active control has been described as any control system in which an external power source is required to provide additional forces to the structure in a prescribed manner, generally through the use of actuators. The signals sent to control the actuators are determined based on feedback from sensors placed on or throughout the structure. Due to the presence of an external power source, the forces applied may either add or dissipate energy from the structure [20].

In order to maximize the performance of an active system, the actuator forces must be prescribed in real-time based on the inputs of the sensors. Assigning the direction and magnitude of these forces can be done in a variety of ways, all of which have their roots in the diverse and mathematically rich field of control engineering. Miller provides a useful overview of the breadth of this topic:

> Civil engineering researchers have applied both classical and modern control techniques to large civil structures, and have addressed many of the same major issues that have been prominent in the aerospace, electrical, and mechanical engineering fields. These issues include such topics as mathematical modeling of structures, identification techniques, reduced-order models, modal truncation and controller interaction with residual modes, placement of control actuators, multivariable controller design techniques, mathematical measures of desired system performance, and

optimal control techniques [39].

In 1972 Yao became the first such researcher to apply control theory to structural problems [20]. Yang followed in 1975 with a study on the application of optimal control strategies for tall buildings subjected to wind loads [68]. Since then, innumerable control algorithms have been developed specifically for civil structures, the basic task of each being to use feedback from sensors to direct the actuator in the best possible way for enhanced serviceability and safety of the structure [33, 55].

Implementation for wind-excited structures

As with passive control systems, there is a significant amount of variety in the design and application of active control systems. More so than with passive systems, however, a majority of active control research has focused on the protection of structures under earthquake loading. Nevertheless, a significant amount of work has also addressed the issues specific to wind-loaded structures, and some control techniques have been adapted for both types of excitation.

Active tendons, also known as active bracing, are an example of an active control technique that has been developed to counteract both earthquake and wind excitation. These devices consist of tendons rigged to the primary structure, the tension of which can be adjusted by actuators. By tightening or slackening these tendons in real-time, it is possible to improve the response of the structure under dynamic loading. Full scale active tendon installation has proven successful for dealing with ground motion and has also been investigated for responding to wind excitation [39, 49].

Other active systems have developed more specifically for counteracting dynamic wind loading, some of which closely resemble successful passive systems. The active mass driver, or AMD, is similar to the passive TMD except that its damper has been replaced by an actuator, allowing for substantially improved control. On the other hand, the active tuned mass damper (ATMD) simply adds an actuator to the original TMD and leaves both the spring and the damper in place. Because the ATMD retains all the components of a passive system, it is sometimes referred to as a "hybrid" control scheme [20].

Both the AMD and ATMD are described more fully in section 2.3, including some successful applications. They have become the most common type of active control implemented in civil structures [10].

Advantages and limitations

The performance benefits of active control are in some cases quite pronounced. Due to its ability to respond in real-time, active control also eliminates most of the tuning limitations inherent in passive devices. However, active control has not been exuberantly embraced by the civil engineering community as a result of some significant limitations.

Most significantly, the attractiveness of active control schemes is diminished by their heavy reliance on external power supplies. In order to output actuator forces of the magnitude necessary to control large civil structures, the power consumption may become large and costly. Additionally, the times at which the control forces are needed most generally coincides with the time when power failure is the most likely, such as during an earthquake or large wind storm. This raises reliability concerns [39].

Beyond the issue of energy supply, engineers also hesitate to embrace non-traditional technologies for structures. The placement of sensors and the design of feedback schemes are beyond the scope of most practicing engineers, and a poorly designed active system may lead to deleterious energy inputs and destabilization of the primary system. These legitimate concerns generally sway designers towards more traditional solutions [55].

1.2.3 Semi-active control

Semi-active control seeks to combine the performance benefits of active control and the reliability of passive control, making it a much more appealing alternative to traditional control schemes in civil structures.

Definition

Semi-active control systems are similar to their fully active counterparts in their reliance on real-time feedback to direct a control system, but they differ in that their external energy requirements are orders of magnitude smaller. Generally, semi-active control devices do not add mechanical energy to the primary system and hence have an inherent stability in terms of bounded-input, bounded-output. Consequently, semi-active devices may be viewed as controllable passive devices [20].

Instead of the application of actuator forces, semi-active control relies on the reactive forces that develop due to variable stiffness or damping devices. That is, by altering the properties of these devices, the response of the system may be favorably modified using only nominal power, usually on the energy scale of a battery. As a result, semi-active control strategies appear to combine the best features of fully active and fully passive systems, leaving them with the greatest likelihood of near-term acceptance for structural applications [55, 59].

Implementation for wind-excited structures

Similar to active control techniques, semi-active control schemes may be developed uniquely or may simply modify and improve existing passive control schemes. Aerodynamic appendages are one example of a novel semi-active technique developed to ameliorate resonance conditions under wind excitation. This concept involves the addition of aerodynamic surfaces to the top of large buildings, the position and orientation of which can be modified using only a small amount of energy. A proper control strategy can then derive the requisite control forces directly from the incident winds [2, 39].

More popular semi-active control schemes have been based on adding semi-active damping or stiffness devices to well-tested passive control devices. These include the semi-active tuned liquid column damper (STLCD), in which the orifice in the tube is given a controllable diameter [26], and the semi-active tuned mass damper (STMD), in which the spring or damping element of the passive TMD is replaced with a device

that has controllable properties. The selection of the semi-active device can vary substantially, an elaboration of which is presented in section 2.4.

Advantages and limitations

The most distinct advantage of semi-active systems is their ability to provide improved control forces with an incredibly low demnad for power. Because this power can be supplied by a battery, this ensures continued functionality even in the event of a power failure, adding reliability to any semi-active control method. It is because of these benefits that enthusiasm towards semi-active structural control schemes has increased in recent years, making it a viable alternative to proven passive devices [20].

While these advantages are in some cases truly significant, semi-active control still has its detractors. Most relevant is the need for sensor technology and computer-controlled feedback, which is as central to semi-active control as to active control. The risk of destabilization has now been removed, but the design engineer must be convinced of the performance benefits of adding semi-active devices before he is willing to embrace a more intricate, less proven technology.

1.3 Selection of a control technique

As has been seen, there are numerous methods for addressing even the specific control problem of wind-excited tall buildings. While several of the control methods have received a great amount of attention in the literature, the greatest precedent lies with mass-based oscillators, whether passive (TMDs) or fully active (AMDs and ATMDs). With the more recent rise of semi-active control strategies, STMDs have also received quite a bit of attention, but none have yet been installed in a full-scale civil structure.

This thesis purposes to expand knowledge of STMD systems, specifically by analyzing their effectiveness as a function of the properties of the variable damping device selected to provide the semi-active control. To do so, the use of tuned mass dampers will be overviewed (chapter 2), various semi-active damping devices will be compared (chapter 3), and performance simulations will be generated (chapter 4).

Comprehensive results for two specific STMD systems will be presented in chapters 5 and 6, both of which will evidence the benefits of adding semi-active control to a traditional tuned mass damper (chapter 7).

Chapter 2

Tuned mass dampers for structures

As mentioned in chapter 1, the most widely accepted control measure for mitigating the response of tall structures under wind loads is the implementation of a tuned mass damper, or TMD. The concept has been well-established and at its base level is relatively uncomplicated. Consisting of a mass, a spring, and a damper, the natural frequency of the TMD is tuned to have a resonance very close to the fundamental mode of the primary structure, which allows a large amount of the structure's vibrational energy to be transferred to the TMD and then dissipated by its damper. This system has been adapted in numerous tall structures, and it has proven to be an effective method for mitigating structural vibration under high wind loads.

This chapter summarizes the vast amount of work done on TMD systems, explains appropriate measures for the optimization of its parameters, and describes the more recent work done in implementing active and semi-active control to enhance and extend the performance of tuned mass dampers.

2.1 Development of TMD theory

Although the basic TMD framework is quite simple, the specific parameters for its mass, stiffness, and damping must be found by using optimal design procedures to maximize its control effectiveness. These expressions are generally developed using a linear single degree of freedom (SDOF) model to represent the vibration of the

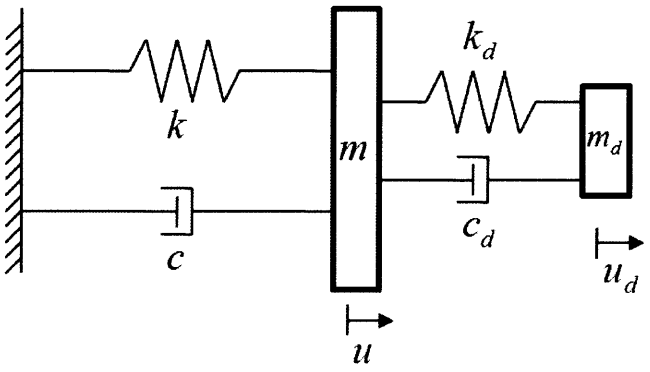

Figure 2-1: Basic TMD model

fundamental mode. The literature on this topic is both extensive and varied, as design equations depend not only on the parameters of the primary structure, but also on system inputs and optimization goals. In all cases closed-form solutions exist for these parameters when the sub-structure has no inherent damping ($c = 0$ in figure 2-1), with numerical and series solutions available for the more complicated case where $c \neq 0$ [5].

2.1.1 Factors influencing TMD optimization

Certainly, not all TMD design procedures are equally beneficial for their placement in structures subjected to wind loading. Before any methods are excluded, however, all TMD design factors will be summarized, with references provided for further information.

Type of excitation input

Except for the special case where $c = 0$, optimal TMD parameters vary based on the type of excitation. The types of loading most commonly considered are

- An excitation force applied directly to the main mass, which for structural applications would include wind loading [5, 18, 44].

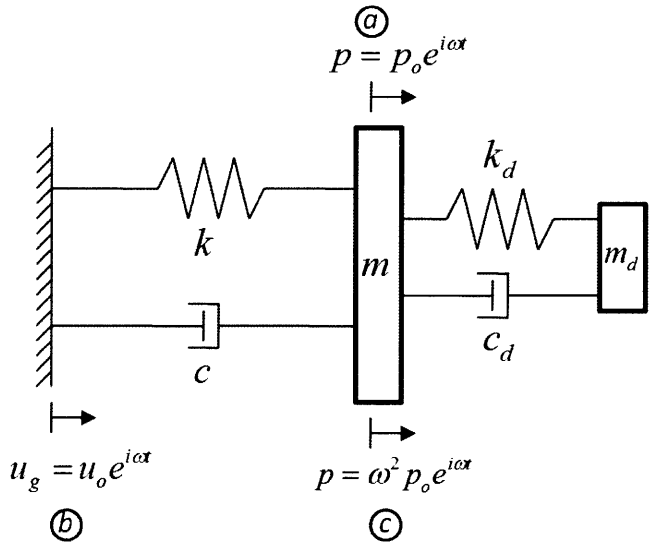

Figure 2-2: Types of excitations

- An acceleration of the structure's base, which is used to model the effects of earthquakes on structures [57, 58].

- An inertial force applied to the main mass, which would describe the effects of an eccentric mass vibrator [52].

Examples of these loadings can be seen in figure 2-2, where ⓐ represents wind excitation, ⓑ represents ground excitation, and ⓒ represents inertial excitation.

Output to be minimized

Selection of optimal TMD parameters further depends on which system output is to be minimized. In general TMD applications these may include the displacement, velocity, or acceleration of the primary mass, as well as the force transmitted to the mass or the relative motion of the mass with respect to the base. Summaries of the results for each of these design goals can be found in [61].

Optimization goal

Even when the excitation input is known and the output to optimize has been selected, there are still three possibilities for optimization criterion from which to choose [5].

- H_∞ optimization minimizes the maximum amplitude response of the system. Expressions are developed by applying minimization techniques to harmonic force inputs [5, 44, 47].

- H_2 optimization minimizes the total vibration energy of the system over all frequencies. In this case, derivations come from minimization of the ensemble mean of the response under random white noise excitation [5, 14, 61].

- Stability maximization attenuates the transient vibration of the system in the shortest amount of time possible. Mathematically, this is accomplished by moving all poles of the transfer function of the system as far to the left of the imaginary axis as possible in the s-plane [41, 64].

Both the H_∞ and H_2 optimization criteria seek improvement for the steady-state response of the structure, while the stability maximization objective aims to improve transient behavior. Figure 2-3 demonstrates how the transfer function of the TMD system varies based on the goal of the optimization.

2.1.2 Optimization scheme for wind-loaded buildings

As can be seen, the procedures for optimizing a TMD are numerous. This necessitates using engineering judgment to select the best expression for the TMD parameters. In the case of tall buildings, both wind and earthquake loading have been considered, but the mitigation of vibrations due to winds is generally the design goal of any TMD system; hence, the model for an excitation force applied to the primary mass will be chosen. As discussed in section 1.1, both displacements and accelerations are dominating design concerns. Tthe selection between these two does not affect the result significantly, so following convention the displacement will be the selected

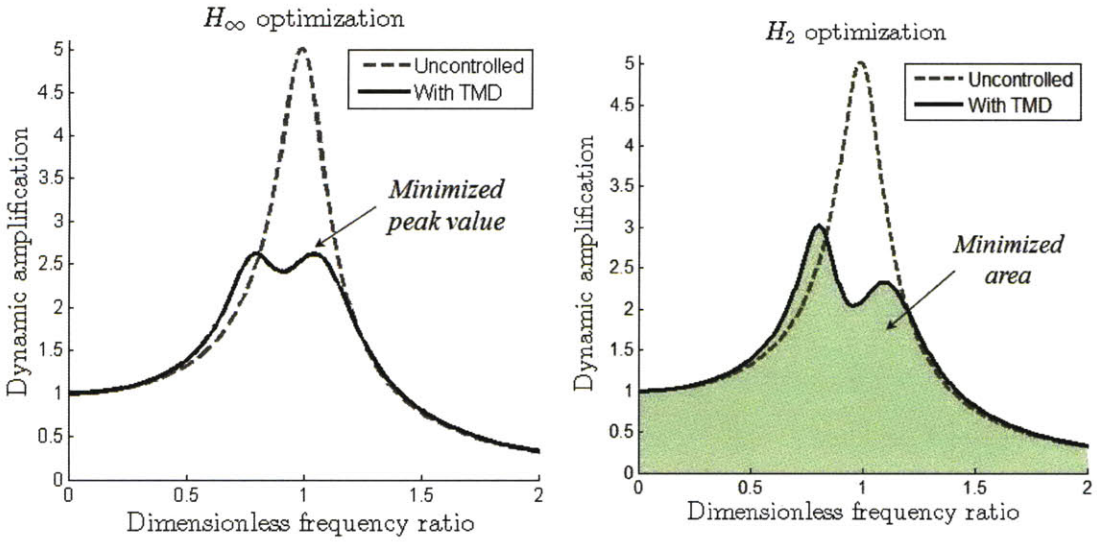

Figure 2-3: Comparison of optimization goals

output[1]. Finally, in civil structures, the primary concern is peak values [13], so H_∞ is the natural design criterion.

Development of parameters

Even for this specific subset of TMD optimization, the literature evidences a significant amount of progression. Indeed, minimization of maximum displacements under harmonic loads was the original objective of early TMD research.

Using a secondary mass to limit displacements at resonance was first proposed by Frahm in 1909 [16]. The benefits of a TMD with a damper was first shown by Ormondroyd and Hartog in 1928, who demonstrated its success experimentally [44]. For a given TMD mass, it was later shown that optimizing the response consisted of two distinct steps: tuning the frequency of the damper and selecting the ideal level of damping. The frequency tuning parameter, f_{opt}, is based on the fact that the TMD introduces a second frequency to the system, which if carefully selected will produce equal responses at the two resonances of the combined system. An expression for f_{opt}

[1]Indeed, as shall be shown in the results sections, the addition of a semi-active device to a TMD has the greatest overall effect when TMD parameters are optimized for displacement rather than acceleration. This is due to the semi-active TMD being more effective for higher frequencies, which is where the dynamic response of the acceleration deviates from optimum for a system optimized for displacement.

was first developed by Hahnkamm in 1932 [5]. The second step involves selection of the optimum damping ratio, ξ_{opt}, the theory for which was first developed by Brock in 1946 [8]. His approach is now known as the "fixed points" theory, since it is based on the recognition that there are two points in the system response (one near each resonance) through which all curves pass regardless of TMD damping; hence, ξ_{opt} is selected such that these points become local maxima.

These parameters were also developed independently by Den Hartog, who put them into wider use with release of his textbook in 1956 [18], but they lacked completeness in that they were only valid for an undamped primary system. In 1981 Randall expanded this theory by producing numerical curve-fitting results for finding f_{opt} and ξ_{opt} when $c \neq 0$ [47]. A variety of other curve-fit solution have also been produced, and recently Asami presented a series solution to this problem [5]. It is believed that an exact analytical solution for damped systems will never be attained, but the numerical and series solutions are certainly sufficient for engineering applications.

Optimization equations

For a give mass ratio, μ, defined as the mass of the TMD divided by the mass of the primary structure, the H_∞ optimized parameters for tuned mass dampers limiting displacements are as follows. In the case of no damping[2]

$$f_{opt} = \frac{1}{1+\mu} \tag{2.1}$$

$$\xi_{opt} = \sqrt{\frac{3\mu}{8(1+\mu)}} \tag{2.2}$$

[2]When $c = 0$, the closed-form analytic solution for H_∞ optimization is identical for all types of excitation inputs described previously.

and in the case of a primary structure with ξ as its damping ratio[3]

$$f_{opt} = \frac{1}{1+\mu} - \xi\frac{1}{1+\mu}\sqrt{\frac{1}{2(1+\mu)}\left(3+4\mu-\frac{AB}{2+\mu}\right)} \tag{2.3}$$

$$\xi_{opt} = \sqrt{\frac{3\mu}{8(1+\mu)}} + \xi\frac{60+63\mu+16\mu^2-2(3+2\mu)AB}{8(1+\mu)(2+\mu)(9+4\mu)} \tag{2.4}$$

where

$$A = \sqrt{3(2+\mu)-\sqrt{\mu(2+\mu)}}$$
$$B = \sqrt{3(2+\mu)+\sqrt{\mu(2+\mu)}}$$

2.2 Application to structures

Though most TMD theory developed for use in mechanical engineering applications, it has proven to be an effective means of addressing the resonance issues in tall buildings described in section 1.1. In many instances, they have been shown to reduce response amplitudes by as much as 40%. The basic concept remains unchanged, with the TMD acting as an energy-absorbing system with parameters optimized to the structure's fundamental mode of vibration. There are, of course, special design considerations due to the much larger scale, but the TMD has been successfully employed in several tall buildings. Current applications include translational tuned mass dampers, in which a large mass is placed on bearings or a near-frictionless oil film and fastened into a structural frame, as well as pendulum tuned mass dampers, in which a large mass is allowed to rock back while hanging from a large rod, the length of which determines its tuning.

[3]The full series, developed by [5], also includes ξ^2 terms, which are excluded here due to their minimal contribution to lightly damped systems. For full expressions, see section 4.2.3

2.2.1 Special considerations

The first and most significant design consideration unique to tall civil structures is the amount of mass that can be placed on the top of the tower. μ, the mass ratio, is the most influential parameter in terms of TMD effectiveness; once the mass ratio is specified, it only remains to size optimal spring and damper elements. However, due the large mass of structures, practical design considerations limit μ to a range of $0.005 - 0.02$ [37].

A second consideration that must be taken into account during the design process is the relative movement of the TMD with respect to the building[4]. In addition to space constraints, stroke limits must be met. For example, in translational tuned mass dampers, pneumatic springs may be used for the stiffness and hydraulic shock absorbers for the dampers, which in both cases have inherit extension limitations [37]. Relative displacements may be decreased by increasing either μ or c_d. Consequently, since the mass ratio is generally fixed, it may become necessary to overdamp the TMD, which has the deleterious effect of increasing the response of the primary structure [50]. This trade-off becomes a matter of engineering judgment.

Thirdly, there is the practical difficulty of creating a low-friction surface for the damper mass. Friction forces must be small enough to enable the damper mass to respond freely even for low levels of building excitation. In translational tuned mass dampers, this may entail using a thin oil film [37].

2.2.2 Current examples

Both translational tuned mass dampers and pendulum tuned mass dampers have been used in significant and progressive structures. This section highlights some examples.

Citicorp Center

The Citicorp Center in New York City was the first to complete installation of a full-scale structural tuned mass damper. When finished in 1977, its 400-ton control

[4]For reference, full-scale lab tests produced relative displacements of around 3.5 feet under the wind loading of a 10-year storm [37].

mass was 250 times larger than any existing TMD. With a mass ratio of 2% of the first modal mass, the damper increased overall structural damping from 1% to 4% of critical, which reduced sway amplitude by a factor of 2. The TMD system consists of a large block of concrete bearing on a thin film of oil, with structural stiffness provided by pneumatic springs [13, 37].

CN Tower, Toronto

The Canadian National Tower in Toronto is unique from a design perspective in that tuned mass dampers had to be added to suppress the motion of the second and fourth modes of vibration. It was not the 553-meter tall tower in its entirety, but rather the 102-meter steel antenna at the top that required suppression of dynamic wind loading effects. Because the first and third modes of the antenna had the same vibrational characteristics as the more heavily damped concrete structure, they did not require any additional damping.

To dampen the vibrations, two doughnut-shaped steel rings with 9 tons of dead-weight were added at elevations corresponding to the peak vibrations of the problematic modes. Each ring was mounted on a universal joint that could rotate in all directions, thereby allowing it to act as a tuned mass regardless of the direction of wind excitation. Energy dissipation is provided by four hydraulically activated dampers per ring [13, 53].

Taipei 101

Taipei 101, the tallest building in the world at the time of its completion in 2004, exemplifies how a tuned mass damper can double as a significant architectural and visual element. Rather than sliding on bearings in an enclosed room, the Taipei 101 TMD rocks like a pendulum in a fully open viewing area at the top of the building. The mass is provided by an impressive 6-meter-diameter steel ball weighing 726 tons. Suspension of this enormous sphere is made possible by four sets of cables, and dynamic energy is dissipated by eight hydraulic pistons each measuring two meters in length. When in full motion, this system is capable of maintaining acceptable levels

of lateral acceleration under wind gusts of up to 150 mph [48].

2.2.3 Passive TMD Limitations

While tuned mass dampers have proven to be effective at mitigating structural vibrations caused by high winds, they also possess some pointed limitations.

The first and most obvious limitation is that, as its named suggests, a TMD is "tuned" to a very narrow band of suppression frequencies. Hence, if other modes of resonance are also significant concerns, the specificity of its tuning renders the TMD ineffective to suppress them [46].

A corollary of this limited tuning range is the risk of a mistuned system. In practical applications, this may occur for two reasons. First, structural properties are only known with a degree of uncertainty, meaning that even a carefully-optimized TMD system is liable to be sub-optimally calibrated to the resonance of the structure's fundamental mode. Second, even if the structural properties are accurately assessed initially, they are prone to vary with time; for example, both variation in mass and deterioration of the structure could negatively affect its tuning [27, 50].

Finally, it is noted that wind excitation is generally neither harmonic nor white noise, both of which have been used as assumptions in TMD optimization. Additionally, even with detailed wind-tunnel models, it is difficult to predict the impact of wind loads due to changes in topography, neighboring buildings, and the results of vortex shedding [50].

These disadvantages do not negate the overall feasibility of TMD systems, but they do threaten to limit their effectiveness. Consequently, methods for improving the passive TMD system with active or semi-active control have been explored.

2.3 Active tuned mass dampers

In an effort to overcome these limitations and to improve performance, measures have been taken to incorporate active control techniques with passive TMD systems,

as mentioned in chapter 1. The basic concept involves adding an external energy source to generate an additional force that complements the force generated by the TMD, usually through the use of an actuator. With the inclusion of sensors and a feedback loop, the actuator force can be adjusted nearly real-time to produce optimized results.

There are many motivations for using an active TMD system, but there are a few particularly significant benefits. First, adding an external force can greatly increase the control system's effectiveness while also mitigating the limitations posed in section 2.2.3. Second, it can allow the size of the mass to be reduced, alleviating potential space and weight constraints. Third, an active system can be used to reduce the relative TMD displacement, thereby addressing limitations on stroke length [53]. As a result of these distinct advantages, the active TMD has become a widely accepted application of active control in civil structures [4].

2.3.1 Development of concept

There are a number of variations to the active TMD concept, ranging from the placement of the actuator to the control scheme used to direct it. This section describes the more common design possibilities and highlights advancements in the theory.

Variations of design

The most basic design is known as an active mass driver (AMD) and consists of a force actuator driving a mass connected to the building by a stiffness element. In this set-up there is no passive energy dissipation; the desired control forces are obtained directly through the reaction of the AMD system acting on the building.

Another scheme is the active tuned mass damper (ATMD), which includes the passive damper of traditional tuned mass dampers. Hence, the actuator is placed in parallel with the stiffness and damping elements and is programmed to enhance the behavior of the passive TMD.

A hybrid variation known as the DUOX system combines an AMD and a passive

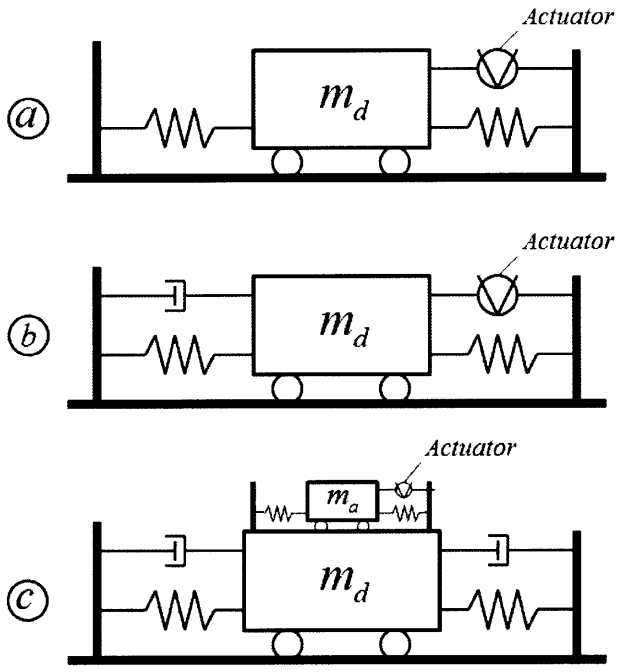

Figure 2-4: Types of active mass drivers

TMD. This design involves attaching an auxiliary mass and an actuator to the tuned mass damper. The purpose of this smaller-scale AMD is to drive itself out of phase with the passive mass damper, producing an additional force that complements the natural motion of the TMD [13, 33].

Basic schematics of each of these devices can be seen in figure 2-4, which portrays the AMD, ⓐ, the ATMD, ⓑ, and the DUOX, ⓒ.

Advancements in theory

A significant amount of literature has been produced on the benefits of actively-controlled tuned mass dampers. This work has included analyses of ATMD effectiveness under both earthquake and wind loading. To date, a majority of published results has concentrated on earthquake-loaded buildings, as this is a frontier that passive TMD systems have proven relatively ineffective at targeting. Nevertheless, since tall structures are more prone to wind-loading issues at their resonant frequencies, work on both issues has been on-going. Because this thesis addresses large

wind-loaded structures, the literature on this topic will be summarized.

The concept of using active control elements to enhance TMD performance was first proposed by Lund in 1979 [32]. In 1980, Soong applied optimal control theory to an ATMD to demonstrate its superiority over passive systems at mitigating wind-induced vibrations [53]. Abdel-Rohman advanced the theory in 1984 by describing how the optimization of the passive TMD parameters must be modified if minimization of energy consumption is to be taken into account [1]. In following years, various attempts were made to produce closed-form optimized solutions of both the passive parameters and the gain coefficients of the closed-loop full-state feedback system [4, 11, 65]. Mackriell further demonstrated ATMD feasibility by using pure acceleration feedback to control simulated high-rise structures subjected to digital time histories of wind-tunnel results [33].

In addition to assessing the overall effectiveness of ATMD systems, work has also been done to specifically address concerns of the actuator stroke. As in the passive TMD case, the relative displacement of the damper mass with respect to the floor can be a significant design issue. Soong demonstrated that this relative displacement can be significantly decreased through use of the ATMD [53]. Ideka was the first to develop guidelines for using LQR control theory to weight the stroke of the actuator [22]. Sakamoto undertook both experimental and theoretical measures to develop an AMD with a limited stroke [51].

2.3.2 Examples

Advances in ATMD theory has been complimented by its success in several structural applications, though predominantly in Japan.

Kyobashi Seiwa Buidling

The first practical application of an AMD was in the Kyobashi Seiwa Building, a slender 11-story building located in Tokyo, Japan. In 1989 two AMDs were installed on the top floor to control both lateral and torsional vibrational modes under ground

or wind excitation. The fully-active system consists of sensors on several locations, a control computer for signal analysis, actuators with 0.01 second response times, and the two large masses. Lateral response of the building was successfully decreased by a factor of three as compared to the uncontrolled structure [10, 13].

Ando Nishikicho building

The Ando Nishikicho building in Japan exemplifies the use of a DUOX active-passive hybrid TMD system. This 14-story building in crowded downtown Tokyo is susceptible to strong wind gusts due to the contours of surrounding buildings. The DUOX control system designed to solve this problem consists of two active mass drivers mounted in orthogonal directions to control vibrations along either primary axis. Sensors were placed on both the AMD and TMD, as well as throughout the building to monitor ground excitation and building response. The computer directs the actuators to both optimize the response of the structure and to limit the stroke of the AMDs [13].

2.3.3 ATMD limitations

The performance benefits of an ATMD are now obvious, but these are not made available without some significant drawbacks.

Perhaps the most serious disadvantage of an active system is the steep increase in cost. Installation of the device itself becomes more complex, as now sensors, feedback connections, and actuator devices must be taken into account. Furthermore, these systems may require both large amounts of power and tedious regular maintenance, both of which add to the long-term operational costs.

Active systems also pose instability risks that need not be considered with passive devices. For example, a malfunction of the system control could cause the actuator to erroneously add energy to the primary structure, thereby having an adverse effect on vibration mitigation. Additionally, any large scale power outage could render the benefits of active control completely useless.

Due to both cost and instability considerations, many have explored alternatives to fully active TMD systems.

2.4 Semi-active tuned mass dampers

As described in section 1.2.3, recent work has championed the promise of semi-active design strategies to blend the performance benefits of active systems with the stability and energy advantages of passive systems. This concept of hybrid design has also been applied to TMD systems. In a semi-active tuned mass damper (STMD), additional forces are developed through variable stiffness or damping devices rather than through the direct application of an active control force.

Utilizing semi-active control with TMD systems is attractive for several reasons. First, it allows for variations in the control force to optimize system performance without the addition of a significant energy source, since devices that vary the stiffness or damping forces require only nominal power. Second, because these control forces dissipate energy rather than add it, they are inherently stable. Consequently, even in the event of a control system malfunction or a system power loss, an STMD may still behave as an effective passive system.

2.4.1 Development of concept

Similar to ATMD design, there are several basic variations of STMD systems that have been considered.

Variations in design

By far the majority of work on STMD systems has focused on improving translational passive TMDs[5], with the reactive control forces coming from installing variable stiffness or damping elements. Semi-active variable stiffness (SAIVS) devices involve replacing the pneumatic springs of the traditional TMD with a mechanical device

[5]Semi-active pendulum TMDs have also been considered. See [38].

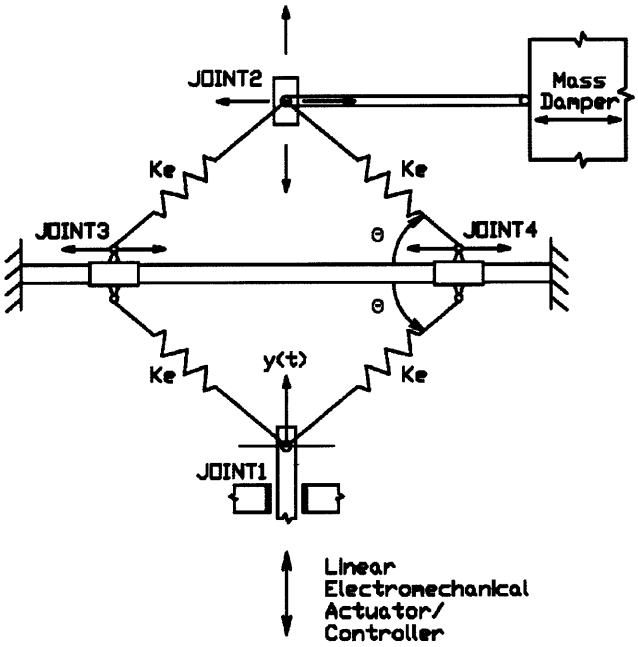

Figure 2-5: Semi-active variable stiffness device [40]

capable of adjusting its stiffness as necessary for optimized performance. This affords the distinct advantage of allowing a continuous retuning of the TMD frequency, thereby improving control and providing robustness against all off-tuning effects. An example of a SAIVS device developed by Nagarajaiah [40] is shown in figure 2-5.

On the other hand, damper-based STMD design involves replacing the passive dissipative element with a variable damping device. Many such devices, including variable-orifice dampers, rheological dampers, and variable friction dampers have already proven successful, with details in the following chapter. These variable dampers are used to adjust the level of energy dissipation in real-time to optimize the performance of the TMD. Due to their documented feasibility in large-scale civil structures, variable damping devices have generally been preferred to the more mechanically intricate SAIVS devices for implementation in STMD systems.

Advancements in theory

As with ATMD studies, the literature on STMDs has focused both on earthquake-loaded and wind-loaded structures, with a noticeable preponderance towards earthquake-excited structures. Because work on both cases is more limited for STMD systems, the significant results for all excitation types will be summarized.

The concept of a semi-active tuned mass damper was first proposed by Hrovat in 1983, who in essence simulated results for a force-clipped ATMD that was prohibited from adding energy to the system [21]. The first practical applications investigated used electrorheological (ER) dampers to supply the semi-active forces; in 1995 Abè developed ER-STMD theory for controlling transient responses under impulse loading [3], and in 1999 Hidaka conducted experimental studies that coupled an ER-STMD with a three-story model building under ground excitation [19]. Both demonstrated improved performance.

With the emergence of magnetorheological (MR) dampers as preferable to ER devices for structural applications (see chapter 3), more recent work has focused on MR-based STMD systems. Koo assessed various groundhook-based control algorithms and demonstrated their effectiveness through an experimental study of a base-excited SDOF model structure coupled with an MR-STMD [27, 28]. Ji further evaluated semi-active control algorithms for controlling an MDOF structure subjected to earthquake loading when there are uncertainties about structural properties [24]. Performance benefits of an MR-STMD under earthquake loading were further documented by Loh through numerical simulations of the response of a 12-story building [30].

Other significant work has focused specifically on wind-loaded structures. Pinkaew was the first to demonstrate the steady-state efficacy of a damper-based STMD by simulating frequency-domain results due to harmonic excitation [46]. Varadarajan proposed a novel device for a stiffness-based STMD capable of retuning to meet the demands of realistic wind excitations and changes in the stiffness properties of the primary structure [59].

At this point, no semi-active TMD devices have been installed in an actual civil structure, but theoretical work remains on-going due to the great potential of semi-active devices.

2.4.2 Limitations and design issues

There are evident advantages in equipping tuned mass dampers with semi-active control, but these, too, come with their own design challenges.

First, while STMD costs may be significantly reduced compared to ATMD costs – particularly with regards to power consumption and maintenance – installation costs still include sensors, control software, and the necessary wiring. Hence, it must be shown that the use of feedback control is still a worthwhile investment.

Second, and more importantly, the effectiveness of any STMD is ultimately limited by the control flexibility afforded by the semi-active device, whether it be through variable stiffness or variable damping. As mentioned previously, the mechanical difficulties associated with variable stiffness devices generally make them a less attractive option, which leaves the designer with the task of choosing the best variable damping device for the STMD system being considered. Realistic damping devices, such as variable-orifice, magnetorheological, or friction-based dampers, have inherent limitations in their maximum force, accessible range of forces, and stroke length. Consequently, it is critical to understand these limitations in order to produce an optimally-designed semi-active tuned mass damper.

Chapter 3

Semi-active damping devices

Selecting an optimal damping device for a given control application involves assessing a host of design considerations, including not only maximum force output, but also reaction time, power requirements, reliability, size, and stroke limitations. This chapter summarizes the capabilities of the three classes of semi-active devices that have been considered for structural applications: hydraulic dampers with a variable orifice, friction dampers, and controllable fluid dampers.

3.1 Variable-orifice damper

The variable-orifice (VO) damper was the first semi-active damping device implemented in structural applications. It consists of a cylinder-piston system with a by-pass valve connected at both ends and behaves essentially like a conventional hydraulic fluid damper with adjustable resistance to fluid flow. By electromechanically controlling an orifice in this valve, it is possible to greatly vary the damping force in real-time. Consequently, VO dampers may be modeled mathematically as linear viscous dampers in which the damping coefficient, c, now becomes a manipulable variable, $c(t)$. A basic schematic of the VO damper can be seen in figure 3-1.

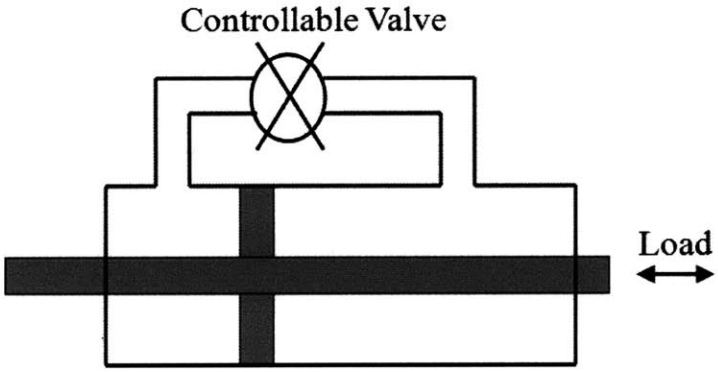

Figure 3-1: Variable-orifice damper schematic [55]

Industrial-sized devices

Kurata [29], Matsunaga [35], and Niwa [42] have each contributed to the development and classification of VO dampers capable of performing on a structural scale. These devices can produce maximum force outputs of 1–2 MN and require a power supply of only 70 W. The dynamic range of the dampers, which is determined by the minimum and maximum values for the damping coefficient, $c(t)$, is in excess of 200. These devices are relatively space efficient, with dimensions of $1.5 \times 0.5 \times 0.5$, in meters, and a mass of around $1,300$ kg.

Structural applications

VO dampers have proven successful in several applications in civil structures. In 1994 Patten led installation of VO dampers on an I-35 bridge in Oklahoma to dissipate energy induced by vehicle traffic, marking the first full-scale implementation of structural control in the United States [45]. Kobori implemented VO dampers to control stiffness elements in a semi-actively controlled building at the Kobori research complex [20]. Kurata was the first to make VO dampers the primary control system of a full-scale building, using several of the 1 MN models. Each of these advancements, among others, has led to acceptance of VO dampers as a viable means of improving control performance on a large scale.

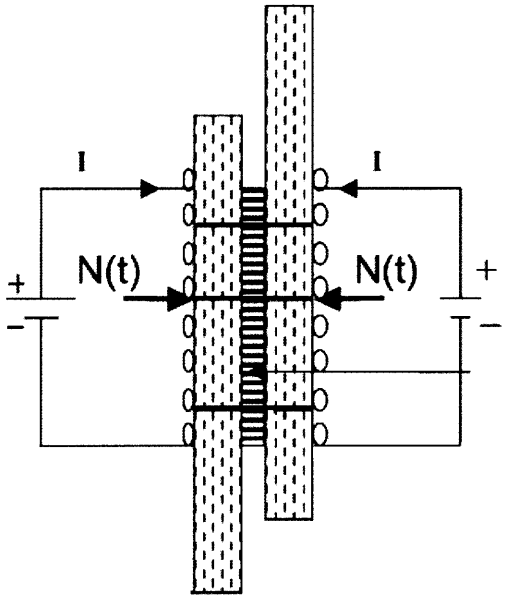

Figure 3-2: Variable-friction damper schematic [69]

3.2 Friction dampers

A second class of semi-active damping devices is based on variable friction elements. These dampers consist of a frictional sliding surface and a clamping device that produces a normal force at the interface. Controllability comes from varying the magnitude of the clamping force in real time. Various techniques have been employed to generate the normal force, including electrically-controlled piezoelectric material [63] and magnetic attractive forces produced by solenoids [69]. A schematic of the latter device is shown in figure 3-2; in this configuration the normal force, $N(t)$ is directly proportional to the square of the current, I, in the solenoids, which are placed on either side of the interface.

Industrial-sized devices and structural applications

Although friction dampers have been lauded due to their insensitivity to temperature, their minimal degradation due to aging, and their complete absence of leakage problems, they have been the least utilized semi-active damper in structural engineering applications [31]. Most of their applications have been in conjunction with other

semi-active devices or in specialized situations. For example, Feng and Yang used friction-controllable fluid bearings in parallel with seismic isolation systems to improve performance under earthquake loading [20]. Xu demonstrated friction damper effectiveness for the control of large truss structures under wind loads [63], but few other systems use friction dampers as the primary control mechanism.

3.3 Rheological dampers

The final class of semi-active damping devices utilizes the controllability of rheological fluids. The essential characteristic of these fluids is their ability to reversibly change from free-flowing linear viscous fluids into semi-solids with a controllable yield strength. This change in material property can be imparted in milliseconds through the application of either an electric field or a magnetic field, depending on if an electrorheological (ER) or magnetorheological (MR) fluid has been chosen [20].

Rheological fluids have garnered a significant amount of attention in the engineering community due to their mechanical reliability. Unlike the other choices for semi-active dampers, rheological dampers have no moving parts except for a piston. Without any electrically controlled valves or additional mechanical components, rheological fluids can provide simple, quick, and quiet interfaces between control electronics and the mechanical system [20].

3.3.1 Electrorheological fluids

ER materials were the first rheological fluids to undergo extensive study. These fluids consist of micron-sized particles suspended in high dielectric strength oils. Upon the application of an electric field, the suspended particles become polarized and fibrate into inter-electrode bridges, producing a solidified material mixture. Once in a solid state, ER fluids experience yield stresses in shear on the order of 10 kPa for static loading and 5 kPa for dynamic loading. Response times vary from 1 to 10 ms, and dynamic ranges exceeding $1,000$ have been obtained [34, 36].

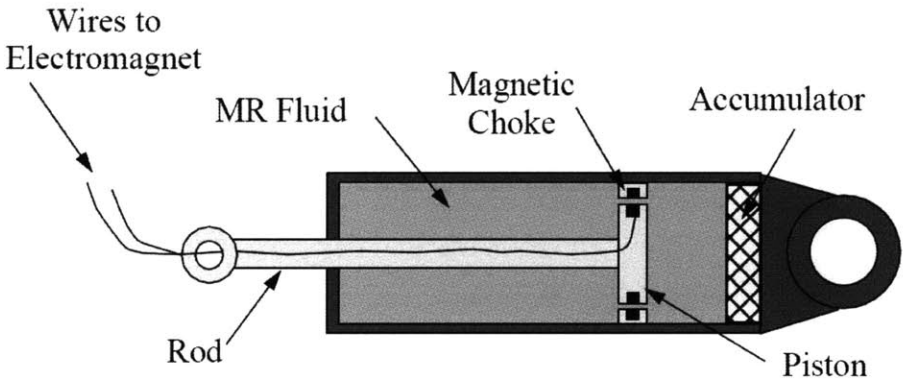

Figure 3-3: Magnetorheological damper schematic [55]

Structural applications

Application of ER technology has been extensive, but it has not been developed on the structural scale. ER fluids have been successfully used in clutches, breaks, tunable engine mounts, shock absorbers, robotics, and aerospace structures [34]. However, ER fluid use diminished by the time structural control gained traction at the end of the twentieth century, primarily because further advancements in MR fluids demonstrated its superiority for control purposes.

3.3.2 Magnetorheological fluids

MR fluids are the magnetic analog to ER fluids. They are comprised of micron-sized magnetically polarizable particles dispersed in a carrier medium such as silicon oil, meaning they take on semi-solid, viscoplastic tendencies when exposed to a magnetic field instead of an electric field. Only recently have they been considered for applications in place of ER fluids [20]. See figure 3-3 for the design of a typical MR damper.

Preferability of MR fluids

With the recent increase in knowledge of MR fluids, several distinctive advantages have surfaced over ER fluids. Perhaps most significantly, MR fluids are capable of

	MR fluids	ER fluids
Max yield stress	50–100 kPa	2–5 kPa
Operable temp.	−40–150 °C	10–90 °C
Impurity sensitivity	No	Yes
Response time	milliseconds	milliseconds
Voltage supply	2–25 V	2,000–5,000 V
Current supply	1–2 A	1–10 mA

Table 3.1: Comparison of MR and ER fluids [55]

achieving a yield strength 20–50 times greater than their ER counterparts. This is because ER fluid is generally limited by the electric field breakdown strength of the carrier liquid, but MR fluids are limited primarily by magnetic saturation, occurring at a much higher threshold.

Other significant advantages involve operability and robustness. While MR and ER dampers require comparable levels of power to operate, the MR damper requires only a low voltage supply (generally 12–24 volts as compared with 2000 or more volts for ER dampers). Outside of power issues, the operational temperatures tolerated by an MR damper range from −40 – 150 °C, more than double the temperature range of ER fluids. Additionally, MR fluids are much less sensitive to contaminants, as their magnetic polarization mechanism us unaffected by additives [20]. Hence, a strong case can be made for the superiority of MR fluids for control purposes. Table 3.1 summarizes comparison details.

Industrial-sized devices

Much effort has been put into harnessing the vast capabilities of MR dampers for structural-scale applications. In 1998 design was completed on a 200 kN MR damper with a dynamic range of 10 at its design velocity. The device, which is now produced by Lord Corporation, has a mass of 250 kg, measures 1 m long, and contains 6 liters of rheological material. Response times average 60 ms, and the device requires only 60 W of power for full functionality [66].

Structural applications

The feasibility of MR dampers in structural control has been well-documented in recent years. Spencer developed a phenomenological model of the MR damper's complicated behavior [54], and Dyke demonstrated its usefulness using control algorithms based on acceleration feedback, the standard sensor output in structures [15]. These rapid advancements led to the first full-scale implementation of an MR damper control system in the National Museum of Emerging Science and Innovation, located in Tokyo, in 2001 [67].

3.4 Choosing a damping device

As has been seen, the characteristics of semi-active damping devices can vary considerably. Settling on a particular device to supply semi-active control may be a project-specific design task, but this study will focus on VO and MR dampers for the following reasons: First, both of them are available on the industrial-sized scales necessary for structural applications. Second, each has already been used in functioning civil structures, providing precedent for their reliability. Third, and critically for the study at hand, they represent two distinct classes of damping devices – those with linear responses and those with non-linear responses. As shall be seen, this will be an essential characteristic in determining the effectiveness of a semi-active tuned mass damper.

Chapter 4

Simulation of Controlled System

In order to provide benchmarks for various STMD systems under wind excitation, it is necessary to accurately simulate how well they mitigate the dynamic response of the primary structure. The numerical techniques used to accomplish this task will be the focus of chapter 4.

4.1 Equations of motion

For a mathematical model that describes the structure as having n degrees of freedom, optimizing control performance is akin to limiting the displacements, velocities, and accelerations in the governing equation of motion

$$\mathbf{M_f}\ddot{\mathbf{U}}_f + \mathbf{C_f}\dot{\mathbf{U}}_f + \mathbf{K}_f\mathbf{U}_f = \mathbf{P}_f - \mathbf{M}_f\mathbf{E}a_g \tag{4.1}$$

where $\mathbf{U}_f$ is the $n \times 1$ vector containing the system displacements, $\mathbf{M}_f$ is the $n \times n$ mass matrix, $\mathbf{C}_f$ is the $n \times n$ damping matrix, $\mathbf{K}_f$ is the $n \times n$ stiffness matrix, $\mathbf{P}_f$ is an $n \times 1$ vector containing the external disturbances (such as wind loading), a_g is the ground acceleration, and $\mathbf{E}$ is an $n \times 1$ vector of ones. Here the subscript f denotes that the equations refer to the free, uncontrolled structure.

For a disturbance mitigation system based on the addition of r active or semi-active tuned mass dampers in which wind loading is the primary concern, equation 4.1

becomes

$$\mathbf{M\ddot{U}} + \mathbf{C\dot{U}} + \mathbf{KU} = \mathbf{P} + \mathbf{WF} \tag{4.2}$$

in which $\mathbf{U}$ is now an $(n + r) \times 1$ vector to include the displacements of the tuned mass dampers, $\mathbf{M}$, $\mathbf{C}$, and $\mathbf{K}$ are $(n + r) \times (n + r)$ matrices, and $\mathbf{P}$ is $(n + r) \times 1$. Here $\mathbf{F}$ has been added as an $r \times 1$ vector of control forces, and $\mathbf{W}$ is an $(n + r) \times r$ matrix that defines the location of those control forces with respect to the degrees of freedom.

This chapter elucidates how equation 4.2 can be used to simulate the benefits of using semi-active tuned mass dampers in actual structures. Presented in the following sections are the rational for determining $\mathbf{M}_f$, $\mathbf{C}_f$, and $\mathbf{K}_f$ for realistically modeled structures; the procedure for designing the r tuned mass dampers; and the technique for calculating the optimal control forces contained in $\mathbf{F}$. All simulations using these methods were performed using MATLAB, the results of which are presented in the chapters to follow.

4.2 Development of model structures

In practice, it is difficult to determine the stiffness and damping properties of a structure without detailed calculations or a finite element analysis. This lack of knowledge is of heightened concern for older buildings in need of retrofitting, as recovery of this information may be nearly impossible. In these cases, not only may the original data be limited, but uncertainties are compounded by fluctuations in structural properties with aging and deterioration.

As an acknowledgement of these limitations, the model structures generated in this study will be based on $\mathbf{M_f}$, the mass properties of the uncontrolled building, and T_o, the fundamental period of the building. The former can generally be reasonably estimated, and the latter can be readily observed and measured. These values will be used to calculate stiffness matrices, based on an optimized stiffness distribution, and damping matrices, based on Rayleigh Damping. In an effort to maintain generality, this will be done for a structure with n degrees of freedom to which r tuned mass

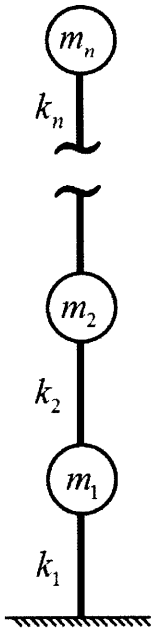

Figure 4-1: Shear beam model of a structure

dampers are being added.

4.2.1 Optimized stiffness distribution

One standard approach for designing the stiffness distribution of a structure is to perform a calibration technique that produces a linear profile of the fundamental mode of vibration. This leads to a structure that is stiffer at the bottom, where bending and shear contribute most significantly, and more efficiently limits deflections at the top of the building. Hence, this design methodology is most beneficial in the tallest of buildings and can even be observed in the profiles of many existing skyscrapers.

Treating the structure as a discrete cantilever shear beam as shown in figure 4-1,

$\mathbf{M_f}$ is a diagonal positive semi-definite matrix of the form:

$$\mathbf{M_f} = \begin{bmatrix} m_1 & & & \\ & m_2 & & \\ & & \ddots & \\ & & & m_n \end{bmatrix}$$

where m_i is the mass of the i^{th} floor. The stiffness matrix of this structure, $\mathbf{K_f}$, can then be formed using

$$\mathbf{K}_f = \mathbf{A^T} diag\{\mathbf{k}_f\}\mathbf{A} \tag{4.3}$$

where

$$\mathbf{k}_f = \begin{bmatrix} k_1 \\ k_2 \\ \vdots \\ k_n \end{bmatrix}$$

and $\mathbf{A}$ is an $n \times n$ matrix such that [56]:

$$\mathbf{A} = \begin{bmatrix} 1 & & & & \\ -1 & 1 & & & \\ & -1 & 1 & & \\ & & \ddots & \ddots & \\ & & & -1 & 1 \end{bmatrix}$$

It is now desired to solve for the elements $\mathbf{k}_f$ such that the fundamental mode has a linear profile:

$$\mathbf{v} = \frac{1}{n} \begin{bmatrix} 1 \\ 2 \\ \vdots \\ n \end{bmatrix}$$

calibrated to have a period of T_o. Using $\omega_o = \frac{2\pi}{T_o}$, this is found from [13]:

$$\mathbf{k}_f = {\omega_o}^2(\mathbf{A^T})^{-1}\mathbf{M}_f\mathbf{v} \tag{4.4}$$

Equation 4.2.1 then produces the system stiffness matrix.

4.2.2 Implementation of Rayleigh damping

In general, the damping matrix of the structure, $\mathbf{C_f}$, cannot be calculated directly. Hence, it is customary to construct this matrix such that it approximates the overall energy dissipation during the response of the system [6]. One common method for doing so is Rayleigh damping, which is based on a linear combination of the mass and stiffness matrices:

$$\mathbf{C}_f = a_0\mathbf{M}_f + a_1\mathbf{K}_f \tag{4.5}$$

These constants are most frequently determined by specifiying the damping ratios, ξ_i and ξ_j, at two arbitrary frequencies pertinent to the structure being considered. For frequencies ω_i and ω_j, this leads to [7, 25]:

$$a_0 = \frac{2\omega_i\omega_j(\xi_i\omega_j - \xi_j\omega_i)}{{\omega_j}^2 - {\omega_i}^2} \tag{4.6}$$

$$a_1 = \frac{2(\xi_i\omega_j - \xi_j\omega_i)}{{\omega_j}^2 - {\omega_i}^2} \tag{4.7}$$

In the majority of simulations presented here, Rayleigh damping of $\xi_i = \xi_j = 0.02$ is assigned directly to the first two modes, $\omega_i = \omega_1$ and $\omega_j = \omega_2$, since $\xi = 0.02$ is common for steel structures.

4.2.3 Design of tuned mass dampers

The use of tuned mass dampers to mitigate undesirable vibrations in structures has typically focused on control of the fundamental mode. Because this mode contains the dominant response of the structure, particularly under wind loading, reduction of its response is generally sufficient for serviceability considerations. However, multiple

tuned mass dampers have also been considered, particularly in situations where both horizontal and torsional motions merit design consideration [9].

Hence, while control of the fundamental mode through the use of a single tuned mass damper will be a focus of this study, the design methodology will be developed for the more general case where r modes of the structural response will be controlled by independently calibrated tuned mass dampers. This allows for a more complete analysis of the effectiveness of improving response through optimal control theory.

Placement of multiple tuned mass dampers

For the discrete shear beam model being developed, r tuned mass dampers will be designed to mitigate vibrations of modes 1 through r. Each of these tuned mass dampers will be placed at the degree of freedom most conducive to the control of that mode in order to maximize their effectiveness. Hence, a modal analysis of the structure must be performed[1] to produce the modal shape vectors:

$$\mathbf{\Phi} = \begin{bmatrix} \boldsymbol{\phi}_1 & \boldsymbol{\phi}_2 & \dots & \boldsymbol{\phi}_r & \dots & \boldsymbol{\phi}_n \end{bmatrix}$$

With this information it is possible to optimize the location of the i^{th} tuned mass damper by placing it at degree of freedom l, chosen such that $\Phi_{li} = max\{\boldsymbol{\phi}_i\}$. Location vectors can then be developed for properly placing mass, stiffness, and damping elements into matrices for the complete $n+r$ degree of freedom system. Let $\mathbf{a}_i$ be the $(n+r) \times 1$ location vector for the i^{th} tuned mass damper and let $\mathbf{b}_i$ be the

[1]This can be done efficiently using the MATLAB command *eig*.

$(n+r) \times 1$ location vector for its stiffness and damping elements. Then[2]:

$$\mathbf{a}_{i,j} = \begin{cases} 1 & \text{if } j = n+i \\ 0 & \text{otherwise} \end{cases} \tag{4.8}$$

$$\mathbf{b}_{i,j} = \begin{cases} 1 & \text{if } j = n+i \\ -1 & \text{if } j = m \\ 0 & \text{otherwise} \end{cases} \tag{4.9}$$

From these the system matrices may be formulated [9]:

$$\mathbf{M} = \begin{bmatrix} \mathbf{M}_f & \mathbf{0} \\ \mathbf{0} & \mathbf{0} \end{bmatrix} + \sum_{i=1}^{r} m_{di} \mathbf{a}_i {\mathbf{a}_i}^{\mathrm{T}} \tag{4.10}$$

$$\mathbf{K} = \begin{bmatrix} \mathbf{K}_f & \mathbf{0} \\ \mathbf{0} & \mathbf{0} \end{bmatrix} + \sum_{i=1}^{r} k_{di} \mathbf{b}_i {\mathbf{b}_i}^{\mathrm{T}} \tag{4.11}$$

$$\mathbf{C} = \begin{bmatrix} \mathbf{C}_f & \mathbf{0} \\ \mathbf{0} & \mathbf{0} \end{bmatrix} + \sum_{i=1}^{r} c_{di} \mathbf{b}_i {\mathbf{b}_i}^{\mathrm{T}} \tag{4.12}$$

where m_{di}, k_{di}, and c_{di} are the mass, damping, and stiffness of the i^{th} tuned mass damper, yet to be optimized.

Tuned mass damper optimization

Following the procedure described by [13], the properties of the i^{th} tuned mass damper may be found by using modal decomposition to isolate the response of the corresponding mode[3]. Then, for a given mass ratio μ, the corresponding mass necessary at degree of freedom l must be

$$m_{di} = \mu \frac{{\tilde{m}_i}^2}{\Phi_{li}} \tag{4.13}$$

[2]Here and throughout, the comma is not used to express index notation but rather to clarify that i does not refer to a dimension of the matrix.

[3]The procedure outlined here is approximate for MDOF systems but exact for SDOF systems, the primary focus of this study. For a more rigorous development of parameters for multiple tuned mass dampers, refer to [9]

where $\tilde{m}_i = \boldsymbol{\phi}_i{}^{\mathrm{T}}\mathbf{M}_f\boldsymbol{\phi}_i$ is the modal mass. Using modal stiffness and damping terms, $\tilde{k}_i = \boldsymbol{\phi}_i{}^{\mathrm{T}}\mathbf{K}_f\boldsymbol{\phi}_i$ and $\tilde{c}_i = \boldsymbol{\phi}_i{}^{\mathrm{T}}\mathbf{C}_f\boldsymbol{\phi}_i$, specifying the stiffness and damping terms for each tuned mass damper is now equivalent to working with a single degree of freedom system, in which

$$k_{di} = m_{di}(f_{opt}\omega_i)^2 \tag{4.14}$$

$$c_{di} = 2\xi_{di}\omega_i m_{di} \tag{4.15}$$

where f_{opt} and ξ_{di} are the optimal tuning and damping parameters.

As described in chapter 2, there are a variety of optimization techniques for determining these values, each depending on the system input and the goal of the optimization. In this study all passive TMD systems will be tuned with the results of Asami [5], which provides series solutions for optimization of maximum displacements under a force excitation. The results obtained are

$$\begin{aligned} f_{opt} =& \frac{1}{1+\mu} - \xi\frac{1}{1+\mu}\sqrt{\frac{1}{2(1+\mu)}\left(3+4\mu-\frac{AB}{2+\mu}\right)} \\ &+ \xi^2\frac{C_0 - 4(5+2\mu)AB}{4(1+\mu)^2(2+\mu)(9+4\mu)} \end{aligned} \tag{4.16}$$

$$\begin{aligned} \xi_{opt} =& \sqrt{\frac{3\mu}{8(1+\mu)}} + \xi\frac{60+63\mu+16\mu^2-2(3+2\mu)AB}{8(1+\mu)(2+\mu)(9+4\mu)} \\ &\xi^2\frac{C_1(A+B)\sqrt{2+\mu}+C_2(A-B)\sqrt{\mu}}{32(1+\mu)(2+\mu)^2(9+4\mu)^3\sqrt{2\mu(1+\mu)}} \end{aligned} \tag{4.17}$$

where

$$A = \sqrt{3(2+\mu)-\sqrt{\mu(2+\mu)}}$$

$$B = \sqrt{3(2+\mu)+\sqrt{\mu(2+\mu)}}$$

$$C_0 = 52+41\mu+8\mu^2$$

$$C_1 = -1296+2124*\mu+6509*\mu^2+5024*\mu^3+1616*\mu^4+192*\mu^5$$

$$C_2 = 48168+112887*\mu+105907*\mu^2+49664*\mu^3+11632*\mu^4+1088*\mu^5$$

Due to the increased amount of variability in the design of active and semi-active systems, an optimal passive TMD may produce sub-optimal results in the controlled case. Consequently, multiple TMD optimization schemes were tested, with the best control results generally achieved using the expressions developed by Tsai [58]. These parameters were found using curve-fitting schemes to minimize the maximum displacements of damped structures under ground excitation[4] and are given by

$$\begin{aligned} f_{opt} =& \left(\frac{\sqrt{1-0.5\mu}}{1+\mu} + \sqrt{1-2{\xi_i}^2} - 1\right) \\ & - (2.375 - 1.034\sqrt{\mu} - 0.426\mu)\xi_i\sqrt{\mu} \\ & - (3.730 - 16.903\sqrt{\mu} + 20.496){\xi_i}^2\sqrt{\mu} \end{aligned} \tag{4.18}$$

$$\begin{aligned} \xi_{di} =& \sqrt{\frac{3\mu}{8(1+\mu)(1-0.5\mu)}} + (0.151\xi_i - 0.170{\xi_i}^2) \\ & (0.163\xi_i + 4.980{\xi_i}^2)\mu \end{aligned} \tag{4.19}$$

4.3 Selection of control algorithm

With all system parameters now established, it is possible to choose a method for finding the optimal control forces, $\mathbf{F}$, and solve the governing equation of motion (equation 4.2). While in general many control techniques may be worth considering, this study focuses on the use of a clipped optimal control algorithm based on a linear quadratic regulator (LQR), for which precedent has been set. Doing so first necessitates the development of state-space formulation of the system.

[4]The ability to improve semi-active performance by choosing an alternate TMD optimization scheme, even one optimized for ground excitation, indicates that the ideal parameters for an STMD may vary notably from all sets of optimized passive parameters. In particular, selection of the TMD tuning ratio, f_{opt}, could likely be altered to further improve STMD results. However, because it is desirable for semi-active systems to behave as passive systems following control failure, only optimal parameters from the literature were explored. For example, while the values given by Tsai are slightly sub-optimal for a wind-excited passive system, overall performance results do not deviate substantially.

4.3.1 Formulation of state-space equations

Because working with a second-order differential equation can prove cumbersome, it is convenient to transform equation 4.2 to a state-space notation that reduces the problem to a set of first-order equations involving the state vector $\mathbf{X}$ [13, 43], where

$$\mathbf{X} = \begin{bmatrix} \mathbf{U} \\ \dot{\mathbf{U}} \end{bmatrix}$$

This leads to a reformulation of equation 4.2:

$$\dot{\mathbf{X}} = \mathbf{A}\mathbf{X} + \mathbf{B}_p\mathbf{P} + \mathbf{B}_f\mathbf{F} \tag{4.20}$$

which involves the constant coefficient matrices

$$\mathbf{A} = \begin{bmatrix} \mathbf{0} & \mathbf{I} \\ -\mathbf{M}^{-1}\mathbf{K} & -\mathbf{M}^{-1}\mathbf{C} \end{bmatrix} \tag{4.21}$$

$$\mathbf{B}_p = \begin{bmatrix} \mathbf{0}_{(n+r)\times 1} \\ diag\{\mathbf{M}_f{}^{-1}\} \\ \mathbf{0}_{r\times 1} \end{bmatrix} \tag{4.22}$$

$$\mathbf{B}_f = \begin{bmatrix} \mathbf{0}_{(n+r)\times r} \\ \mathbf{M}^{-1}\mathbf{W} \end{bmatrix} \tag{4.23}$$

where $\mathbf{A}$ is $2(n+r) \times 2(n+r)$, $\mathbf{B}_p$ is $2(n+r) \times 1$, and $\mathbf{B}_f$ is $2(n+r) \times r$. $\mathbf{W}$ is the $(n+r) \times r$ force location matrix and can be formed from the stiffness location vectors:

$$\mathbf{W} = -\begin{bmatrix} \mathbf{b}_1 & \dots & \mathbf{b}_r \end{bmatrix}$$

By making this transformation into state-space notation it becomes more direct to numerically integrate equation 4.2 and more straightforward to apply an optimal control law.

4.3.2 Clipped optimal control

Guidelines for choosing a particular control method are rather general, and several options may be viable. One shown to be effective for semi-active damping devices is the clipped optimal control algorithm, proposed by Hrovat [21] for semi-active tuned mass dampers and recommended by Dyke [15] for use with magnetorheological dampers. Clipped optimal control was further applied to semi-active tuned mass dampers by Pinkaew [46], who demonstrated effective results in the frequency domain, and by Ji [24], who demonstrated its validity through a comparison with three other control algorithms. Following their precedent, clipped optimal control will be used in this study[5].

The first part of the clipped optimal control strategy involves finding the control vector $\mathbf{F} = \mathbf{F}(t)$ that minimizes the quadratic performance index given by

$$J = \int_0^\infty \left(\mathbf{X}^{\mathrm{T}}\mathbf{Q}\mathbf{X} + \mathbf{F}^{\mathrm{T}}\mathbf{R}\mathbf{F}\right) dt \tag{4.24}$$

where $\mathbf{Q}$ is a positive semi-definite weighting matrix and $\mathbf{R}$ is a positive definite weighting matrix that penalizes extreme control forces. These matrices are generally found heuristically to meet control and cost considerations, but they are typically diagonal matrices that take the form

$$\mathbf{Q} = \begin{bmatrix} q_{d,i}\delta_{ij} & \mathbf{0} \\ \mathbf{0} & q_{v,i}\delta_{ij} \end{bmatrix} \tag{4.25}$$

$$\mathbf{R} = \left[r_i\delta_{ij}\right] \tag{4.26}$$

where the q_d and q_v terms weight displacement and velocity feedbacks, respectively, and the r terms weight the various control forces. For fully active control devices, all q_d terms are often set to zero to avoid potential instability due to displacement

[5]Comparative studies by Wu [62] and Yang [70] demonstrated H_∞ control methods to have comparable effectiveness when used for wind-loaded buildings, with an advantage over linear quadratic controllers when robustness is a concern. Because this study is not concerned with system uncertainties, use of these methods was not considered advantageous, though H_∞ techniques are recommended for studies in which robustness is a fundamental design issue.

feedback [13, 43].

Solution of equation 4.24 leads to an optimal control force based on the feedback law

$$\mathbf{F}(t) = -\mathbf{K}_c\mathbf{X}(t) \tag{4.27}$$

in which $\mathbf{K}_f$ is a constant gain vector formed from

$$\mathbf{K}_c = \mathbf{R}^{-1}{\mathbf{B}_f}^{\mathrm{T}}\mathbf{P}_c \tag{4.28}$$

where $\mathbf{P}_f$ is a symmetric matrix that satisfies the reduced-matrix Ricatti equation

$$\mathbf{A}^{\mathrm{T}}\mathbf{P}_c + \mathbf{P}_f\mathbf{A} - \mathbf{P}_c\mathbf{B}_f\mathbf{R}^{-1}{\mathbf{B}_f}^{\mathrm{T}}\mathbf{P}_c + \mathbf{Q} = \mathbf{0} \tag{4.29}$$

Using equations 4.27, 4.28, and 4.29 it is possible to calculate the optimal control force vector for the user-specified weighting matrices. The second component of the control law involves commanding the control device to perform the optimal action given its inherent constraints, such as force saturation. In the case of semi-active damping devices only dissipative forces can be exerted, giving further limitations to controllability. The details of the control law, including clipping strategies, vary by device and are presented more fully in section 4.5.

4.4 Simulation strategy for frequency-range response

The effectiveness of any control scheme, whether passive or active, can be investigated by performing a dynamic amplification analysis. That is, by surveying the stead-state response of the structure as a function of excitation frequency, it is possible to address issues of resonance and to characterize a control scheme's efficacy in vibration suppression. Because closed-loop feedback control schemes can produce highly non-linear responses, it is not possible to directly generate such results.

Hence, to quantify the frequency-range effectiveness of semi-active tuned mass dampers, numerical techniques must be employed. First, a system input is chosen that

ranges over a broad band of harmonic excitations; second, a time-domain numerical integration scheme is executed; and third, Fourier transformations are obtained to produce transfer functions in the frequency domain.

4.4.1 System input

In order to recover useful information in the frequency domain, the external disturbances must contain a broad range of frequencies. Since the present study involves an analysis of wind loading on the primary structure, the external disturbances are limited to

$$\mathbf{P} = p(t) \begin{bmatrix} \mathbf{E}_f \\ \mathbf{0}_{r\times 1} \end{bmatrix} \tag{4.30}$$

where $p(t)$ is a time-dependent function that must contain the necessary frequency content. One common technique is to use a "chirp" excitation in which

$$p(t) = \sin \omega(t)t \tag{4.31}$$

Here $\omega(t)$ varies linearly from ω_{min} to ω_{max} over the duration of the input excitation. ω_{min} and ω_{max} must be selected to satisfactorily enclose all frequencies of interest, specifically any system resonances.

4.4.2 Time domain numerical integration

The response of the structure under this loading can be found by integrating equation 4.20. Assuming time independent feedback parameters and known initial conditions at time t_o, the total solution is given by the Duhamel integral matrix [13]

$$\mathbf{X}(t) = \mathbf{e}^{\mathbf{A}(t-t_o)}\mathbf{X}(t_o) + \int_{t_o}^{t} \mathbf{e}^{\mathbf{A}(t-t_\tau)}\big(\mathbf{B}_p\mathbf{P}(\tau) + \mathbf{B}_f\mathbf{F}(\tau)\big)d\tau \tag{4.32}$$

wher $\mathbf{e}$ is a matrix exponential. In the more general case where parameters may be time dependent, the closed-form solution must give way to a time-step discretization scheme in which $t \to t_j$ and $t_{j+1} = t_j + \Delta t$. An expansion for $\mathbf{e}^{\mathbf{A}t}$ then transforms

equation 4.32 into

$$\mathbf{X}_{j+1} = \mathbf{e}^{\mathbf{A}\Delta t}\mathbf{X}_j + \mathbf{A}^{-1}(\mathbf{e}^{\mathbf{A}_j\Delta t} - \mathbf{I})\left(\mathbf{B}_p\mathbf{P}_j + \mathbf{B}_f\mathbf{F}_j\right) \tag{4.33}$$

By starting with an initial state vector, $\mathbf{X}_0 = \mathbf{X}(t_o)$, equation 4.33 provides an accurate estimate for $\mathbf{X}_{j+1}$ and may be used successively to obtain the system response [13].

4.4.3 Calculation of dynamic amplication factors

Once the time history of a response has been calculated, the frequency-range response can be found by computing the Fourier transforms of the outputs and inputs. In general,

$$H_{ij}(\omega) = \frac{\mathcal{F}\left[u_i(t)\right]}{\mathcal{F}\left[p_j(t)\right]} \tag{4.34}$$

where $\mathcal{F}$ is the Fourier transform, $u_i(t)$ is the response of degree of freedom i, and $p_j(t)$ is the load applied to degree of freedom j. H_{ij} is referred to as the transfer function for the response at i due to a load at j; due to the principle of reciprocity, $H_{ij} = H_{ji}$ for all i, j pairs [25].

Under the wind disturbance being considered, the load is the same for all degrees of freedom. Namely,

$$p_1 = \cdots = p_n = p(t)$$

as defined in equation 4.31. Consequently, equation 4.34 reduces to

$$H_i(\omega) = \frac{\mathcal{F}\left[u_i(t)\right]}{\mathcal{F}\left[p(t)\right]} \tag{4.35}$$

leaving n distinct transfer functions for the response of the primary structure.

When damping is present, transfer functions contain an imaginary component; furthermore, because they describe an input-output relationship, their scaling is dependent on the units used for each. In a general assessment of a system's dynamic behavior, it is therefore convenient to work with a dynamic amplification function, de-

fined as the frequency-dependent ratio between the maximum dynamic displacement and the maximum static displacement:

$$A_{d,ij}(\omega) = \frac{p_j}{u_{s,ij}} |H_{ij}(\omega)| \quad (4.36)$$

where $A_{d,ij}$ is the dynamic amplification function for displacement, $u_{s,ij}$ is the deflection at degree of freedom i due to a load applied statically at degree of freedom j of magnitude p_j.

As described in chapter 2, tuned mass dampers may be needed more to limit accelerations than displacements, for occupant comfort is a driving concern in most flexible high-rise buildings. Consequently, it is worthwhile to investigate the effect of control devices on mitigating maximum accelerations in the structure. Following the steps of equations 4.34 and 4.36, a result analogous to the dynamic amplification function can be obtained for SDOF systems:

$$A_a(\omega) = m \left| \frac{\mathcal{F}\left[\ddot{u}(t)\right]}{\mathcal{F}\left[p(t)\right]} \right| \quad (4.37)$$

4.5 Systems compared

The simulation techniques outlined in this chapter were applied to model structures with six categorizations of control. While the semi-active tuned mass dampers are the focus of this study, results were generated for structures without control, with passive control only, and with fully active control to provide useful comparative benchmarks. The summary that follows explains the basis of these simulations, including techniques for clipped optimal control and an explanation of accessible control forces.

4.5.1 Free response

The free response simulations solve equation 4.1 without the addition of any tuned mass dampers or control forces. Mitigation of the sharp resonance of the fundamental mode is the goal of all control measures.

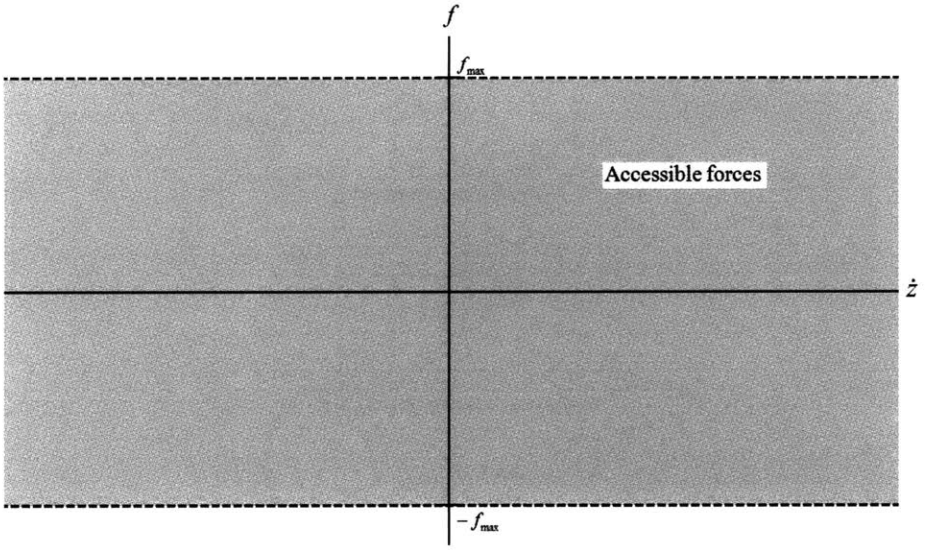

Figure 4-2: Forces accessible by an actuator

4.5.2 Passive TMD

Results for passive tuned mass dampers come from the solution of equation 4.2 with $\mathbf{F} = \mathbf{0}$. Because the optimization of the tuned mass dampers has been standardized, as described in section 4.2.3, the control effectiveness of the passive system depends entirely on the selection of μ, the mass ratio. Hence, any improvements in mitigation of resonance comes at the expense of adding more mass to the top of the building.

4.5.3 ATMD

As described in chapter 2, the active tuned mass damper uses a full-scale actuator, capable of adding energy to the system. The only limitations on the potential control force come from constraints on the cost, as introduced by the control force weighting matrix $\mathbf{R}$, and clipping due to any force saturation limits inherit in the actuator. Figure 4-2 graphically demonstrates the accessible forces for a given saturation limit, f_{sat}. As has already been shown in the literature, use of clipped optimal control with a low concern for cost can lead to near complete mitigation of resonance effects [53].

4.5.4 Limited ATMD

What is here termed a "limited ATMD" refers to an ATMD that has been given the additional constraint of only being able to produce dissipative forces. This concept was first developed by Hrovat [21] and represents an upper bound for the effectiveness of any semi-active tuned mass damper, making it useful for comparison purposes. Mathematically, simulations are equivalent to using a full-scale ATMD with the addition of the dissipation constraint

$$f_{l,i} = -f_{sat} \leq f_i \frac{1 + sgn\,(f_i \dot{z}_i\,)}{2} \leq f_{sat} \tag{4.38}$$

where f_i refers to the optimal force for the actuator on the i_{th} tuned mass damper, z_i is the relative velocity of the tuned mass damper with respect to the building, and $f_{l,i}$ is the actual control force outputted by the limited ATMD.

A graph of the resulting forces available for this system are shown in figure 4-3. As has been demonstrated by Hrovat, mitigation around resonance is comparable to that attainable by an actuator without any limitations, thereby demonstrating validity to the concept of semi-active tuned mass dampers. It remains only to find a realistic damping device capable of achieving similar results.

4.5.5 Variable-orifice STMD

As described in chapter 3, a variable-orifice damper is one candidate for use in a semi-active tuned mass damper based on a variable damping device. The basic mathematical model for this device treats it as a linear viscous damper with controllable damping coefficient $c(t)$, which can vary between limiting values c_{min} and c_{max}. Hence, the magnitude of the control force is now also limited by the magnitude of the relative TMD velocity. In addition to the constraint of equation 4.38, the accessible control force is now limited to

$$\begin{aligned} f_{vo,i} &= -f_{sat} \leq c_i(t)\dot{z}_i \frac{1 + sgn\,(f_i \dot{z}_i\,)}{2} \leq f_{sat} \\ c_{min} &\leq c(t) \leq c_{max} \end{aligned} \tag{4.39}$$

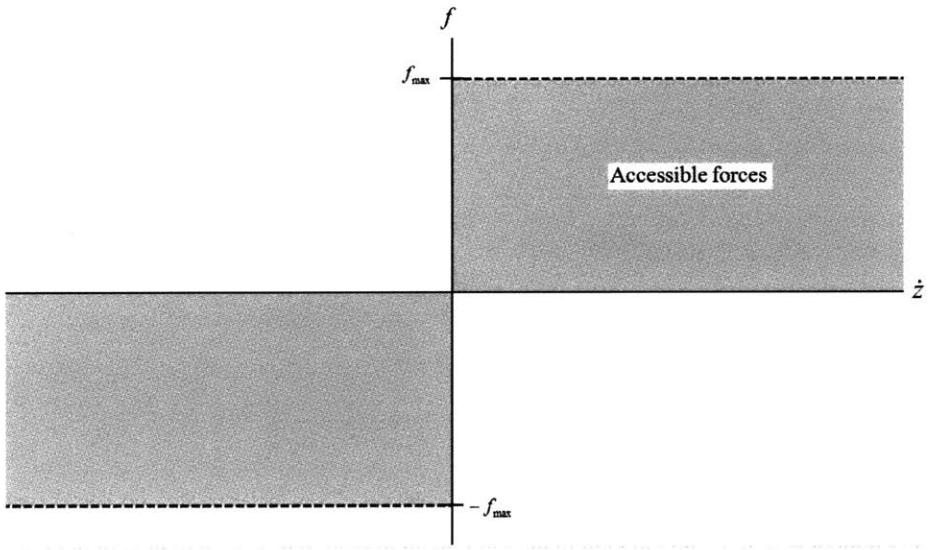

Figure 4-3: Forces accessible by a semi-active actuator

The result is a much more limited band of accessible forces, as shown in figure 4-4, and performance that falls between that of the limited ATMD and the passive system. The control objective is to come as near to the limited ATMD results as possible for a given damping device.

4.5.6 Magnetorheological STMD

The second variable damping device compared in this study is the magnetorheological damper. Chapter 3 highlights the capabilities of MR dampers. The mathematical model selected for this study is a modified version of the Bingham model, described more fully in chapter 6. Because this is a non-linear device, the control force must be produced by assigning a voltage to the mathematical model rather than by prescribing a force directly. Clipped optimal control laws have been developed by Dyke [23]. This study uses

$$\begin{aligned} f_{mr,i} &= -f_{sat} \leq g_{mr}\,[V(t)\,] \leq f_{sat} \\ V(t) &= V_{max}\frac{1+sgn\,(f_i\dot{z}_i\,)}{2} \end{aligned} \tag{4.40}$$

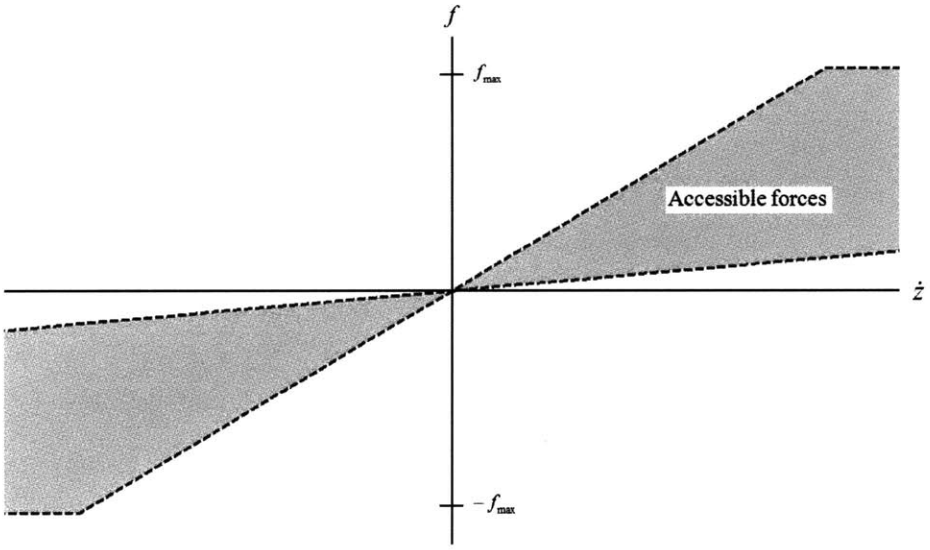

Figure 4-4: Forces accessible by a variable-orifice semi-active damper

where g_{mr} is a function that outputs the force of the MR damper for a given mathematical model, $V(t)$ is the voltage assigned by the control law, and V_{max} is the maximum voltage that can be prescribed. See figure 4-5 for a display of the accessible forces and equation 6 for the formulation g_{mr}.

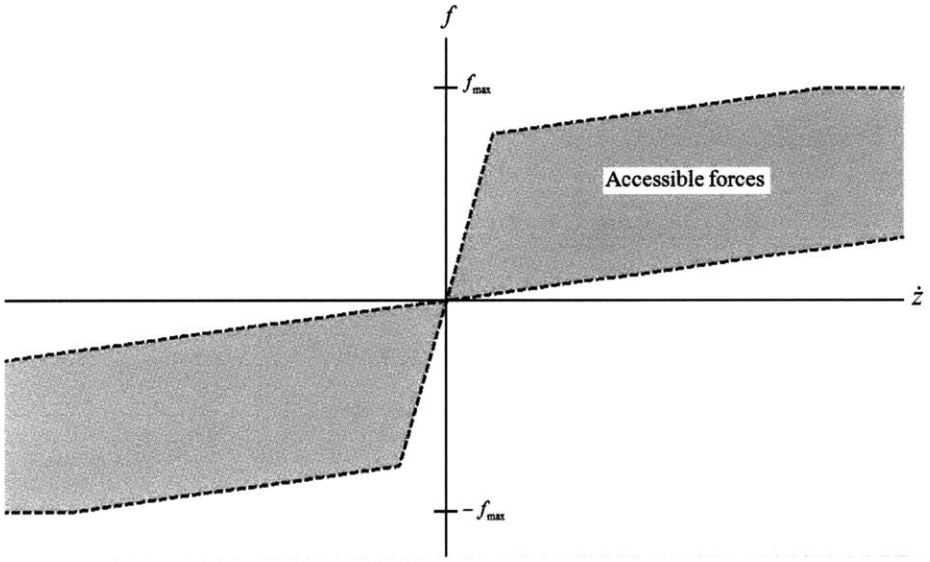

Figure 4-5: Forces accessible by a magnetorheological semi-active damper

Chapter 5

Results for Variable-Orifice STMD

As described in chapter 3, the variable-orifice damper is one candidate to provide the reactive forces necessary for an effective semi-active tuned mass damper (VO-STMD). This device has been selected for further analysis as a representative case of variable dampers with linear responses. Such devices behave essentially as viscous dampers whose damping coefficient, c, may be adjusted in real time.

This chapter follows the simulation procedure described in the previous chapter and bases control forces on the mathematical model explained in section 4.5.5. An overview of the analysis is provided before results are presented in full.

5.1 Overview of analysis

Since realistic damping devices have inherent limitations in their control effectiveness, semi-active tuned mass dampers should be designed to maximize their performance under these constraints. In an effort to categorize the capability of STMD systems, two variables will be defined:

- D_r = the dynamic range of a damping device, which quantifies the difference between its maximum and minimum force outputs.

- C_r = the damping reduction factor of the STMD design, which quantifies the difference between the optimal damping for a passive TMD, c_d, and the mini-

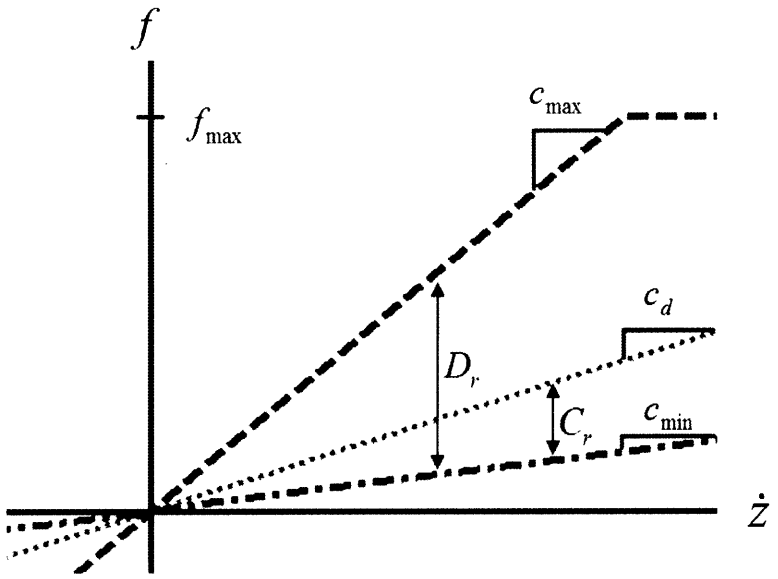

Figure 5-1: Dynamic range and damping reduction factor

mum damping attainable by a given damping device.

In the case where a variable-orifice damper is used as the semi-active device, these variables will be described by

$$D_r = \frac{c_{max}}{c_{min}} \tag{5.1}$$

$$C_r = \frac{c_d}{c_{min}} \tag{5.2}$$

where c_{max} and c_{min} may vary significantly depending on the damping device selected.

Figure 5-1 indicates how D_r and C_r affect the range of accessible control forces for a variable-orifice STMD; note that $\dot{z}$ refers to the relative velocity of the tuned mass with respect to the primary structure.

5.1.1 Dynamic range implications

Assuming that a given STMD system is constructible and meets all stroke limitations, the dynamic range of its damping device is perhaps the most critical characteristic in determining its potential effectiveness. As can be seen in figure 5-1, the value

given for D_r directly controls the range of accessible control forces. For $D_r = 0$, the best result could be to reproduce the results of a passive TMD, but as $D_r \to \infty$ the controllability will approach that of the limited ATMD as described in section 4.5.4.

In fact, the dynamic range of a damper is more critical to the success of an STMD than is the maximum force output of a given damping device. That is, even if a device has the potential for a high force output (such as by having a significant c_{max} in the case of a variable-orifice damper), the range of accessible forces may be significantly limited if its minimum force output is not significantly below its maximum. Furthermore, for design purposes, constraints on the maximum force capacity of a device may be overcome by installing several dampers in parallel provided that their dynamic range is not the limiting factor.

Figure 5-2 demonstrates the effect the dynamic range can have on the steady-state performance of a VO-STMD. As can be seen, the VO-STMD performance improvement is rather sensitive to dynamic range for low D_r values but levels off as D_r increases.

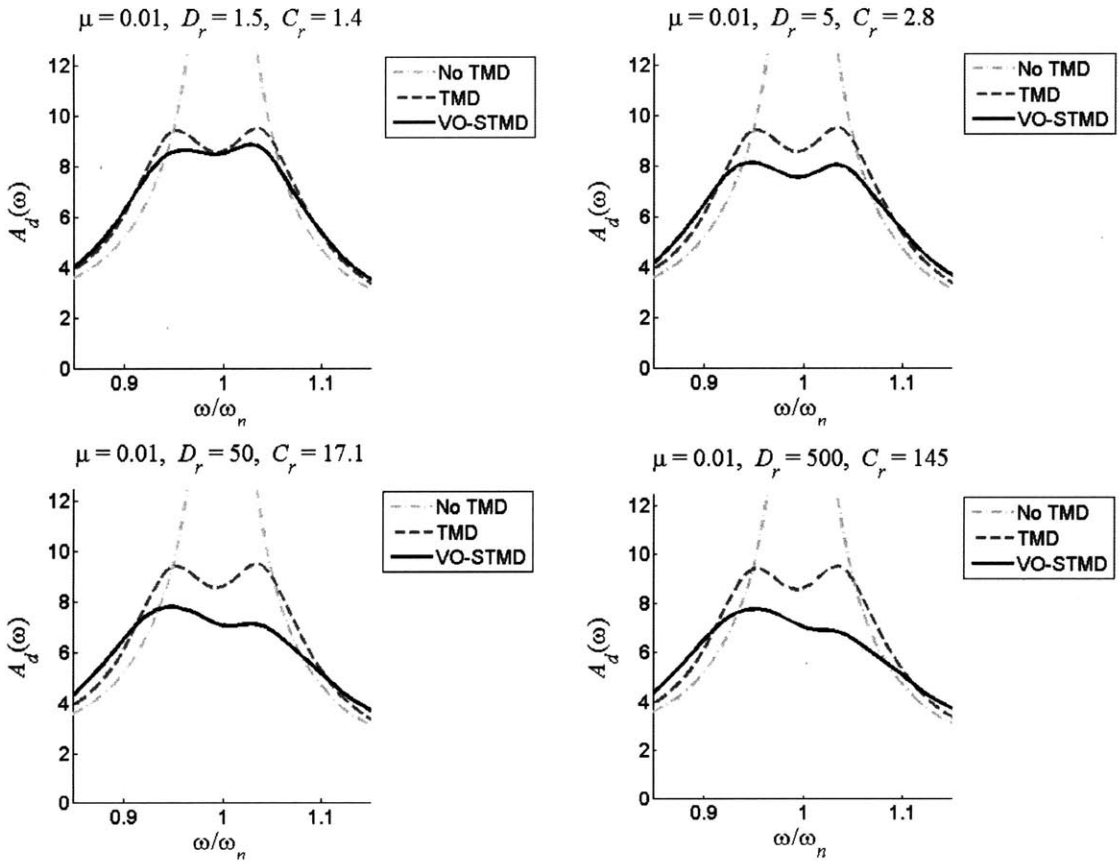

Figure 5-2: Variation based on dynamic range

5.1.2 Damping reduction factor implications

While the dynamic range is an unalterable limitation of the selected damping device, the damping reduction factor is fundamentally a design issue. That is, the determination of C_r may not significantly alter the range of accessible control forces, but it it can significantly affect how beneficial that range of forces is to the overall performance of the STMD. For example, if $C_r \leq 1$, any control forces will exceed those of the optimally-tuned passive TMD, thereby resulting in an over-damped system. Similarly, if C_r is specified too highly, the controlled system may fall short of producing optimal forces. Hence, there is some optimal value for C_r constrained by

$$1 \leq C_r \leq D_r \tag{5.3}$$

The optimal value must be found heuristically and indeed may vary widely based on the dynamic range of the damper, the selection of a control algorithm, and the performance goal of the overall system.

Figure 5-3 displays results for various values of C_r for an STMD with a dynamic range of $D_r = 10$. As can be seen, an improperly designed system can produce controlled results that are inferior to those of the passive system.

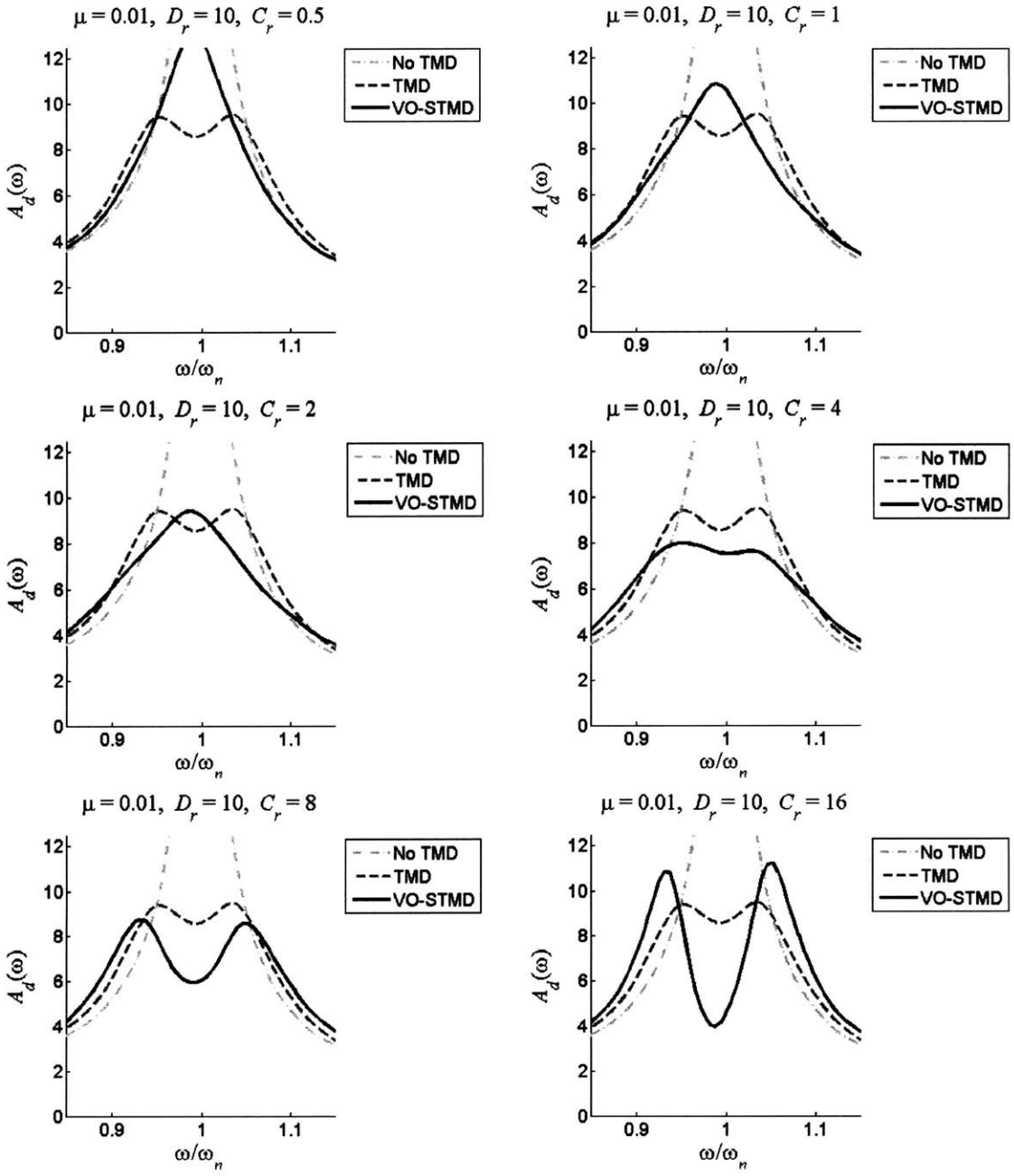

Figure 5-3: Variation based on damping reduction factor for $D_r = 10$

5.1.3 Evaluative measures

By varying both D_r and C_r, the effectiveness of variable-orifice STMD systems will be investigated and compared with equivalent passive systems. In order to accomplish this, performance indices will be established; results for equivalent passive systems will be produced; and comparisons of various system characteristics will be presented.

Performance indices

As described in section 4.4.3, the two primary design considerations for the structural control of high-rise buildings are displacements and accelerations. Hence, the performance indices used in this study focus on the ability of the STMD to limit these values, with two evaluations for each:

$$J_1 = \max \{A_d(\omega)\} \tag{5.4}$$

$$J_2 = \max \{A_a(\omega)\} \tag{5.5}$$

$$J_3 = \frac{1}{0.3\omega_n} \int_{0.85\omega_n}^{1.15\omega_n} A_d(\omega)\, d\omega \tag{5.6}$$

$$J_4 = \frac{1}{0.3\omega_n} \int_{0.85\omega_n}^{1.15\omega_n} A_a(\omega)\, d\omega \tag{5.7}$$

J_1 and J_2 are to be emphasized, as peak response values represent the primary concern for structures. J_3 and J_4 have been chosen to represent the overall effectiveness of STMD vibration mitigation in a region $\pm 15\%$ of the resonance frequency (ω_n), the bandwidth in which passive TMD systems are considered to be effective[1] [13]. Consequently, optimizing the STMD for J_3 and J_4 values corresponds to an H_2 optimization, in which the overall dissipation of energy is emphasized.

[1]For SDOF systems, dynamic effects are relatively small outside of this narrow band of frequencies, and the behaviors of the systems under consideration are almost identical. In the case of MDOF structures where secondary modes may be problematic, these performance indices are inadequate to fully categorize the improvements of controlled tuned mass dampers over their passive counterparts.

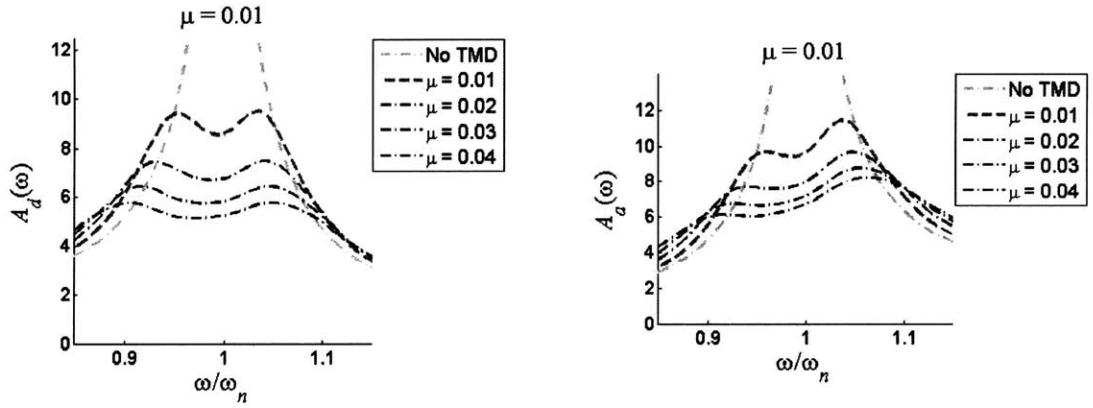

Figure 5-4: Variation based on dynamic range

Equivalent passive performance

With these evaluative criteria established, it is useful to generate benchmark performance indices for equivalent passive systems. Since the effectiveness of optimally-calibrated passive tuned mass dampers is a function of μ, passive results for $J_1 \ldots J_4$ may be plotted directly against the selected mass ratio. Figure 5-4 shows representative $A_d(\omega)$ and $A_a(\omega)$ results for varying mass ratios, and figure 5-5 organizes results in terms of the four performance indices. Because an ultimate design goal of STMD systems is to reduce the required mass, these results will be used to measure the comparative effectiveness of all STMD systems being considered in this study.

Effective damping

Another means of assessing control effectiveness is to compare results based on "effective damping," ξ_e, defined as the damping ratio necessary in an SDOF system to provide equivalent vibration mitigation. For an SDOF system, the maximum amplfication function values for displacement ($J_{1,f}$) and acceleration ($J_{2,f}$) are equivalent and are determined directly by the damping ratio:

$$J_{1,f} = J_{2,f} = \frac{1}{2\xi\sqrt{1-\xi^2}} \tag{5.8}$$

where the subscript f denotes the free, uncontrolled structure [25].

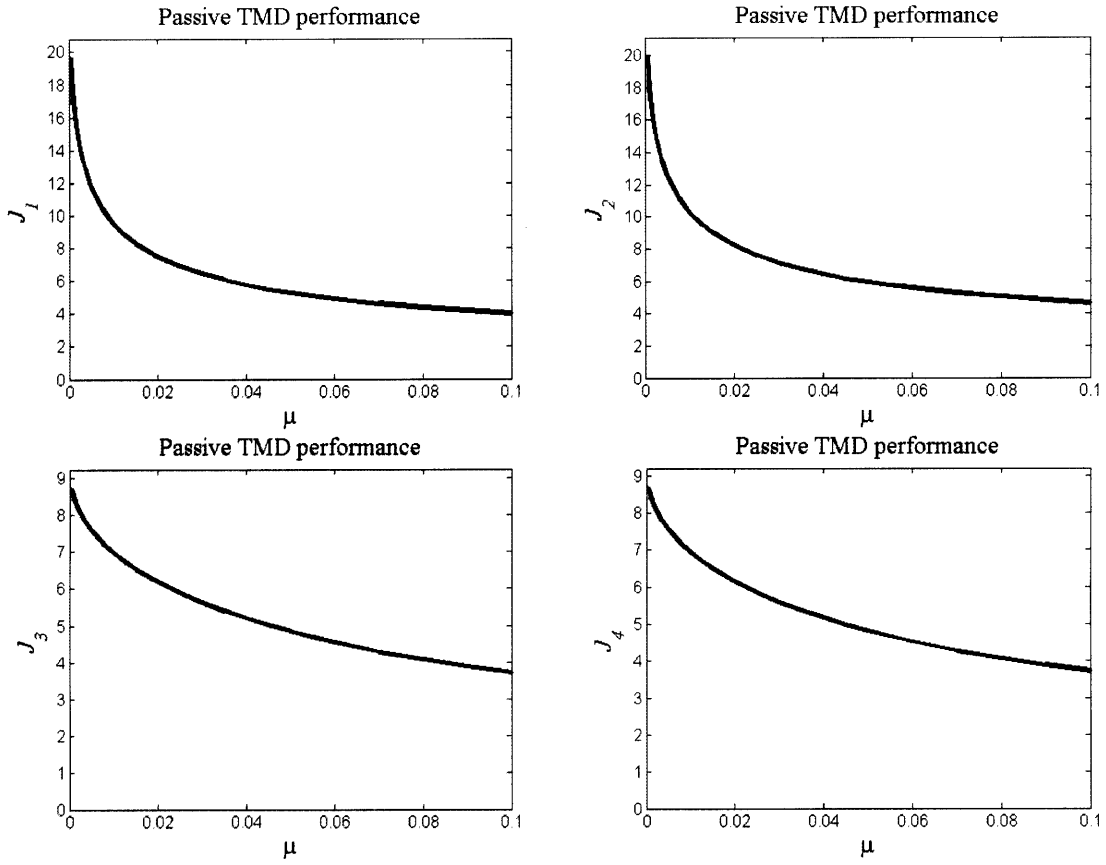

Figure 5-5: Performance indices for passive systems

Hence, once J_1 or J_2 have been found for a controlled system using the formulation given in section 5.1.3, equation 5.8 can be used to establish the effective damping of an equivalent SDOF system:

$$J_i = \frac{1}{2\xi_e\sqrt{1-\xi_e{}^2}} \tag{5.9}$$

for $i = 1$ or 2, depending on whether maximum displacement or maximum acceleration is the quantity of interest[2]. Solving for ξ_e and discarding negative or imaginary solutions leads to

$$\xi_e = \sqrt{\frac{1}{2} - \frac{\sqrt{J_i{}^2 - 1}}{2J_i}} \tag{5.10}$$

Relative STMD motion

A serious design consideration for tuned mass dampers in structures is the relative displacement between the mass and the building floor on which it rests. Large movement of the mass can complicate the design of spring, damper, and actuator connections and also raises concerns for the stroke limit of any semi-active damping device being considered. While this study focuses on the optimization of performance, attention will also be paid to relative displacements to provide comparison with equivalent passive tuned mass dampers.

Actual relative displacements depend heavily on the size of the building and the location of the tuned mass damper, so this parameter will be addressed in a relative manner to maintain generality. For assessment of STMD systems, results for the maximum relative displacements will be presented in terms of the maximum relative displacement observed in a passive system with the same mass ratio.

Maximum force output

Since variation in C_r will affect the maximum force attainable for a semi-active damper with a given dynamic range, data will also be presented on the maximum force output required by a given STMD system. This will provide insight into the size of semi-active damper necessary or, for smaller-scale devices, the number of semi-active

[2]Note that for controlled systems, $J_1 = J_2$ is no longer guaranteed.

dampers that must be placed in parallel. As in the case of relative displacements, results will be presented in comparison form, with the maximum damper force of an optimally-tuned passive TMD used for reference.

5.1.4 Broken system considerations

A significant factor to take into account for any active or semi-active system is its behavior during a malfunction of the control system. If designed correctly, one of the benefits of implementing a semi-active system is that it can still perform effectively as a passive device when this occurs. In the case of a VO-STMD, or any other STMD with a linearly-variable damping device, there is an accessible level of damping, c_d, that allows the STMD to perform like an optimized passive TMD. Hence, the ideal failure mode would involve the variable-orifice damper automatically adjusting to c_d as a default level of damping.

If, however, such a "safety mode" were also to fail, it is likely that the variable-orifice damper would output forces only at its minimal damping level, $c_{min} = \frac{c_d}{C_r}$. Since the optimal value for C_r can vary widely, as described in section 5.1.2, the resulting reduction in system damping may be very significant. These adverse conditions were investigated by comparing the performance indices, $J_1 \ldots J_4$, of passive TMD systems in which the damping has been adjusted to c_{min} for various C_r values. Figure 5-6 shows representative results for $A_d(\omega)$ using the mass ratio $\mu = 0.02$ and design C_r values of 1.2, 2, 4, and 8. Performance results for a variety of C_r values are summarized in figure 5-7.

As these figures demonstrate, an impaired control system with no safety mode will have very damaging effects on performance, in some cases resulting in worse control than a passive TMD with less than 10% of the mass. Hence, it is imperative that any STMD system be well-equipped to deal with power outages or control deficiencies by defaulting to the optimized level of damping.

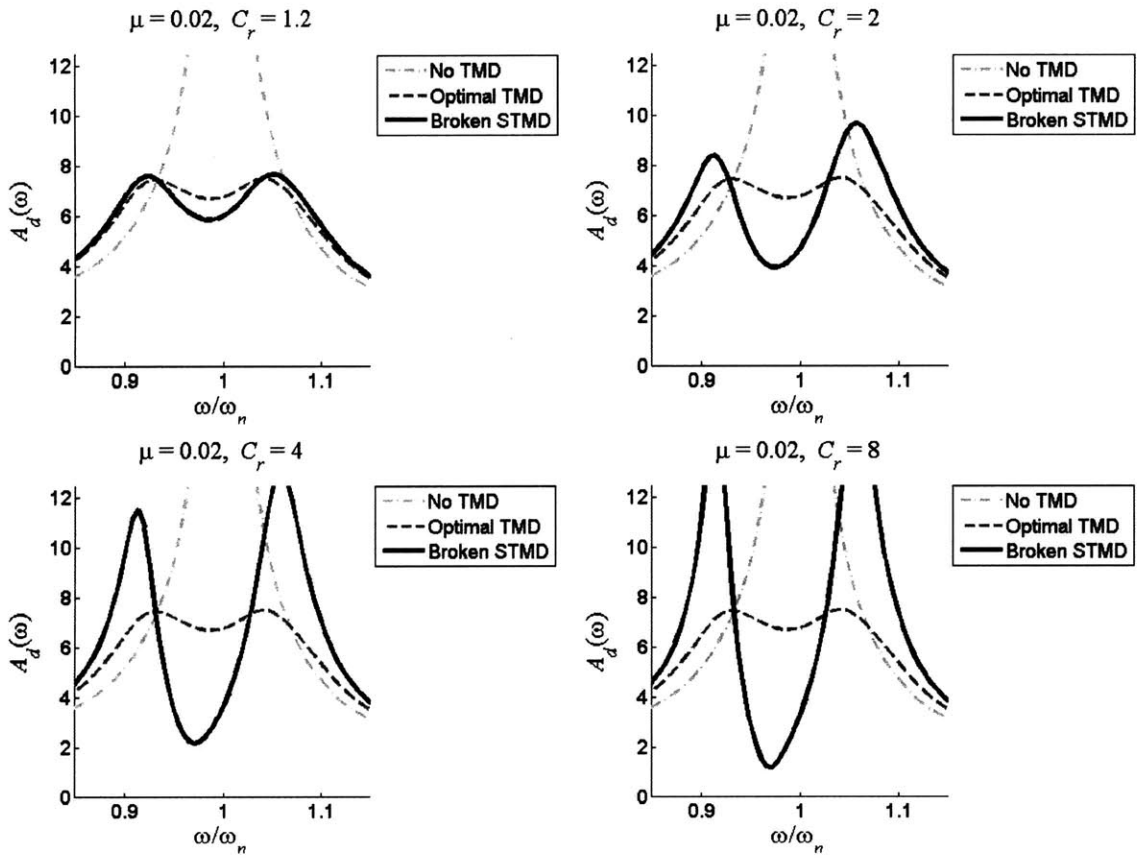

Figure 5-6: Dynamic amplification factors for malfunctioning systems

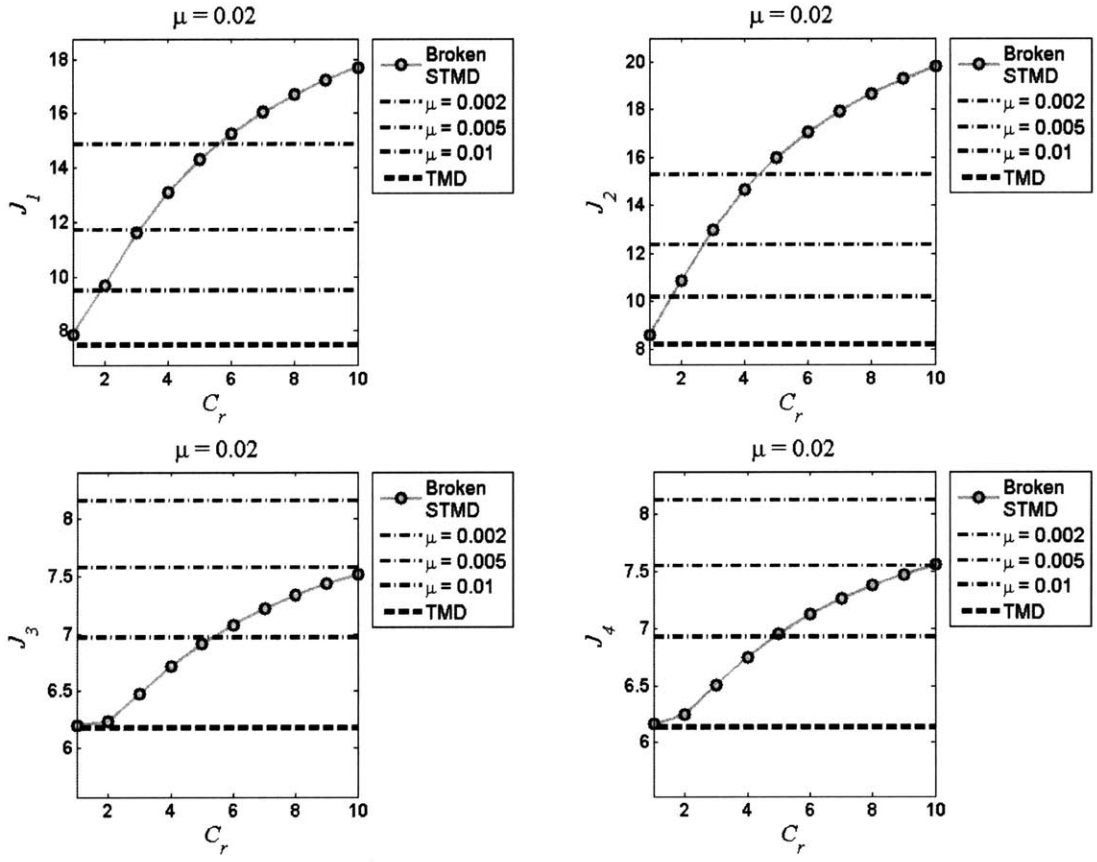

Figure 5-7: Performance indices for malfunctioning systems

5.2 Results for $\mu = 0.01$

Results for the preceding evaluative measures will first be presented for a mass ratio of $\mu = 0.01$. Though in practice the mass ratio may range from $\mu = 0.005$ to $\mu = 0.02$ [37], 1% of the modal mass of the fundamental mode is a typical value for sizing a TMD [13]. All results presented here were obtained with the heuristically determined weighting matrices

$$\mathbf{Q} = \begin{bmatrix} 1 & & & \\ & 0.1 & & \\ & & 70 & \\ & & & 0.1 \end{bmatrix}$$

$$\mathbf{R} = \begin{bmatrix} 10^{-12} \end{bmatrix}$$

5.2.1 C_r optimization

With the goal being to measure STMD effectiveness as a function of its dynamic range, it is first necessary to find the optimal value of C_r for each D_r being considered. Here, values of D_r being analyzed include

$$D_r = 2,\ 5,\ 10,\ 20,\ 50,\ \text{and}\ 100$$

For each of these six values of D_r, simulations were run with an array of values for C_r. By tracking the four performance indices for each run, it was then possible to obtain sets of C_r values that minimized $J_1 \ldots J_4$. The following four figures present these results for each of the performance indices and each of the D_r values under consideration. This makes apparent how the optimal C_r value may vary depending on which performance index is set as the design criteria. Additional lines have been added to demonstrate how STMD performance compares to passive systems with larger mass ratios.

By tracking the minimum values in each of the previous figures, four sets of op-

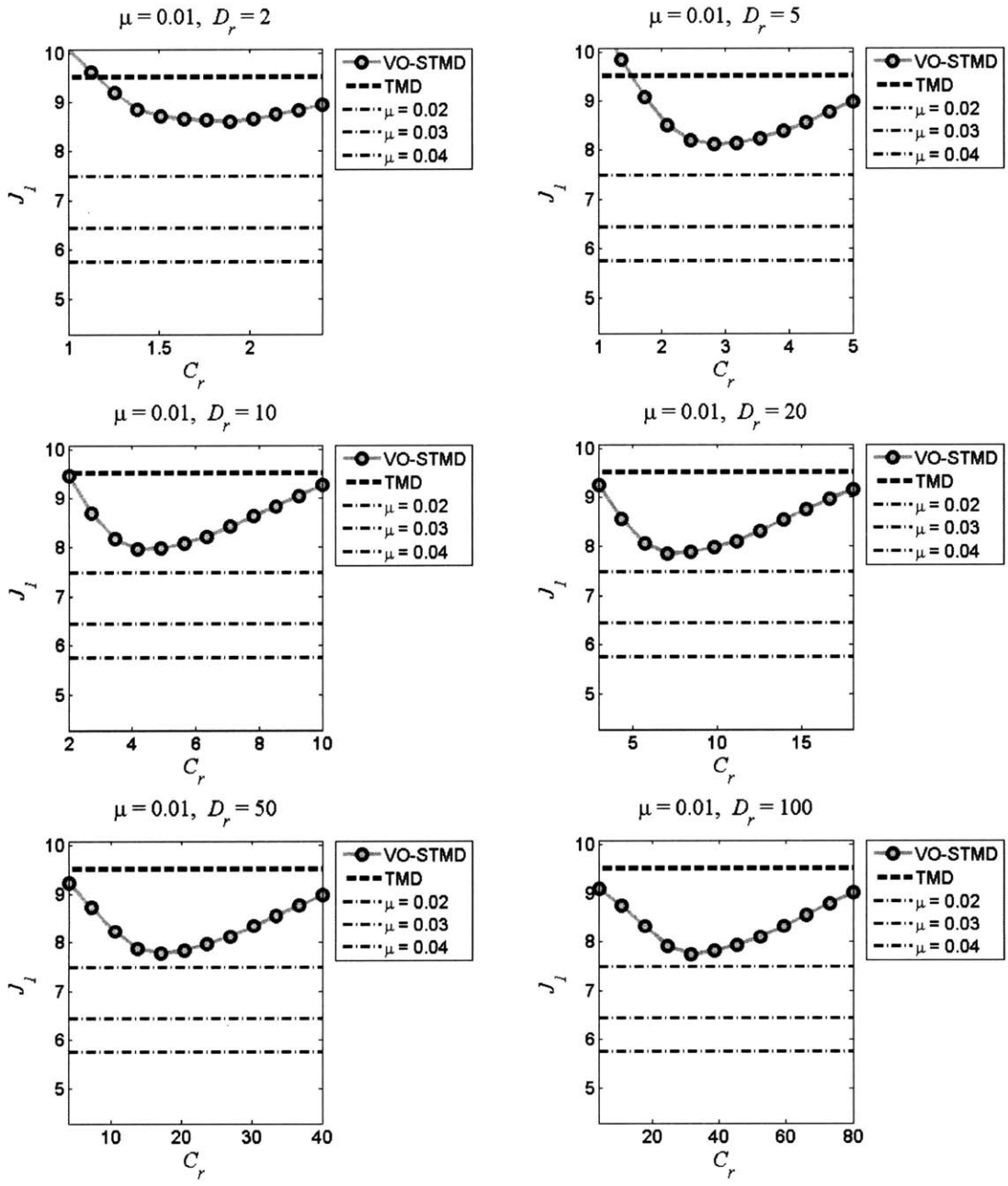

Figure 5-8: $\mu = 0.01$: Finding optimal C_r values for J_1

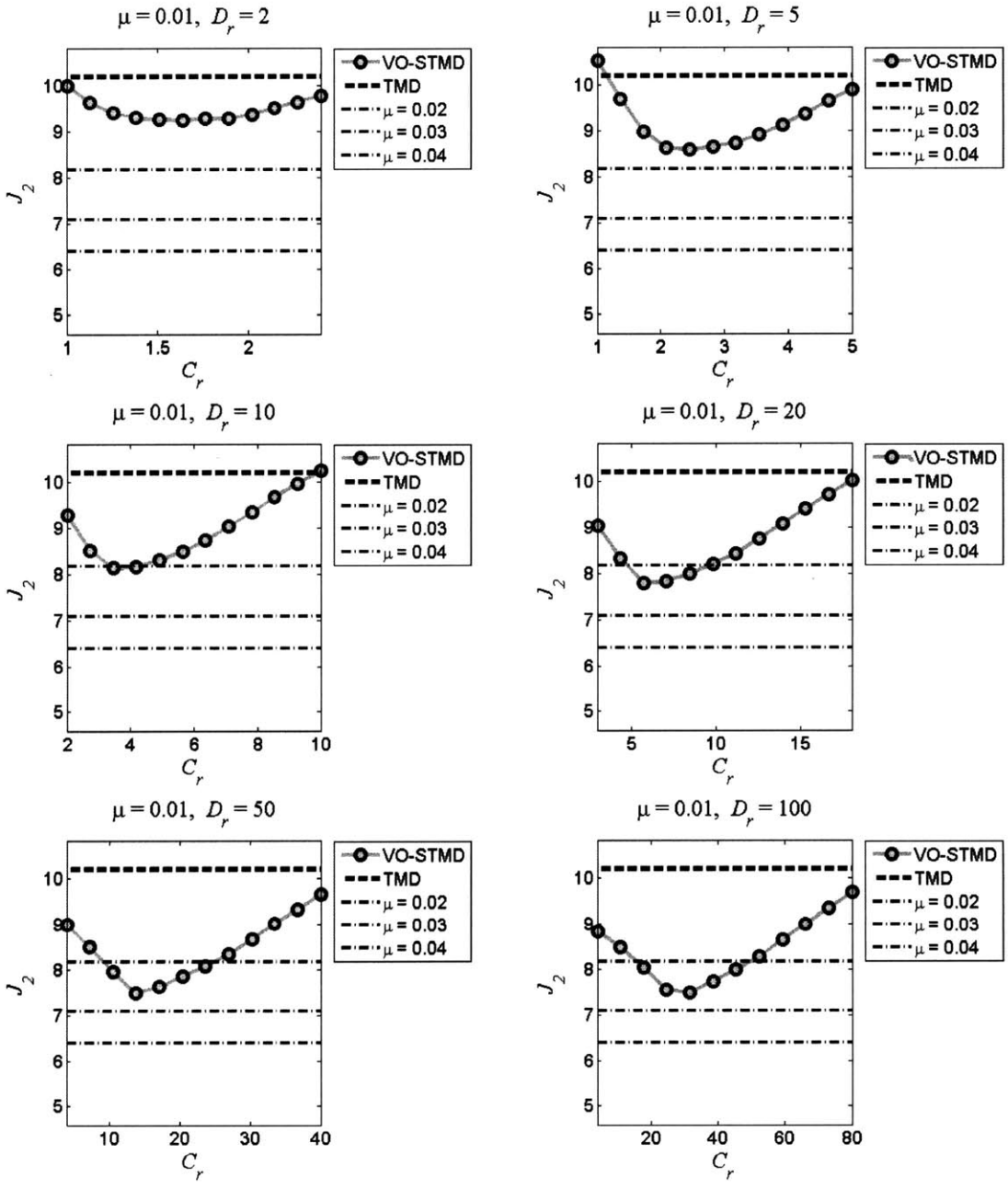

Figure 5-9: $\mu = 0.01$: Finding optimal C_r values for J_2

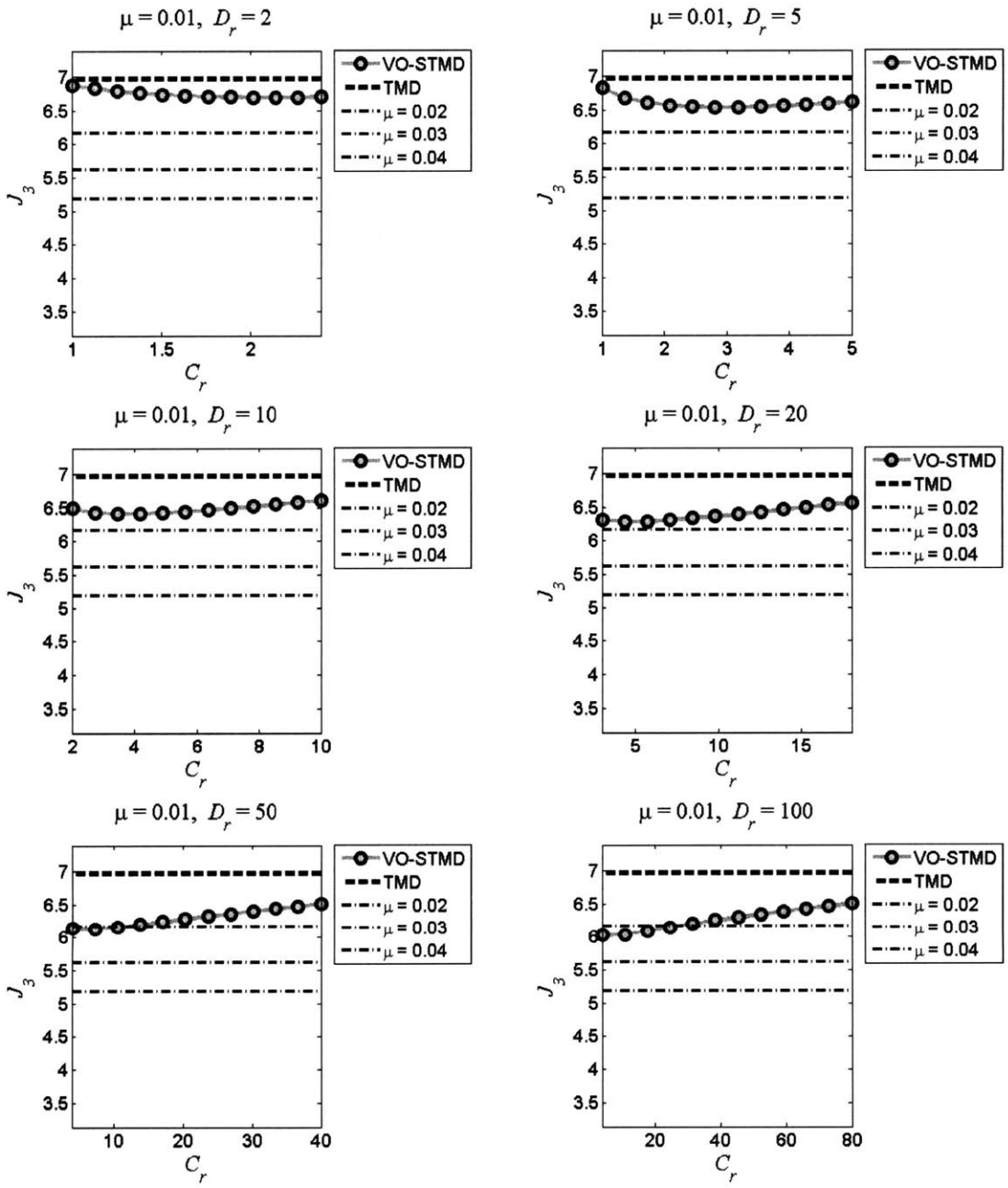

Figure 5-10: $\mu = 0.01$: Finding optimal C_r values for J_3

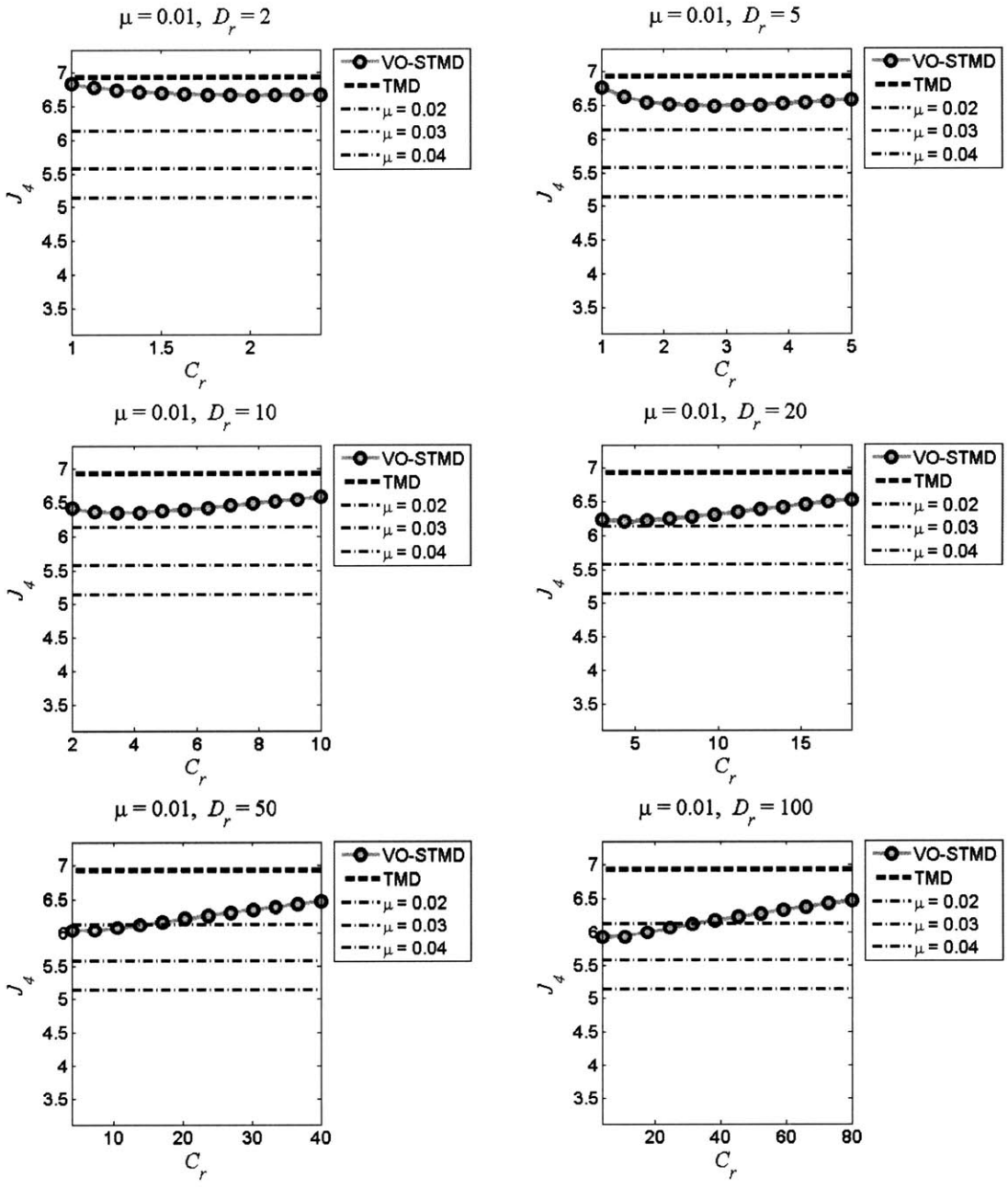

Figure 5-11: $\mu = 0.01$: Finding optimal C_r values for J_4

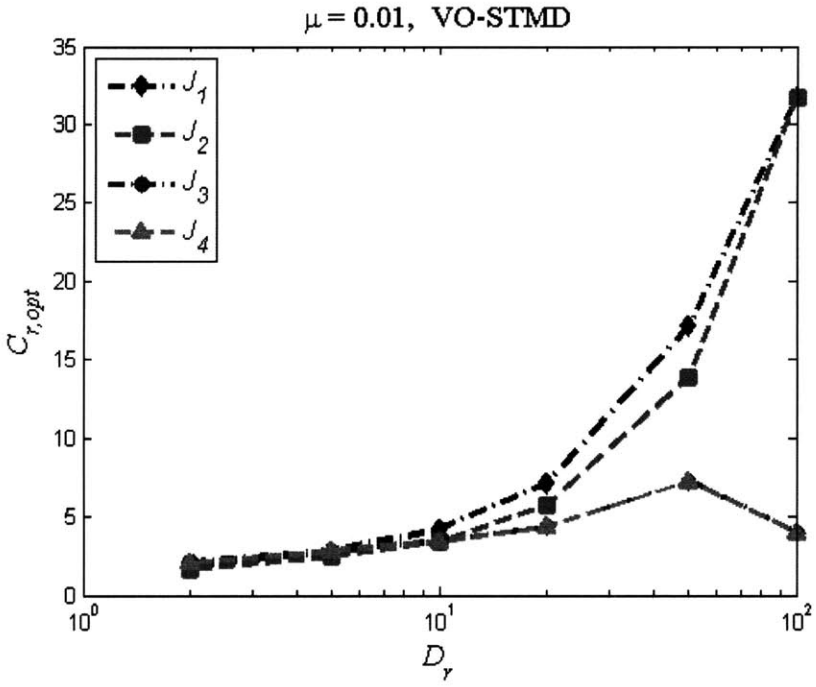

Figure 5-12: Summary of optimal C_r values for $\mu = 0.01$

timal values C_r can be obtained depending on which performance goal is selected. Hence, if the TMD system is to be optimized for any one of the criteria, $J_1 \ldots J_4$, the corresponding set of optimized C_r values should be used. The results are presented in figure 5-12

5.2.2 D_r variability

Based on the values of C_r presented in figure 5-12, the optimized performance of the variable-orifice STMD can be plotted as a function of the damper's dynamic range. The figures that follow highlight some of the results:

- Figure 5-13 shows optimized results for all four performance indices, assuming that each may be optimized independently.
- Figure 5-14 shows results for all four performance indices using only C_r values from the optimized J_1 results.
- Figure 5-15 presents $A_d(\omega)$ simulations for minimization of J_1.
- Figure 5-16 presents $A_a(\omega)$ simulations for minimization of J_1.

The C_r values that minimized J_1 were chosen even for figures 5-14 through 5-16 because the minimization of maximum displacements is generally the design goal of a passive TMD. Since, of course, there can be only one design value for C_r, this was the data selected for comparison of results.

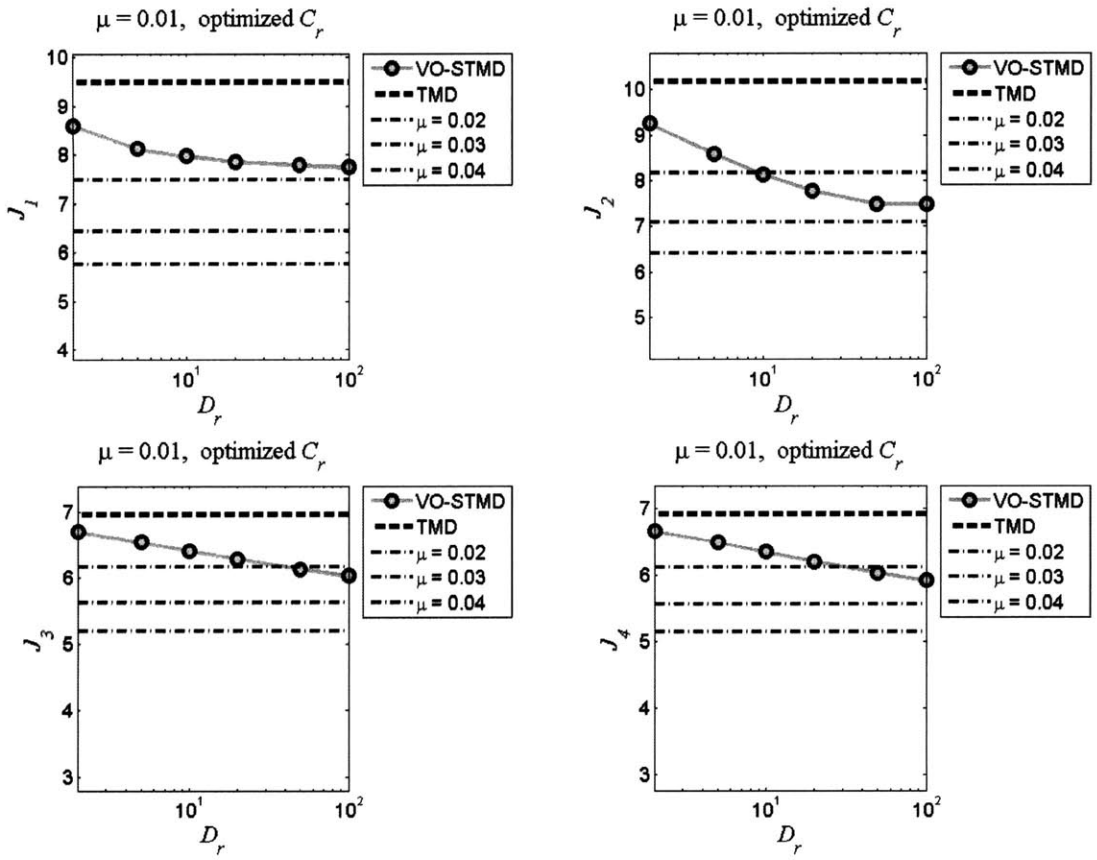

Figure 5-13: $\mu = 0.01$: Independently optimized results as a function of D_r

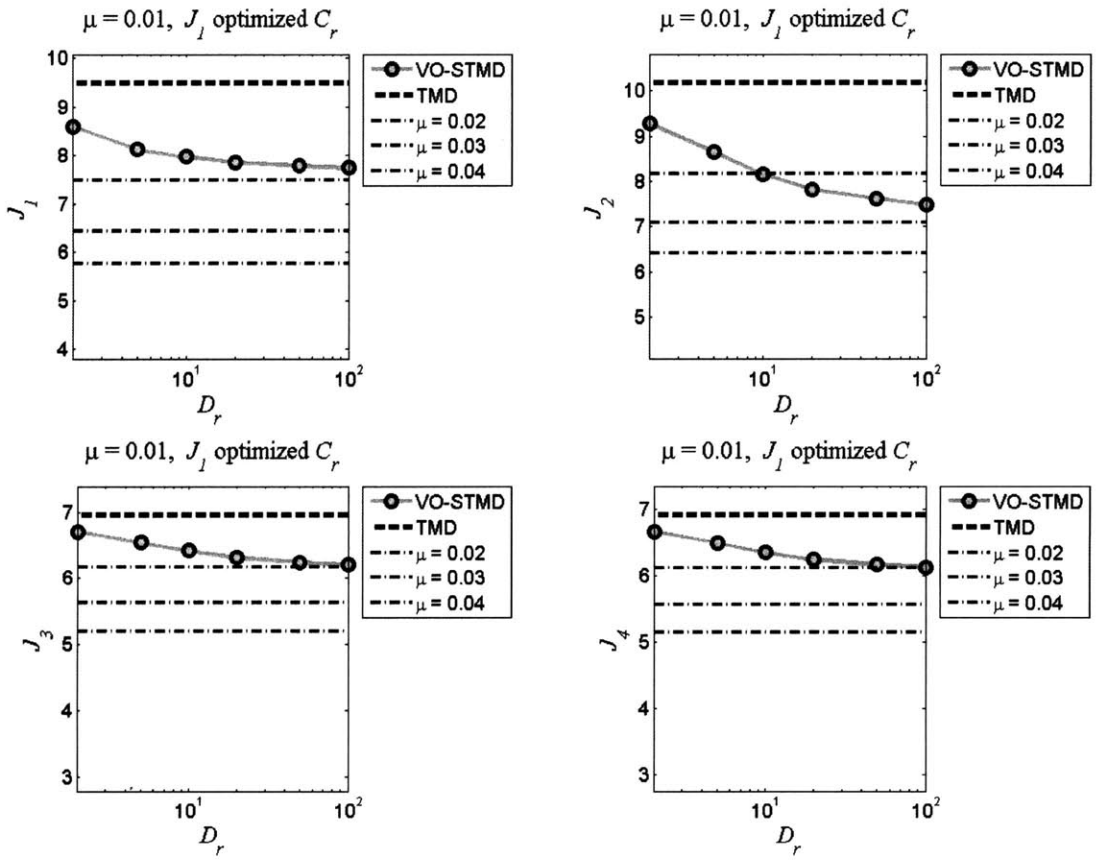

Figure 5-14: $\mu = 0.01$: J_1 optimized results as a function of D_r

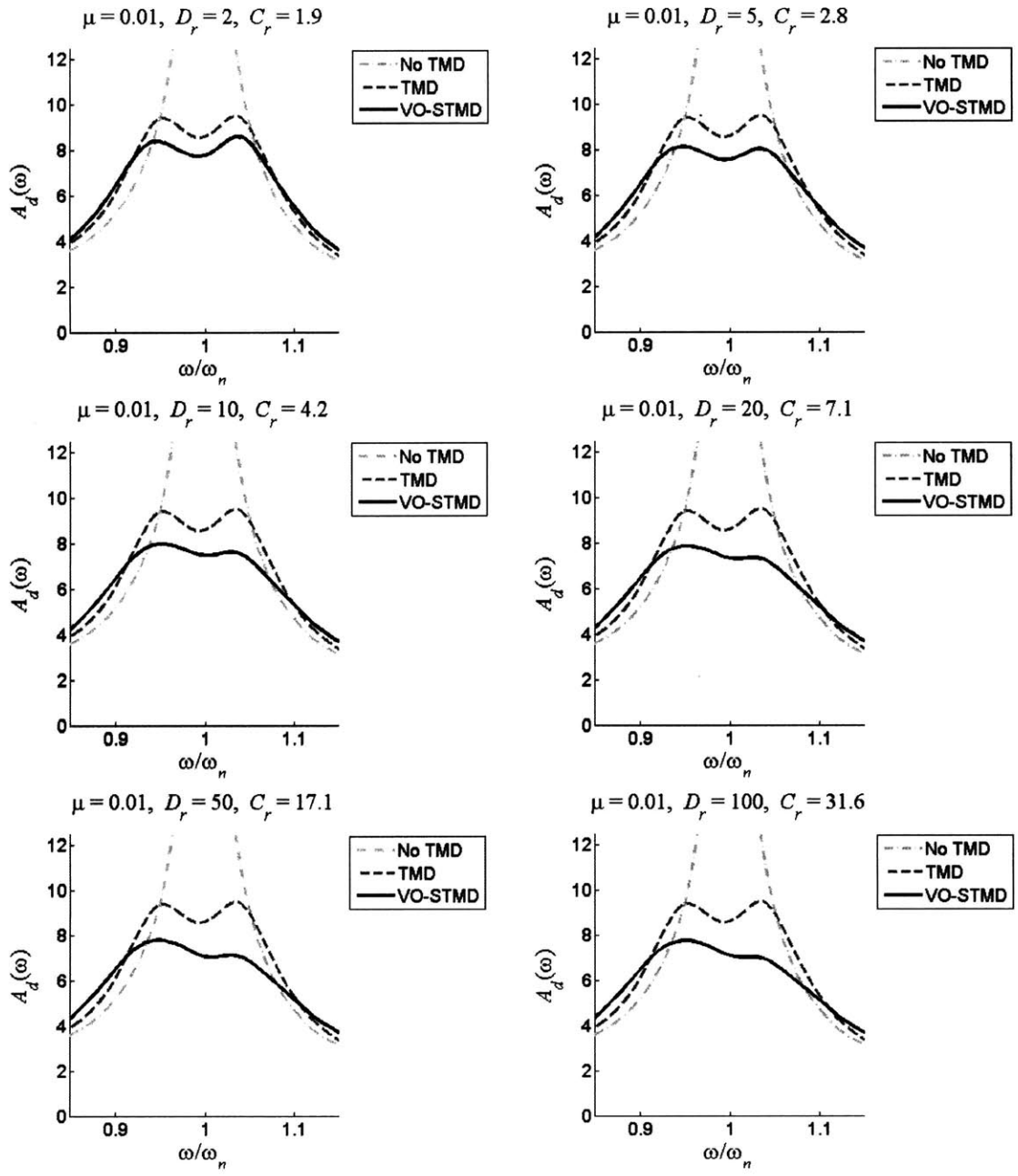

Figure 5-15: $\mu = 0.01 : A_d(\omega)$ simulations for minimized J_1

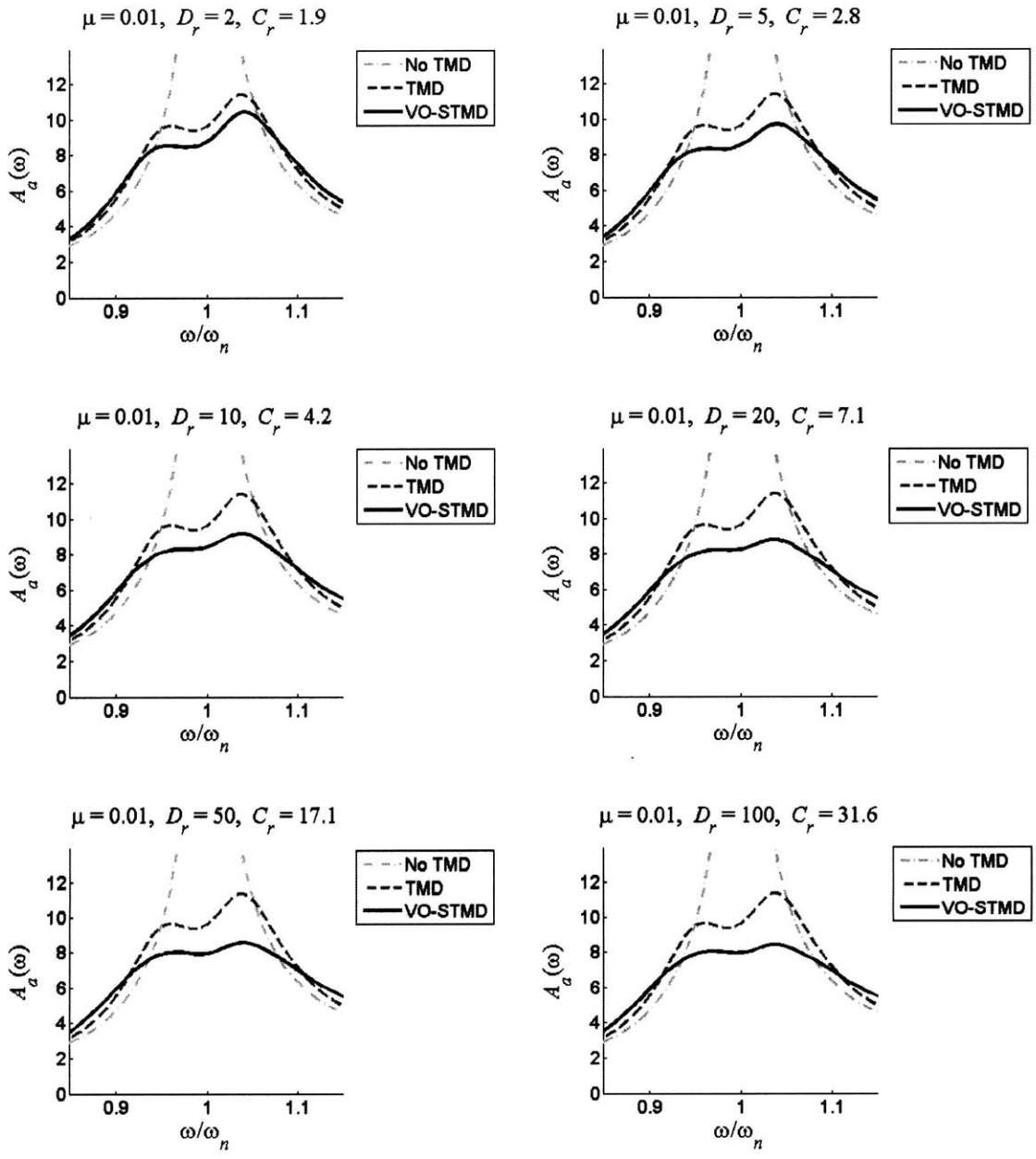

Figure 5-16: $\mu = 0.01 : A_a(\omega)$ simulations for minimized J_1

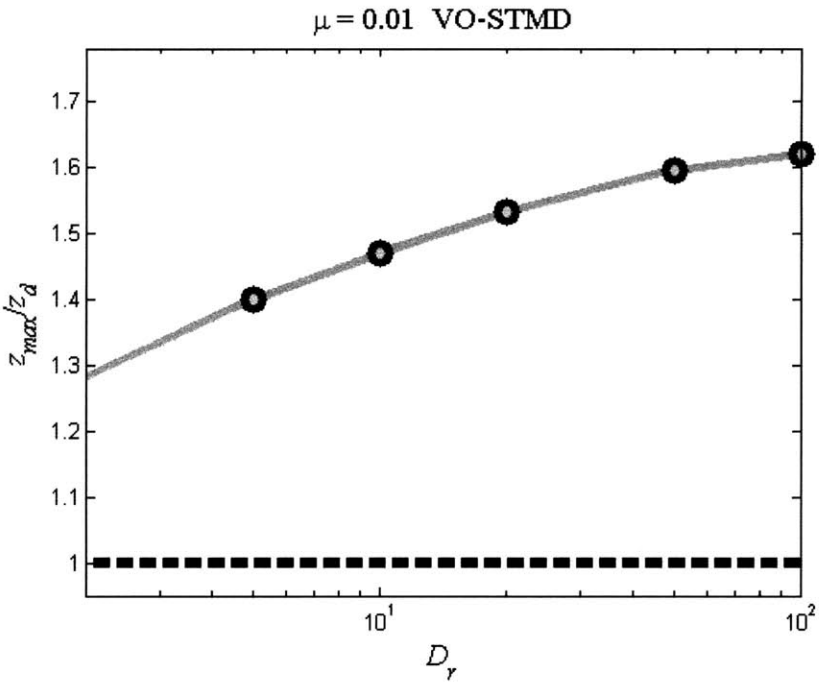

Figure 5-17: $\mu = 0.01$: Relative STMD displacement

5.2.3 Other performance measures

As described in section 5.1.3, each simulation also tracked the maximum relative displacement of the TMD and the maximum force output of the semi-active damper. Representative results for minimized J_1 simulations are given in figures 5-17 and 5-18. While relative displacement, z, levels off with increasing D_r, there is continued growth in F_{max}.

5.3 Results for $\mu = 0.03$

The second set of results presented for the variable-orifice STMD will be for a mass ratio of $\mu = 0.03$. While this is in general a very large mass for a TMD in structures, it is here presented for two reasons. First, there is a trend that the importance of D_r in determining the effectiveness of an STMD increases noticeably as the prescribed mass ratio gets larger; consequently, the results for $\mu = 0.03$ make this readily apparent.

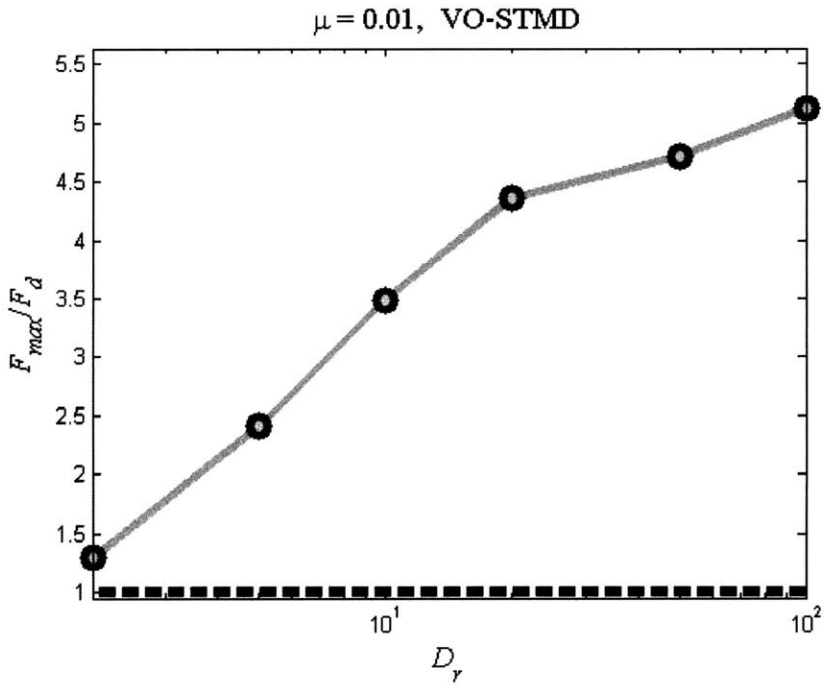

Figure 5-18: $\mu = 0.01$: Maximum damper force

Second, in the only current publication addressing the frequency-range response of STMD systems, $\mu = 0.03$ is the mass ratio considered [46]. This work claims STMD effectiveness equivalent to a passive system with a quadrupled mass ratio but does not justify the use of a dynamic range exceeding $3,000$; hence, it provides a useful benchmark for demonstrating the benefits of a study that explicitly addresses this issue.

The weighting matrices used for $\mu = 0.03$ are

$$\mathbf{Q} = \begin{bmatrix} 1 & & & \\ & 0.1 & & \\ & & 20 & \\ & & & 0.1 \end{bmatrix}$$

$$\mathbf{R} = \begin{bmatrix} 10^{-12} \end{bmatrix}$$

5.3.1 C_r optimization

As before, the values of D_r being analyzed include

$$D_r = 2,\ 5,\ 10,\ 20,\ 50,\ \text{and}\ 100$$

The two figures that follow present the J_1 and J_2 results for the arrays of C_r values considered. From this point forward, results for J_3 and J_4 will no longer be plotted against C_r due to their lesser importance. However, their optimized results will still be summarized by including plots for J_3 and J_4 as functions of D_r. Figure 5-21 again summarizes the optimal C_r values for each performance index.

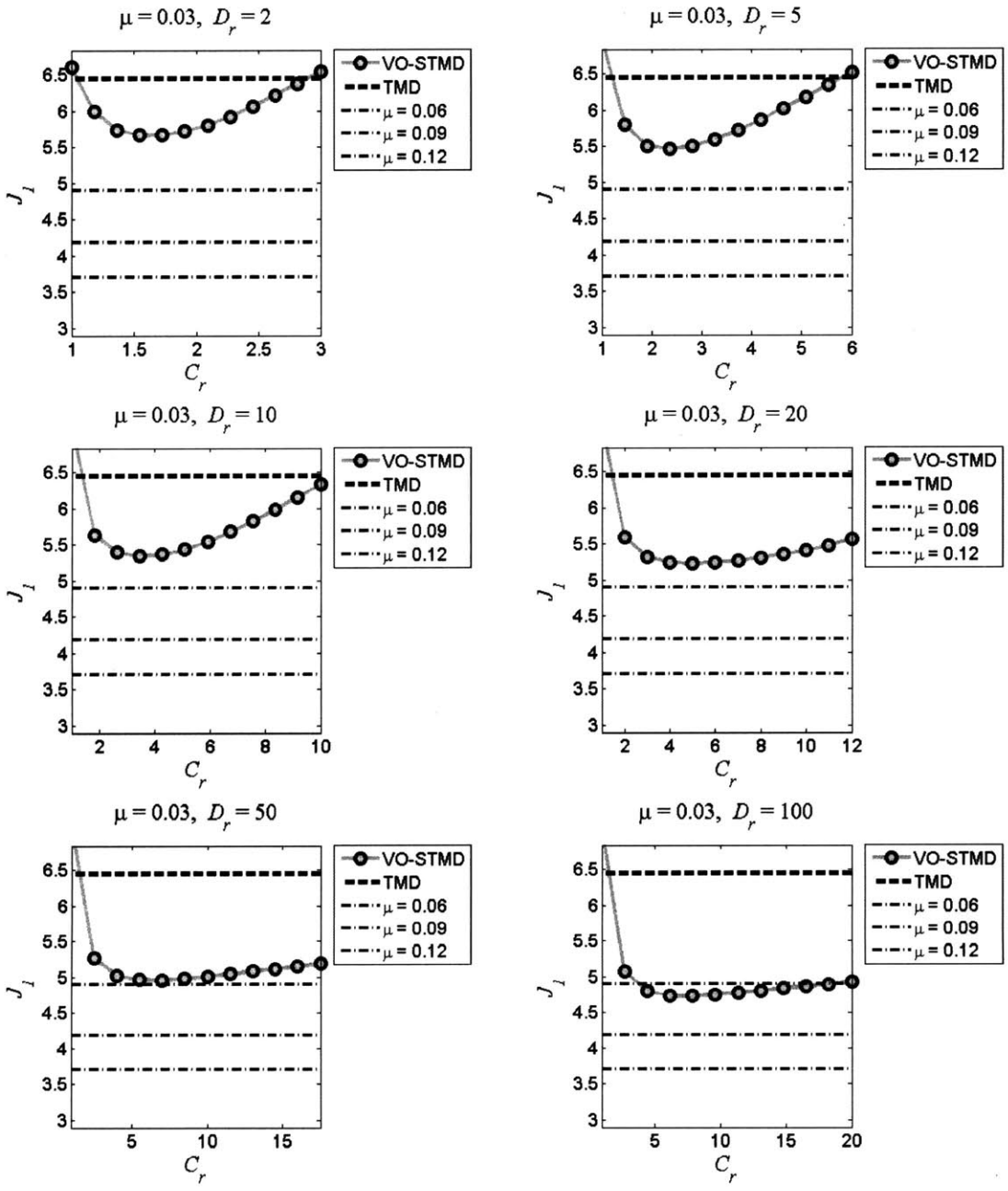

Figure 5-19: $\mu = 0.03$: Finding optimal C_r values for J_1

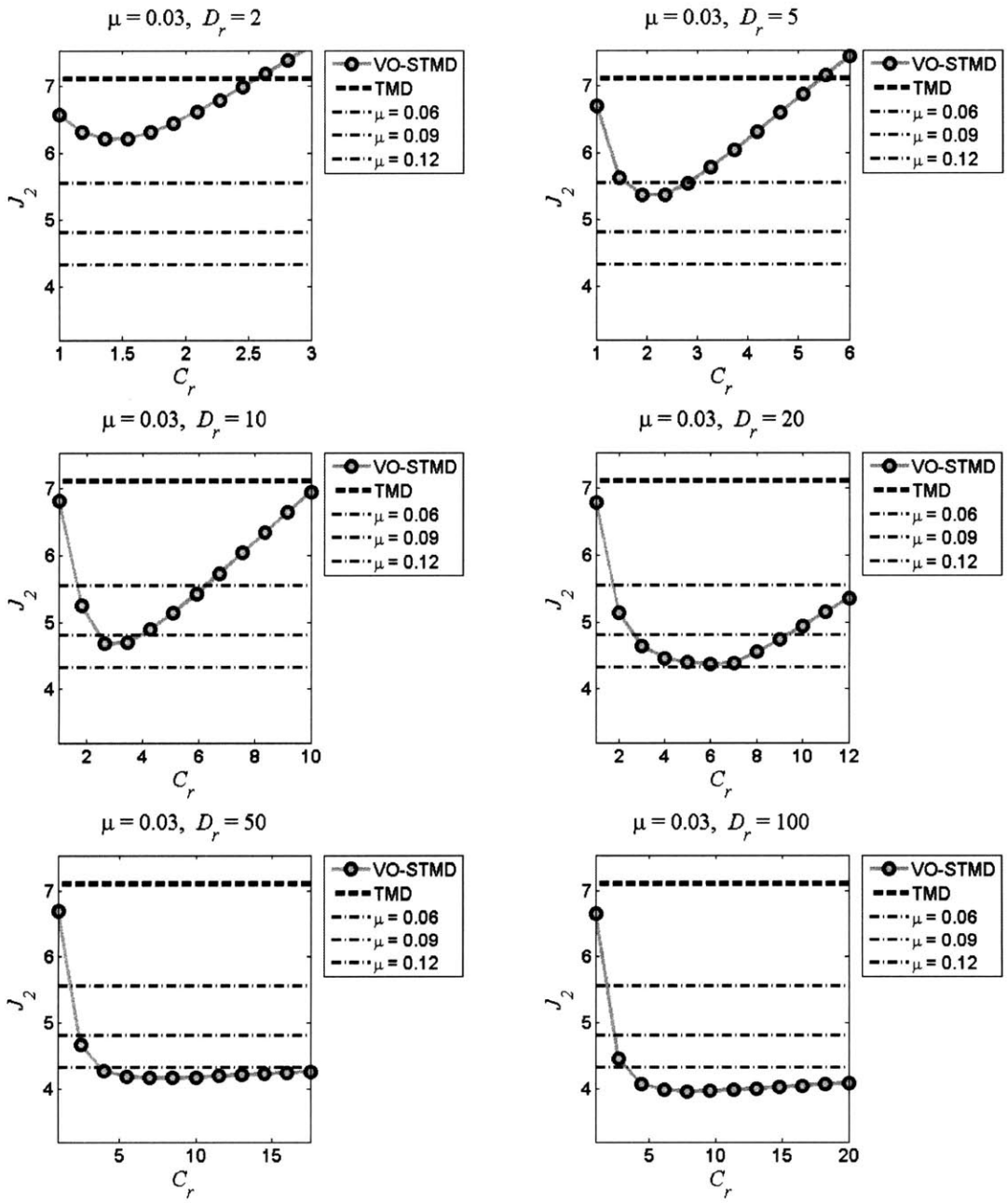

Figure 5-20: $\mu = 0.03$: Finding optimal C_r values for J_2

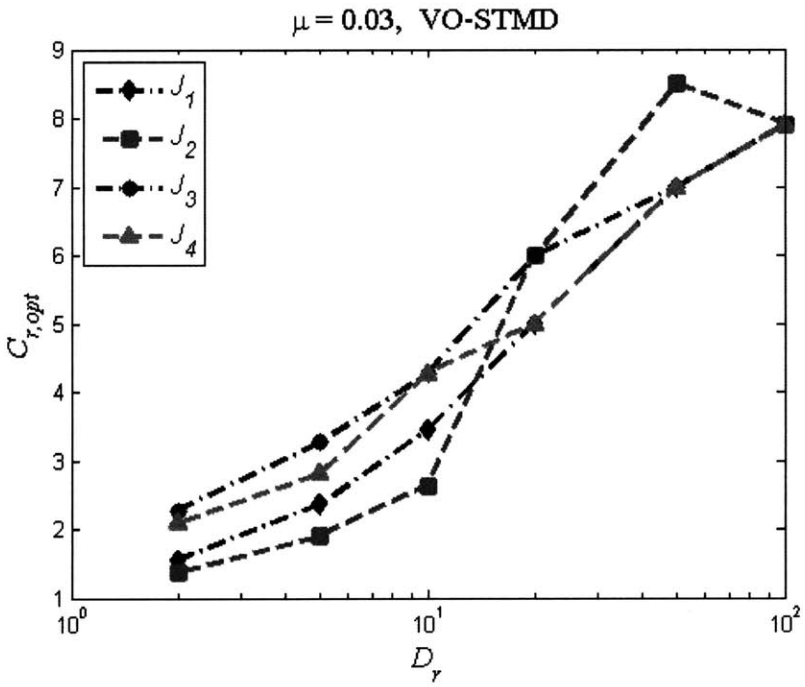

Figure 5-21: Summary of optimal C_r values for $\mu = 0.03$

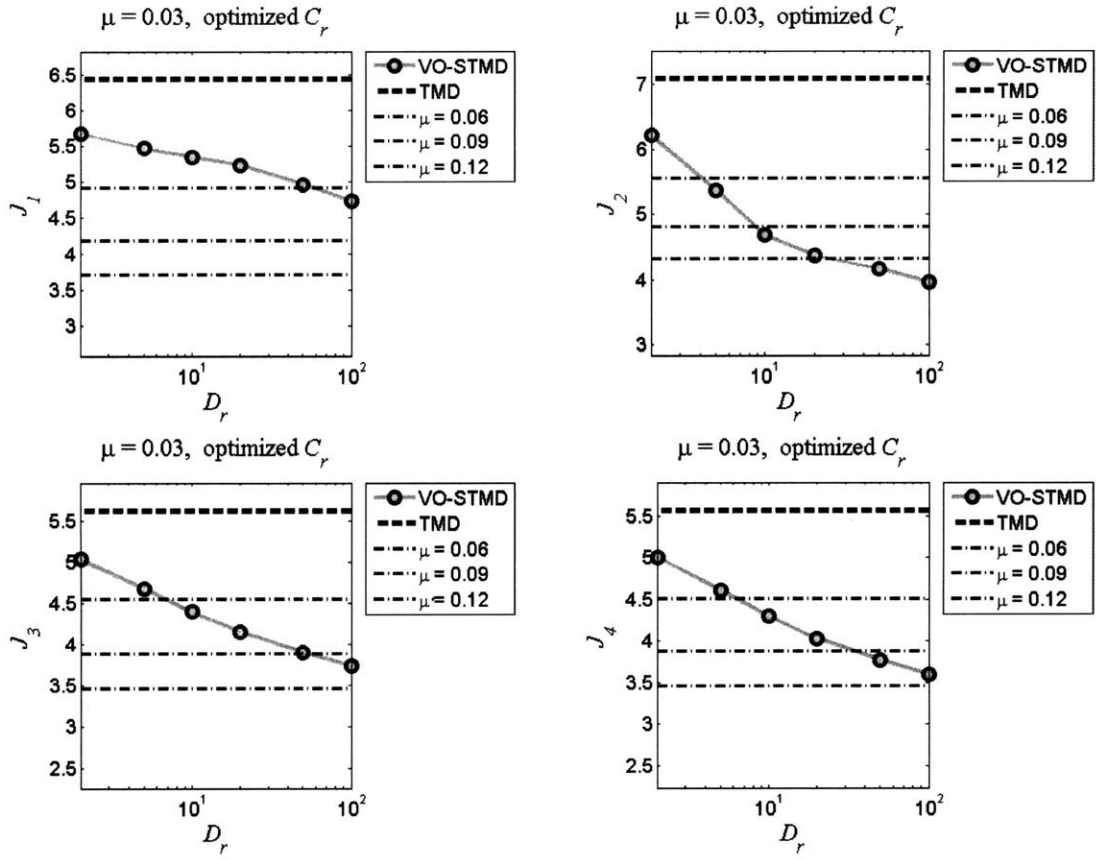

Figure 5-22: $\mu = 0.03$: Independently optimized results as a function of D_r

5.3.2 D_r variability

Based on the values of C_r presented in Figure 5-21, the optimized performance of the variable-orifice STMD can be plotted as a function of the damper's dynamic range. As in the previous section, the following results will be highlighted:

- Figure 5-22 shows optimized results for all four performance indices, assuming that each may be optimized independently.
- Figure 5-23 shows results for all four performance indices using only C_r values from the optimized J_1 results.
- Figure 5-24 presents $A_d(\omega)$ for minimization of J_1.
- Figure 5-25 presents $A_a(\omega)$ for minimization of J_1.

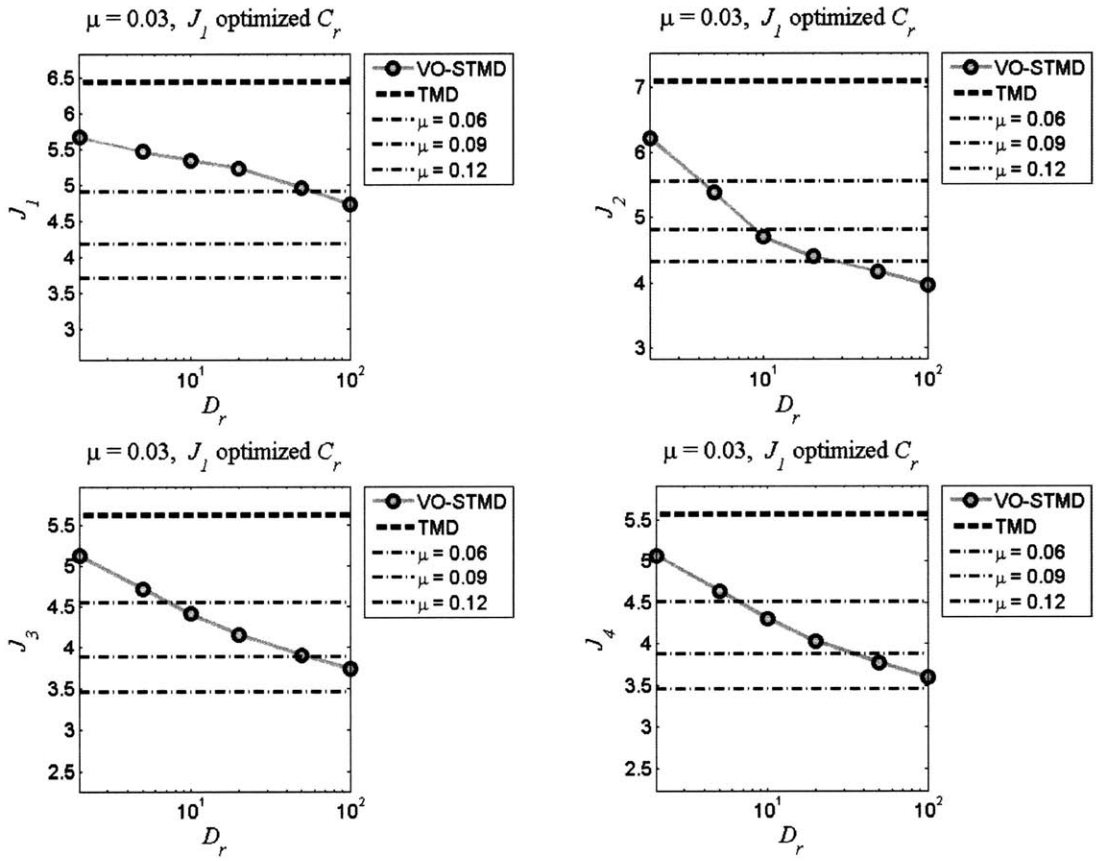

Figure 5-23: $\mu = 0.03$: J_1 optimized results as a function of D_r

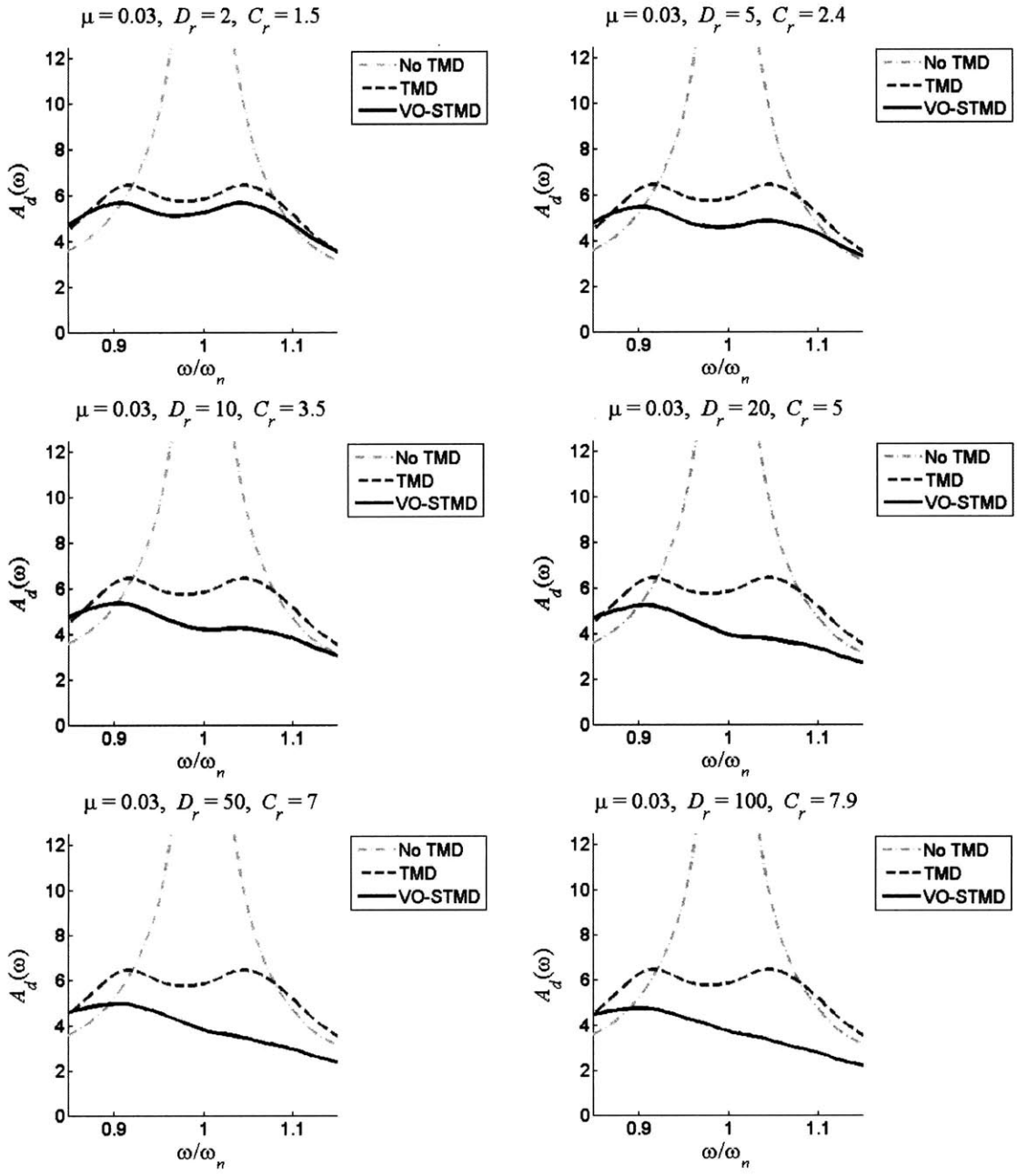

Figure 5-24: $\mu = 0.03 : A_d(\omega)$ simulations for minimized J_1

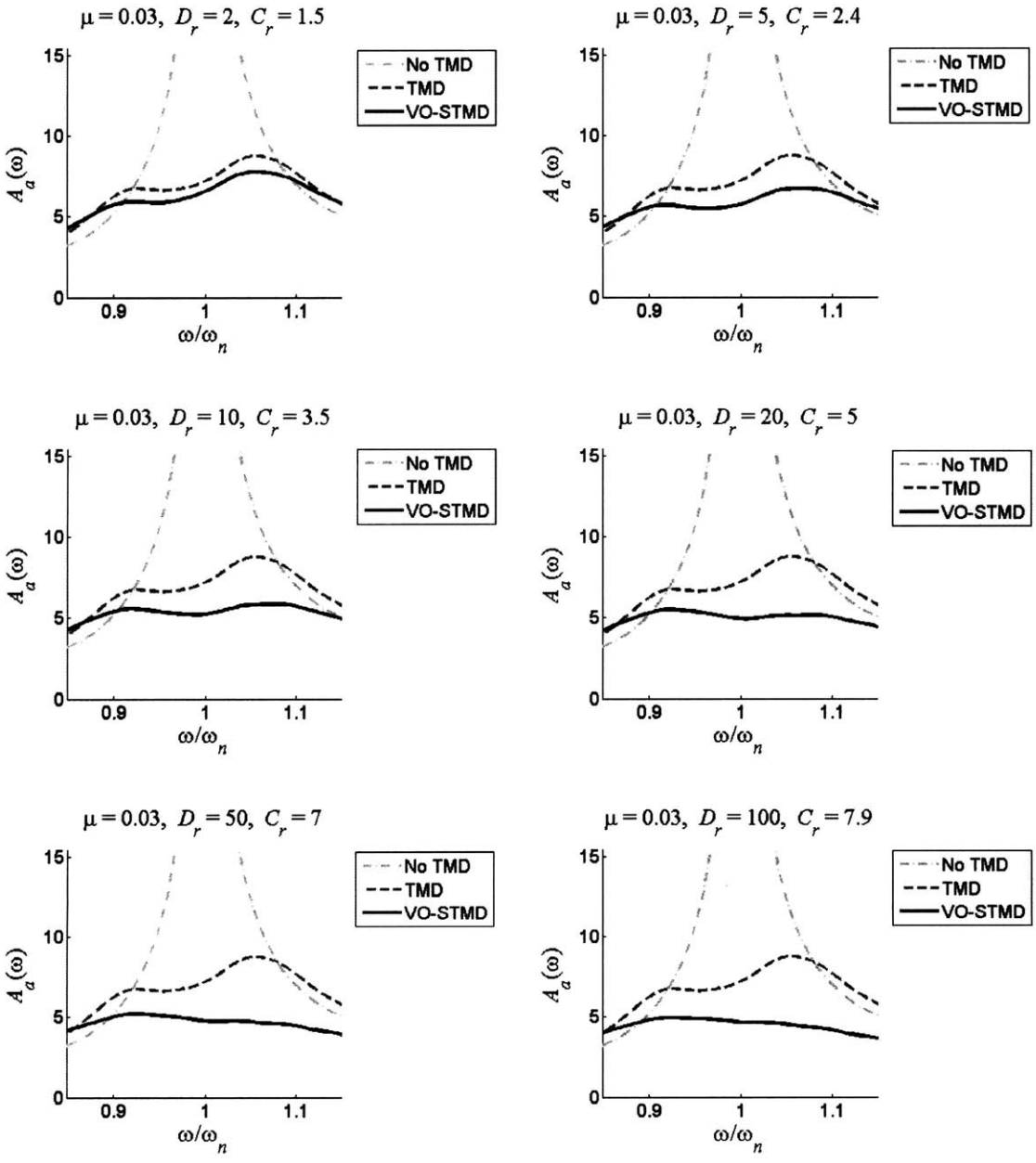

Figure 5-25: $\mu = 0.03 : A_a(\omega)$ simulations for minimized J_1

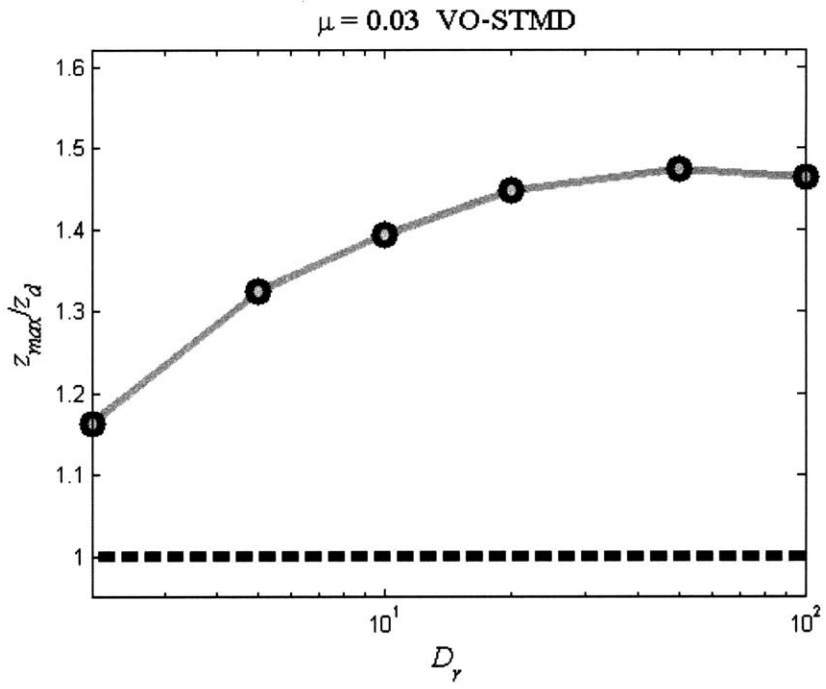

Figure 5-26: $\mu = 0.03$: Relative STMD displacement

5.3.3 Other performance measures

Relative motion and maximum force results for simulations that minimized J_1 are given in figures 5-26 and 5-27. As can be seen, relative displacements are essentially equivalent for $\mu = 0.01$ and $\mu = 0.03$ when comapared with their passive counterparts. However, the maximum damper force output, which is already larger for higher mass ratios, has increased significantly for $\mu = 0.03$. This is due largely to the fact that lower C_r values are now optimal, implying that c_{max} – and therefore f_{max} – will increase accordingly.

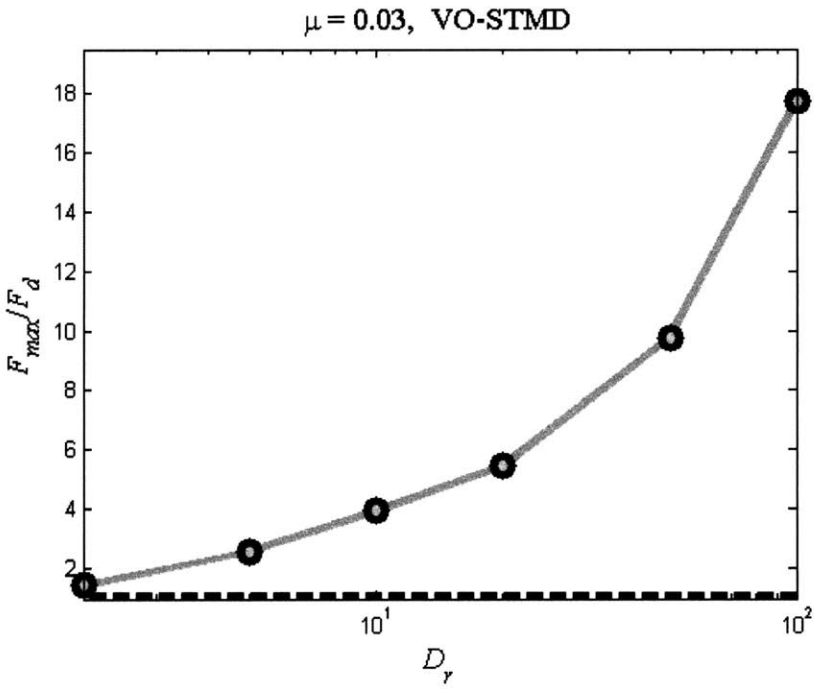

Figure 5-27: $\mu = 0.03$: Maximum damper force

5.4 Other mass ratios

In an effort to more fully categorize the relationship between mass ratio and STMD effectiveness, the analysis presented for $\mu = 0.01$ and $\mu = 0.03$ was also performed for realistic mass ratios of 0.005, 0.0075, 0.015, 0.02, and 0.025. This section compares optimized results of these analyses by presenting only the most relevant outputs:

- Figure 5-28 shows optimized J_1 results.
- Figure 5-29 shows J_2 results using C_r values obtained in the J_1 optimization.
- Figure 5-30 presents representative $A_d(\omega)$ results for $D_r = 10$ and C_r obtained through J_1 optimization.
- Figure 5-31 presents representative $A_a(\omega)$ results for $D_r = 10$ and C_r obtained through J_1 optimization.

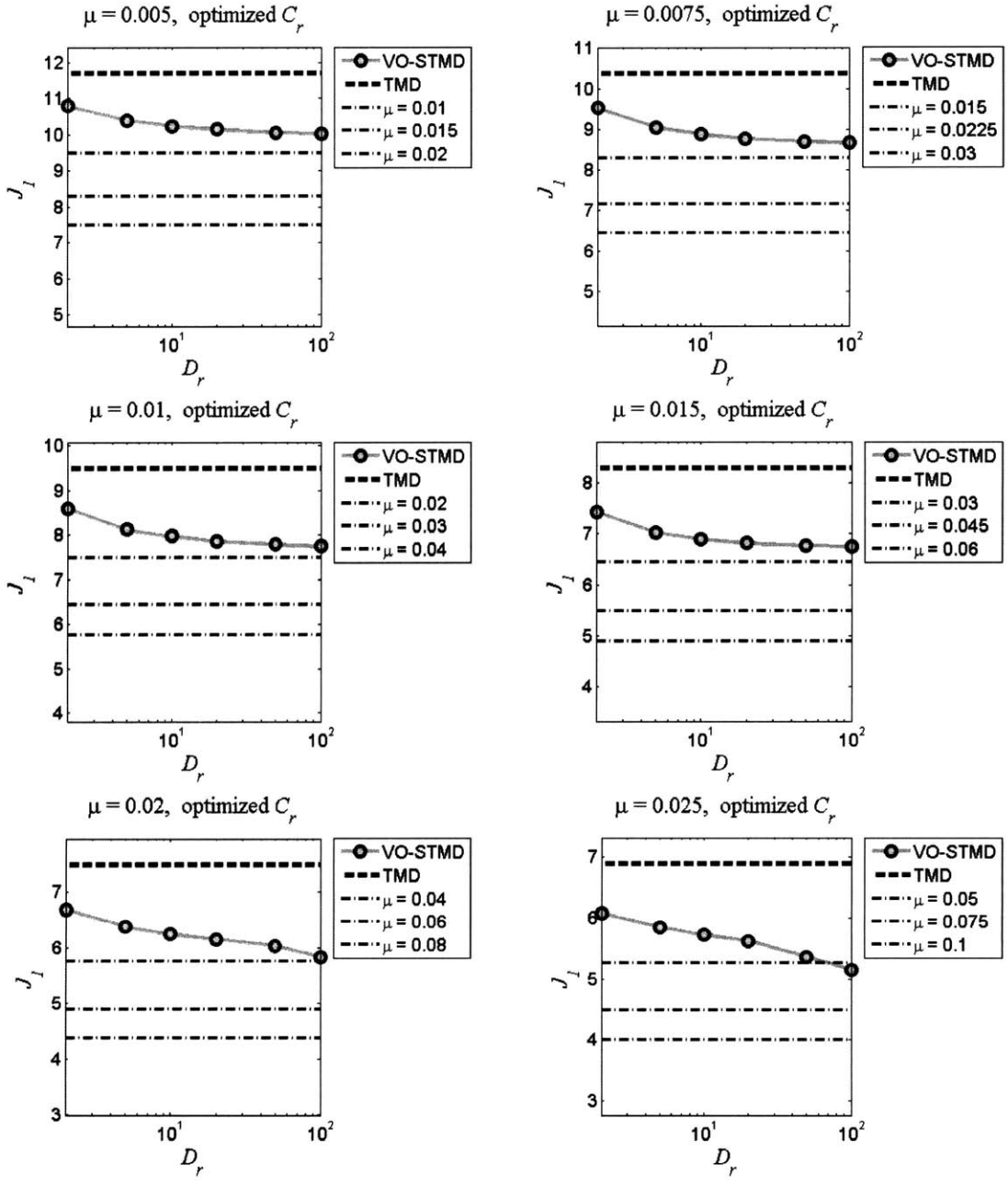

Figure 5-28: Optimized J_1 results for various mass ratios

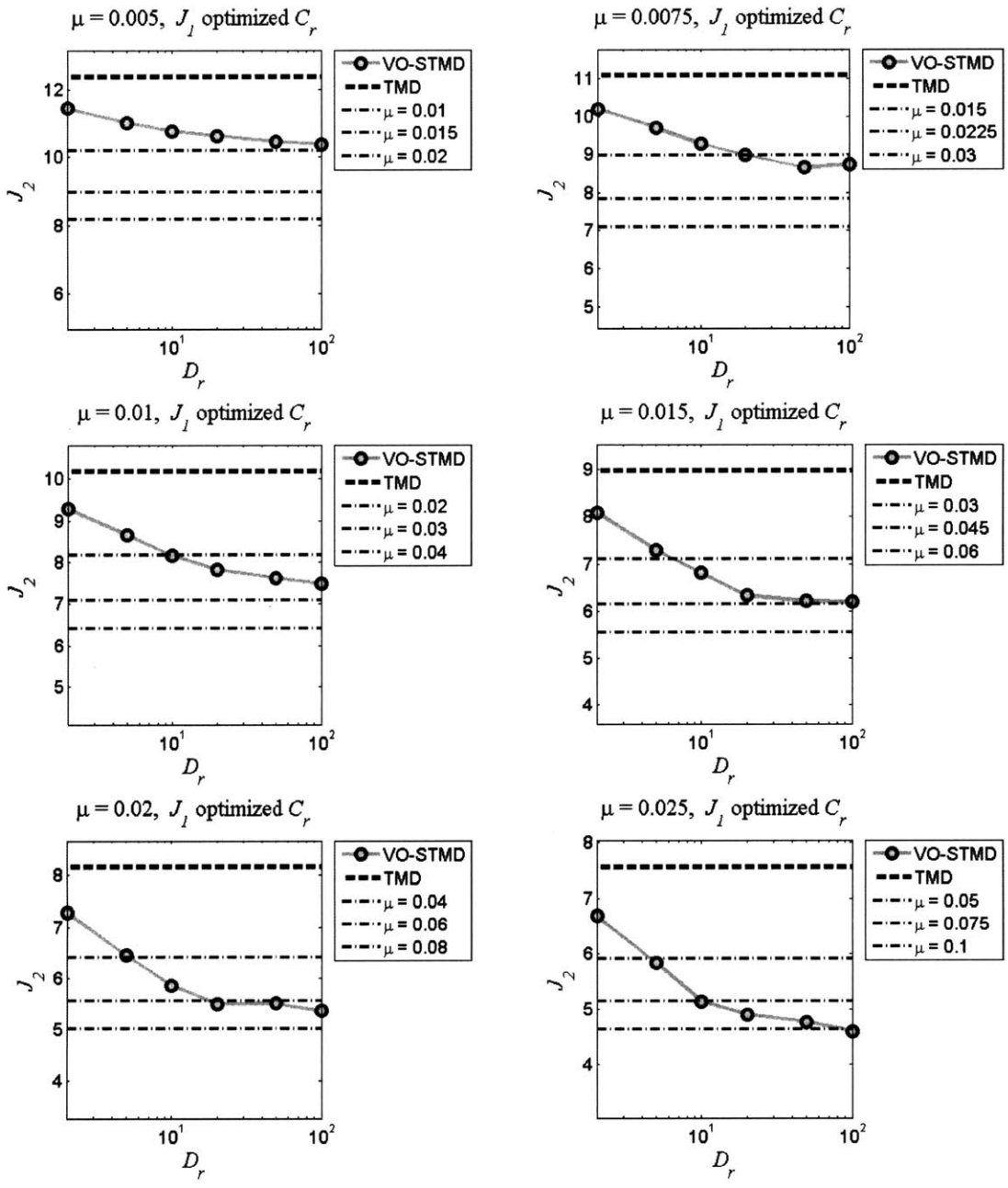

Figure 5-29: J_2 results for optimized J_1 for various mass ratios

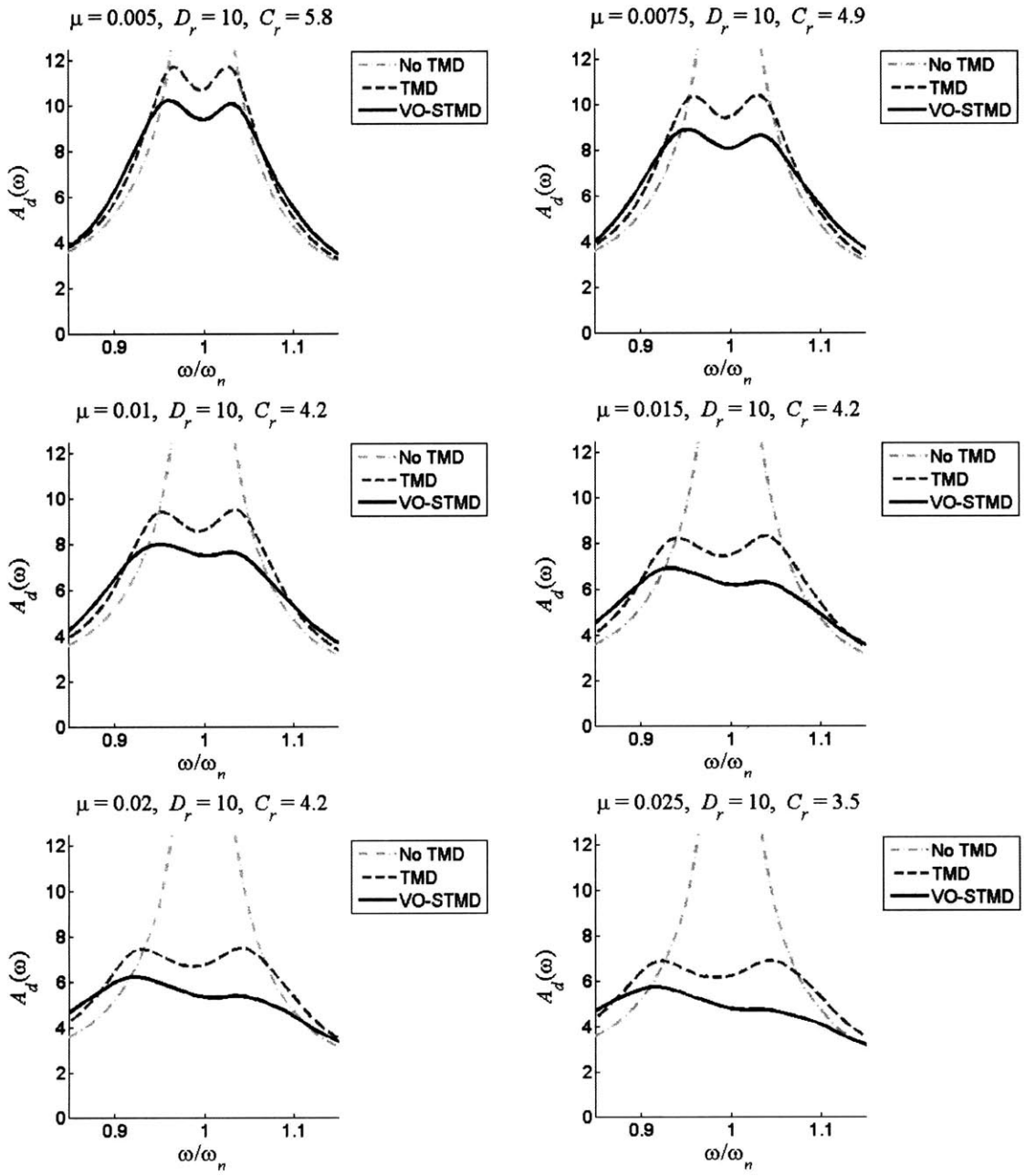

Figure 5-30: $D_r = 10$: $A_d(\omega)$ simulations for minimized J_1

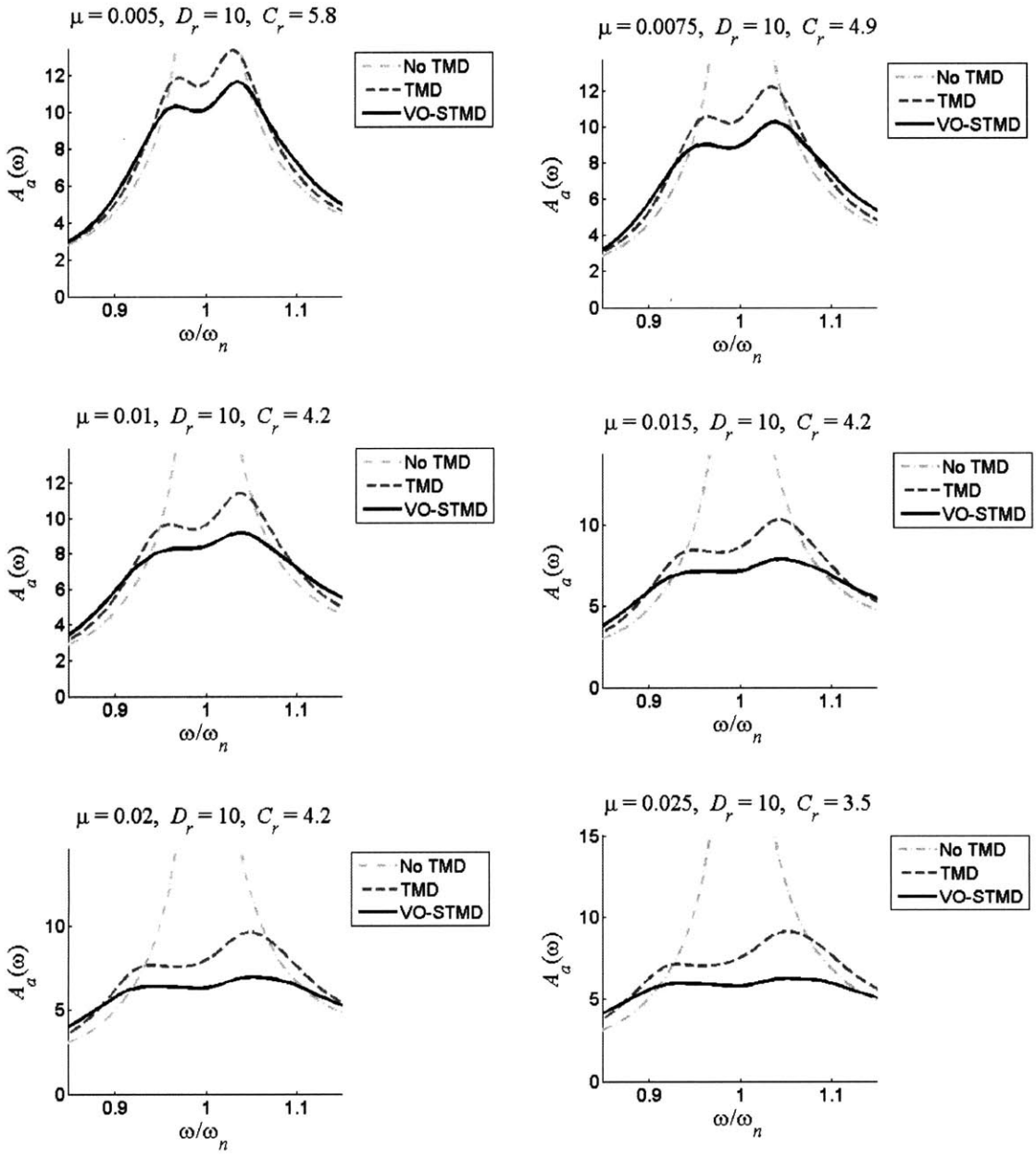

Figure 5-31: $D_r = 10$: $A_a(\omega)$ simulations for minimized J_1

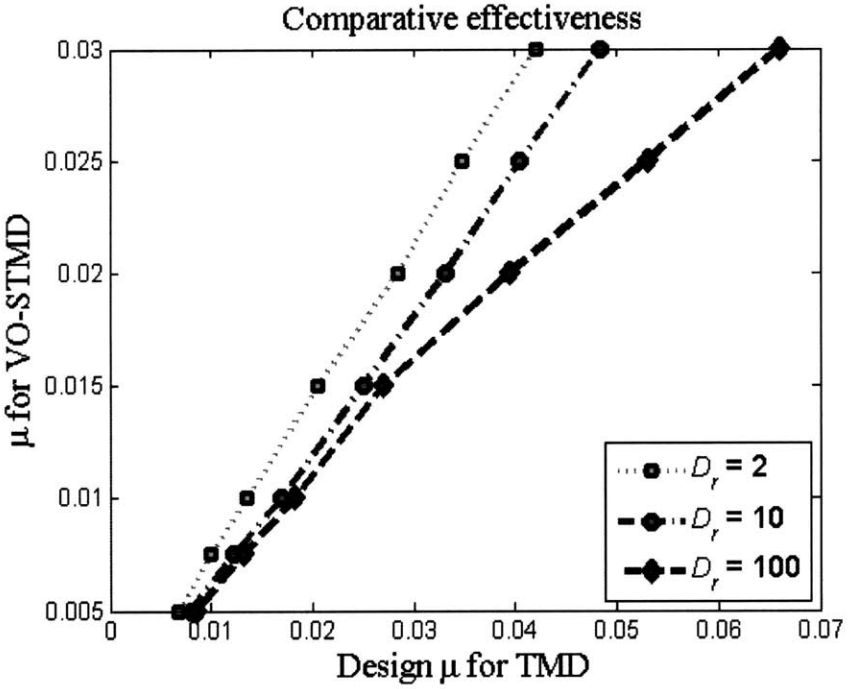

Figure 5-32: Relative effectiveness of VO-STMD

5.5 Summary of results

As has been demonstrated, the performance of variable-orifice STMD systems shows considerable improvement over their passive counterparts. Even with a nominal dynamic range of $D_r = 10$, the results for all performance criteria either met or exceeded those of passive systems with 60% more mass.

This is significant because one possible design objective in choosing a semi-active system could be to decrease the required mass. Particularly in retrofit situations, space or weight constraints may present difficult design issues that could be ameliorated through the addition of a semi-active damper. Hence, it is worthwhile to document how the required mass for an STMD compares with the required mass for a passive TMD. Figure 5-32 summarizes the results for all VO-STMD studies performed, which include full results for several D_r values using the following mass ratios:

$$\mu = 0.005,\ 0.0075,\ 0.01,\ 0.015,\ 0.02,\ 0.025, \text{ and } 0.03$$

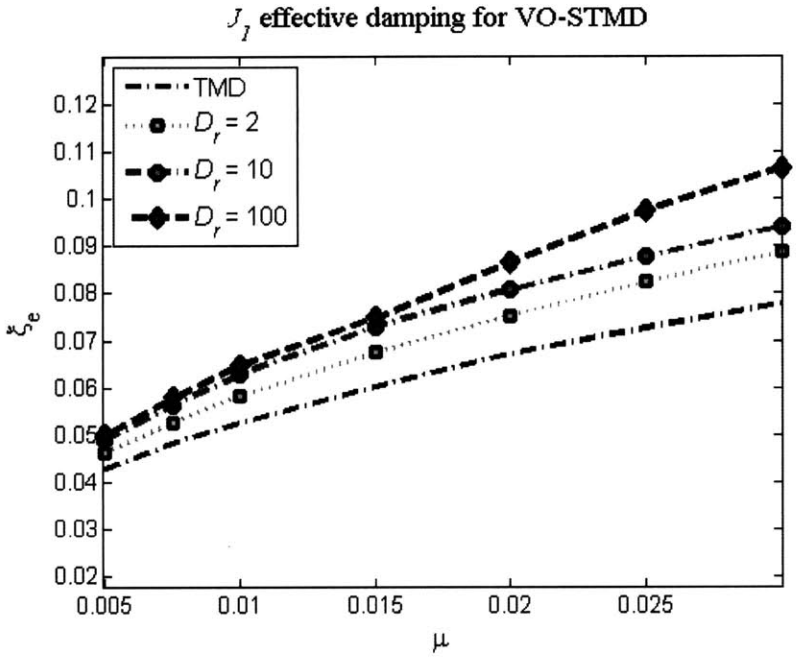

Figure 5-33: Effective damping ratios for peak displacements

The results shown in figure 5-32 were taken using the J_1 criteria, which in almost all instances represents the worst case results for each of the performance criteria previously defined[3]. Hence, the advantages of using a semi-active device in a TMD system are readily apparent from the standpoint of decreasing the requisite mass ratio.

A secondary way of viewing STMD performance improvement is by assessing the effective damping of the controlled system as described in section 5.1.3. In engineering practice, it is common to determine how much damping a structure needs for serviceability and then to select a control system whose capability matches the need. Figures 5-33 and 5-34 summarize the effective damping provided by VO-STMD systems in terms of peak displacements (figure 5-33) and peak accelerations (figure 5-34). Hence, these may function as design charts: once the requisite damping has been determined and the dynamic range of the VO damper has been selected, the necessary mass ratio may quickly be found.

[3]This is the expected result given that the passive systems were optimized for J_1, making it the most difficult to improve through additional control measures.

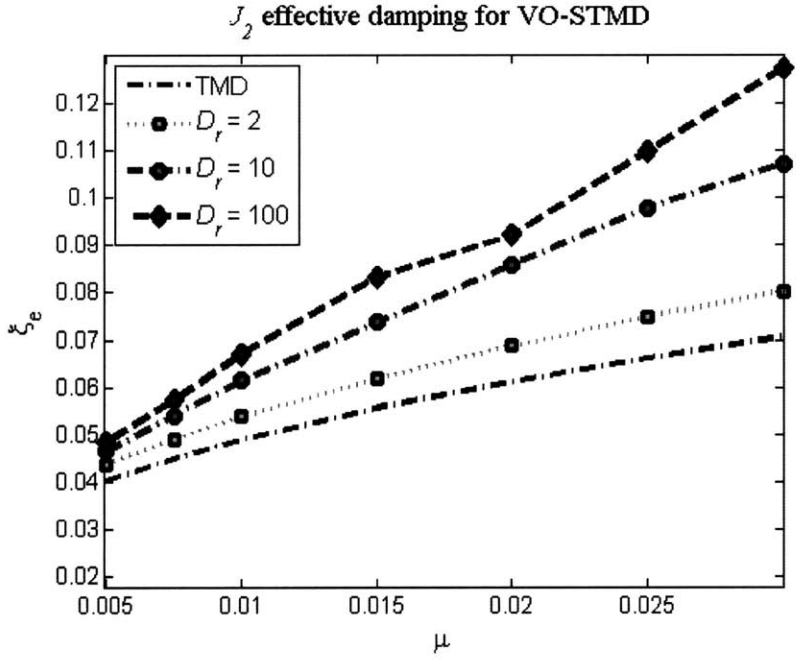

Figure 5-34: Effective damping ratios for peak accelerations

Note that the inherent damping of the simulated structure is 2%, making this the baseline for all performance benefits. The simulations considered also focus on passive TMD systems optimized to limit maximum displacements; hence, the passive results shown in figure 5-34 may be slightly improved if the mitigation of maximum accelerations is the design goal. Even with a displacement-based optimization, however, it is observed that the effective damping of STMD systems is more significant for J_2 then for J_1.

As evidenced in figure 5-30, this is because STMD systems exhibit greater control at higher input frequencies, particularly for larger mass ratios. Since $A_a(\omega)$ is more problematic at higher frequencies due to the addition of a $\omega^2/{\omega_n}^2$ term, STMD systems appear better suited to mitigate acceleration than displacements; see figure 5-31 for comparison. This suggests than an STMD system may be designed to limit peak displacements while actually improving peak accelerations more significantly. Since acceleration often governs the design of wind-loaded structures, this is a particular advantageous feature of STMD systems.

Chapter 6

Results for Magnetorheological STMD

Another possible device for a damper-based STMD is the magnetorheological damper. As elucidated more fully in chapter 3, MR dampers have attracted a significant amount of attention for their viability in semi-active control of structures, making them an appealing candidate for use with a tuned mass damper. Hence, MR-STMD systems will be analyzed and used as a representative case of variable dampers with non-linear responses. As shall be shown in this chapter, the introduction of non-linearity leads to superior STMD performance as compared to systems using linearly-varying dampers.

This chapter follows the simulation procedure described in chapter 4 and bases control forces on the formulation explained in section 4.5.6. The mathematical model used for the MR damper is a modification of the classic Bingham model and can be expressed mathematically as

$$g_{mr}\left[V(t)\right] = c_{min}\dot{z} + \begin{cases} 10 f_c \frac{V(t)}{V_{max}} \frac{\dot{z}}{\dot{z}_{max}} & \text{if } |\dot{z}| \leq 0.1\dot{z}_{max} \\ f_c \frac{V(t)}{V_{max}} \text{sgn}(\dot{z}) & \text{otherwise} \end{cases} \tag{6.1}$$

where $V(t)$ is the applied voltage, $0 \leq V(t) \leq V_{max}$; c_{min} is the minimum damping when $V(t) = 0$; f_c is the equivalent Coulomb friction force when $V(t) = V_{max}$; $\dot{z}$ is

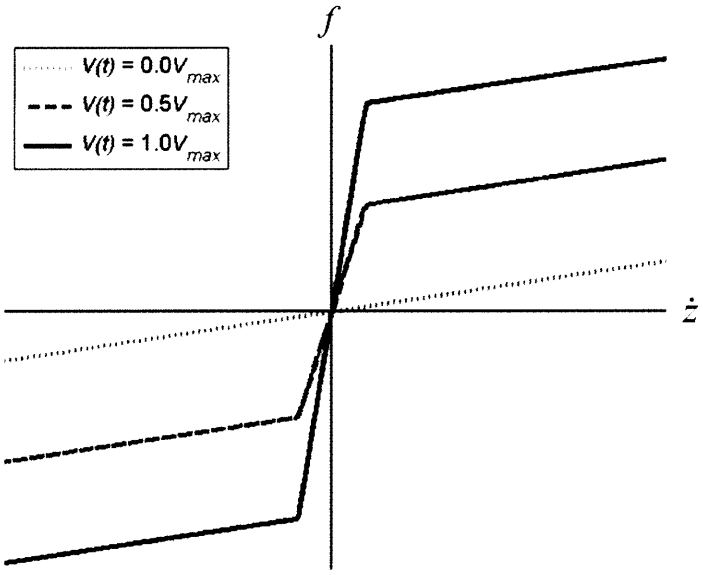

Figure 6-1: Modified Bingham model

the relative velocity of the TMD with respect to the building; and $\dot{z}_{max}$ is the design value for the maximum relative velocity, above which saturation limits are reached.

The purpose of adding the transition zone for $|\dot{z}| \leq 0.1\dot{z}_{max}$ is to avoid generating unrealistic control forces when the relative velocity is very small. Based on experimental results for large-scale MR dampers, the traditional Bingham model, which does not take this transition zone into account, is overly generous in this region. Figure 6-1 shows simulations for this mathematical model for various constant values of $V(t)$.

6.1 Overview of analysis

Due to the non-linear nature of MR-dampers, the definitions developed in chapter 5 must be slightly modified. While the damping reduction factor, C_r, remains mathematically unchanged, the dynamic range, D_r must now take into account this non-linearity by being defined at a particular velocity. For convenience, this term will be based on the secant damping at the design value for the maximum velocity, $\dot{z}_{max}$[1].

[1]In general, defining D_r at $\dot{z} = \dot{z}_{max}$ produces the most favorable results for a given value of D_r. However, this definition was selected to follow accepted convention for assigning a dynamic range

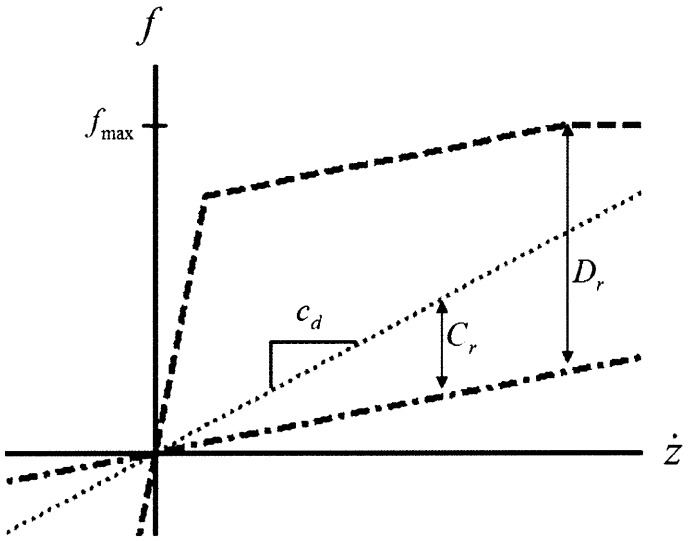

Figure 6-2: Dynamic range and damping reduction factor for MR-STMD

The resulting expressions are

$$D_r = \frac{f_c}{\dot{z}_{max} c_{min}} + 1 \tag{6.2}$$

$$C_r = \frac{c_d}{c_{min}} \tag{6.3}$$

where c_d is optimal damping for the passive TMD, and where f_c, $\dot{z}_{max}$, and c_{min} may vary significantly depending on the damping device selected.

Figure 6-2 demonstrates how D_r and C_r are found and how they affect the range of accessible control forces for an MR-STMD.

6.1.1 Dynamic range implications

Just as with the variable-orifice damper, if stroke and force requirements can be met, the dynamic range is perhaps the most significant factor in determining how effective a magnetorheological damper might be at improving the performance of a passive TMD. Figure 6-3 demonstrates the influence the dynamic range has on the steady-state performance of an MR-STMD by highlighting simulation results for markedly

to MR dampers. See reference [66].

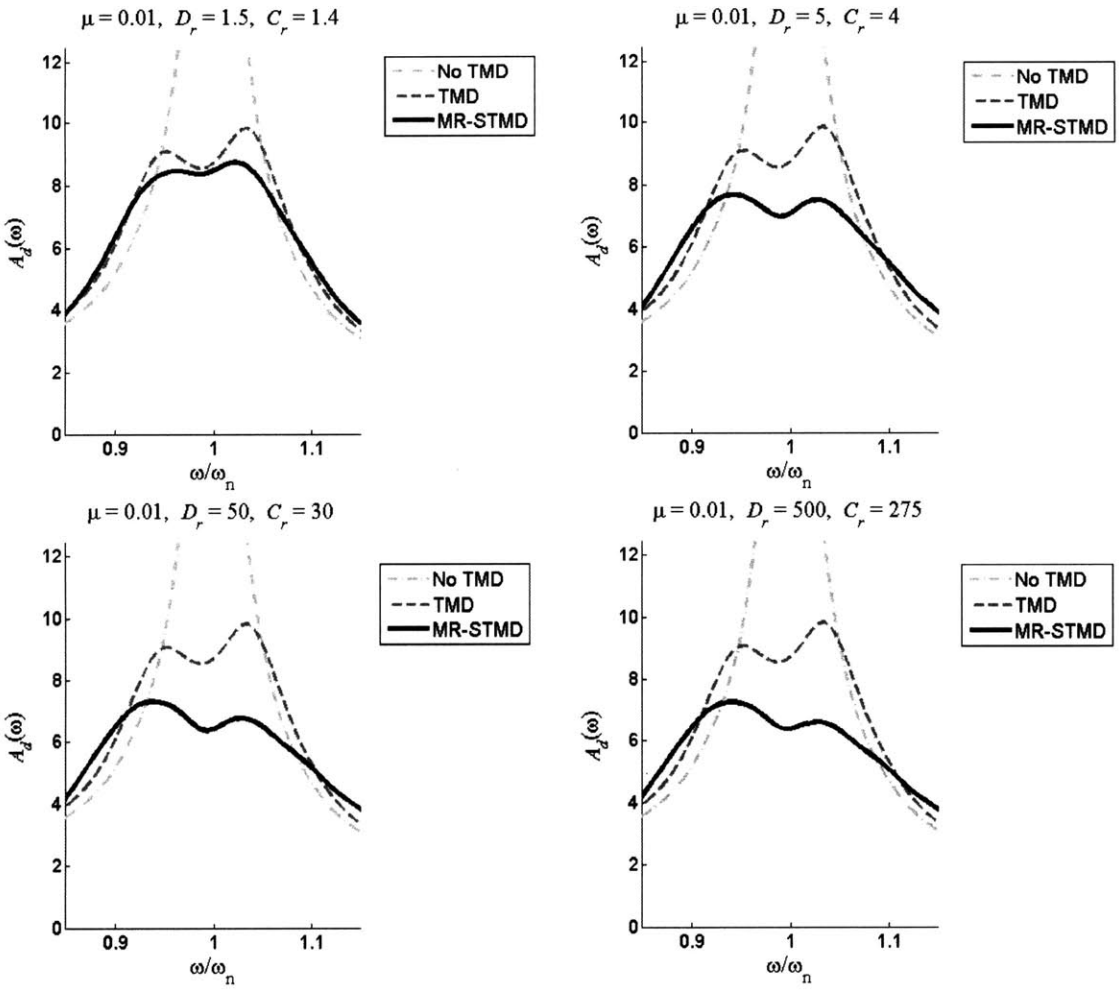

Figure 6-3: Variation based on dynamic range for MR-STMD

different D_r values. As is evident, most of the benefits of an MR damper are accessible even for relatively small values for D_r.

6.1.2 Damping reduction factor implications

The effects of selecting an optimal dynamic reduction factor for a given value of D_r are also similar between the VO-STMD and the MR-STMD, with heuristic optimization methods being required. For comparison, results are presented in figure 6-4 for various values of C_r for an MR-STMD with a dynamic range of $D_r = 10$. Again, it is evident that poorly selected C_r values can result in unacceptable performance results, though performance is less sensitive to C_r for the MR-STMD than for the VO-STMD.

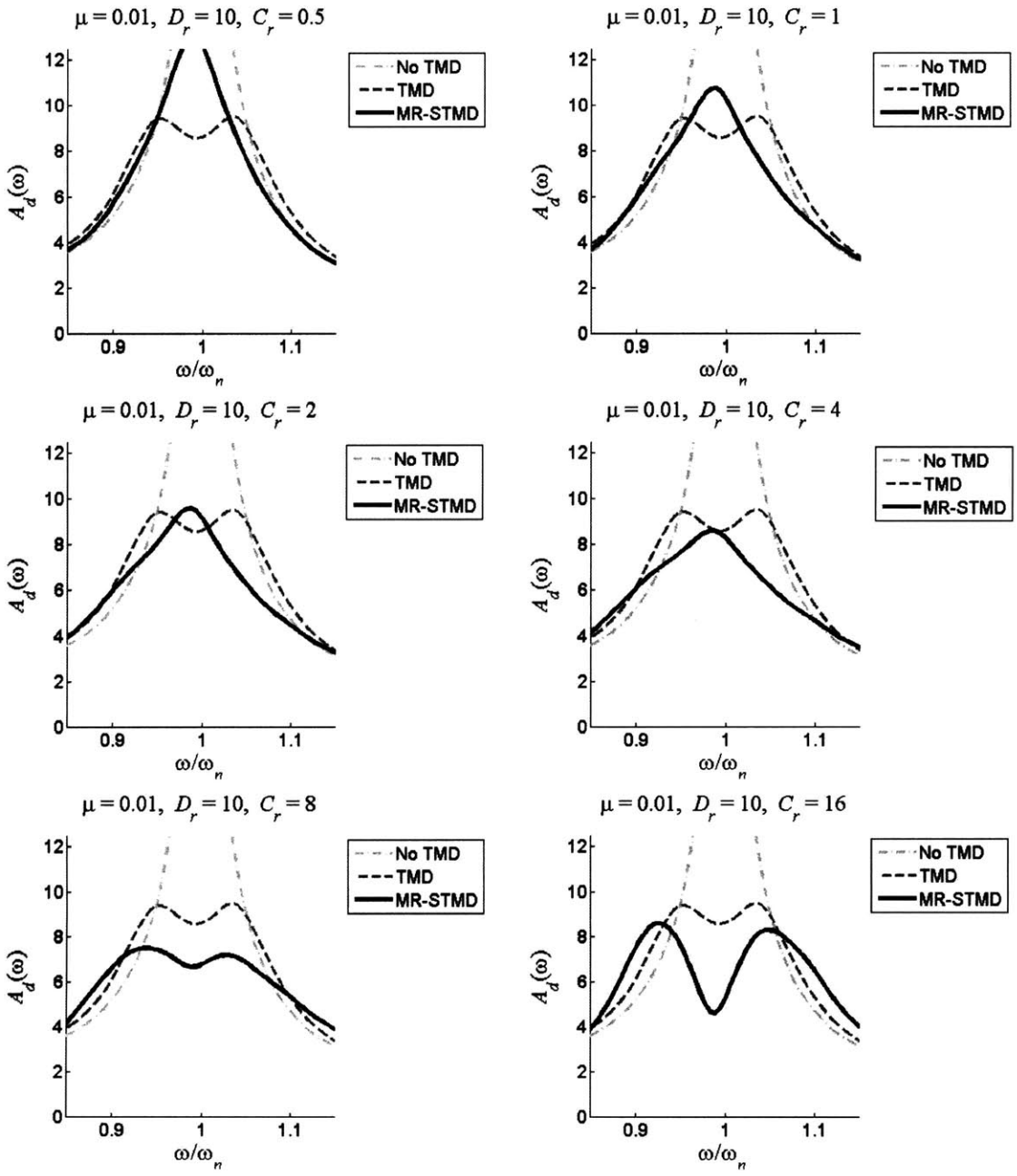

Figure 6-4: Variation based on damping reduction factor for $D_r = 10$

6.1.3 Evaluative measures

The effects of varying both D_r and C_r will be evaluated using the same performance measures described in section 5.1.3. $J_1 \ldots J_4$ will used as the evaluative criteria, passive systems will be used for comparison, effective damping will be calculated, and maximum displacements and force outputs will be assessed.

6.1.4 Broken system considerations

One of the key differences between MR dampers and VO dampers is that there is no accessible level of damping that can allow the system to behave like an optimally-tuned passive TMD should the control system fail. There exists a constant level of voltage, $V(t)$, for which an uncontrolled system is the most beneficial, but its performance falls short of the optimal response attainable by a VO-STMD. This is a trade-off that must be taken into account when considering the reliability of the semi-actively controlled system.

To demonstrate this more explicitly, figure 6.1.4 shows simulations results for an MR-STMD in which the MR damper has been set to a constant voltage. As evident in these simulations, some voltages produce better results than others, making it desirable to find the optimal voltage level for "passive" performance. Ideally, the system will default to this voltage should any problems occur. Figure 6.1.4 further demonstrates the behavior of a passive MR-STMD for each of the four performance indices.

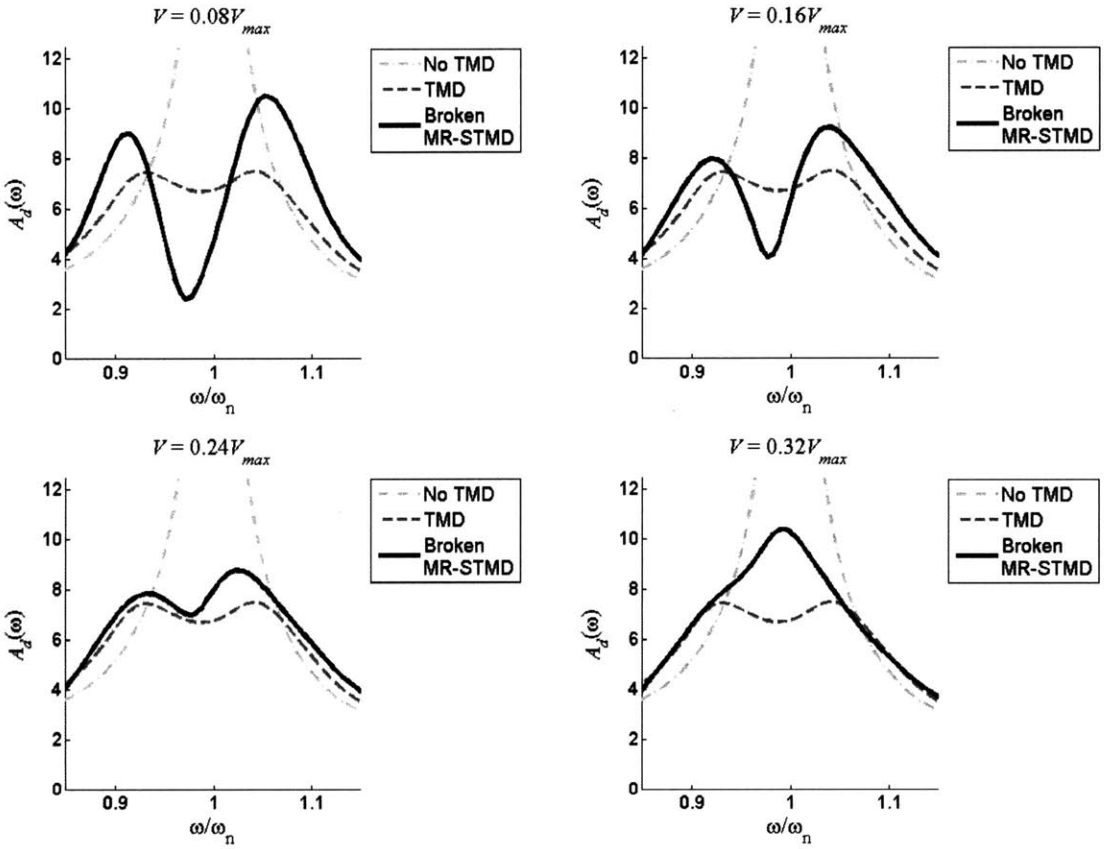

Figure 6-5: Dynamic amplification factors for malfunctioning systems with fixed $V(t)$

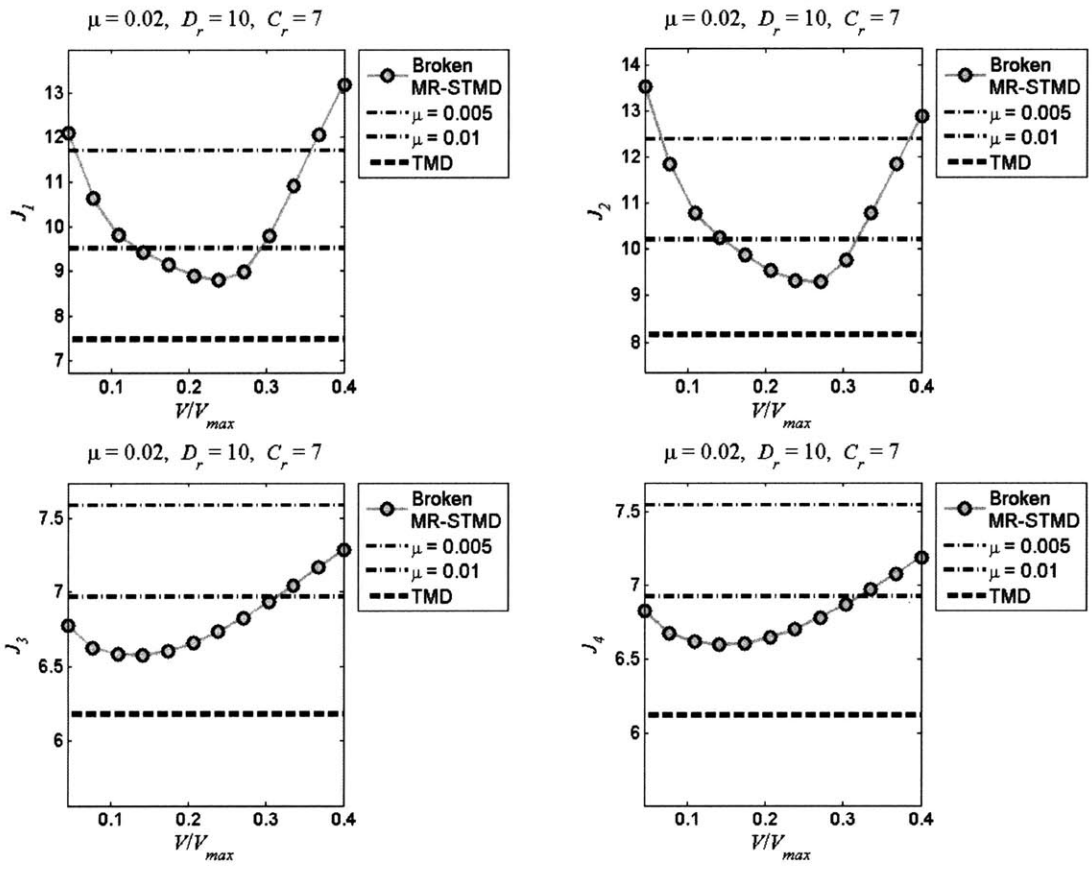

Figure 6-6: Performance indices for malfunctioning systems with fixed $V(t)$

6.2 Results for $\mu = 0.01$

Results will be presented in the same manner as the previous chapter except that now both VO-STMD results and MR-STMD results will be plotted together for comparison. In all cases, the same $\mathbf{Q}$ and $\mathbf{R}$ weighting matrices have been used as introduced in chapter 5, as well as the same values of D_r. What follows are results for a mass ratio of 0.01.

6.2.1 C_r optimization

The optimal values for C_r were found heuristically as for the VO-STMD. Figures 6-7 through 6-10 give results for each of the four performance indices, with plots presented for each of the D_r values under consideration. In general, the optimal C_r values for the MR-STMD are greater than those for the VO-STMD.

By tracking these optimum values, four sets of optimal C_r values can be obtained depending on which performance goal is selected. Results for these "design values" can be seen in figure 6-11.

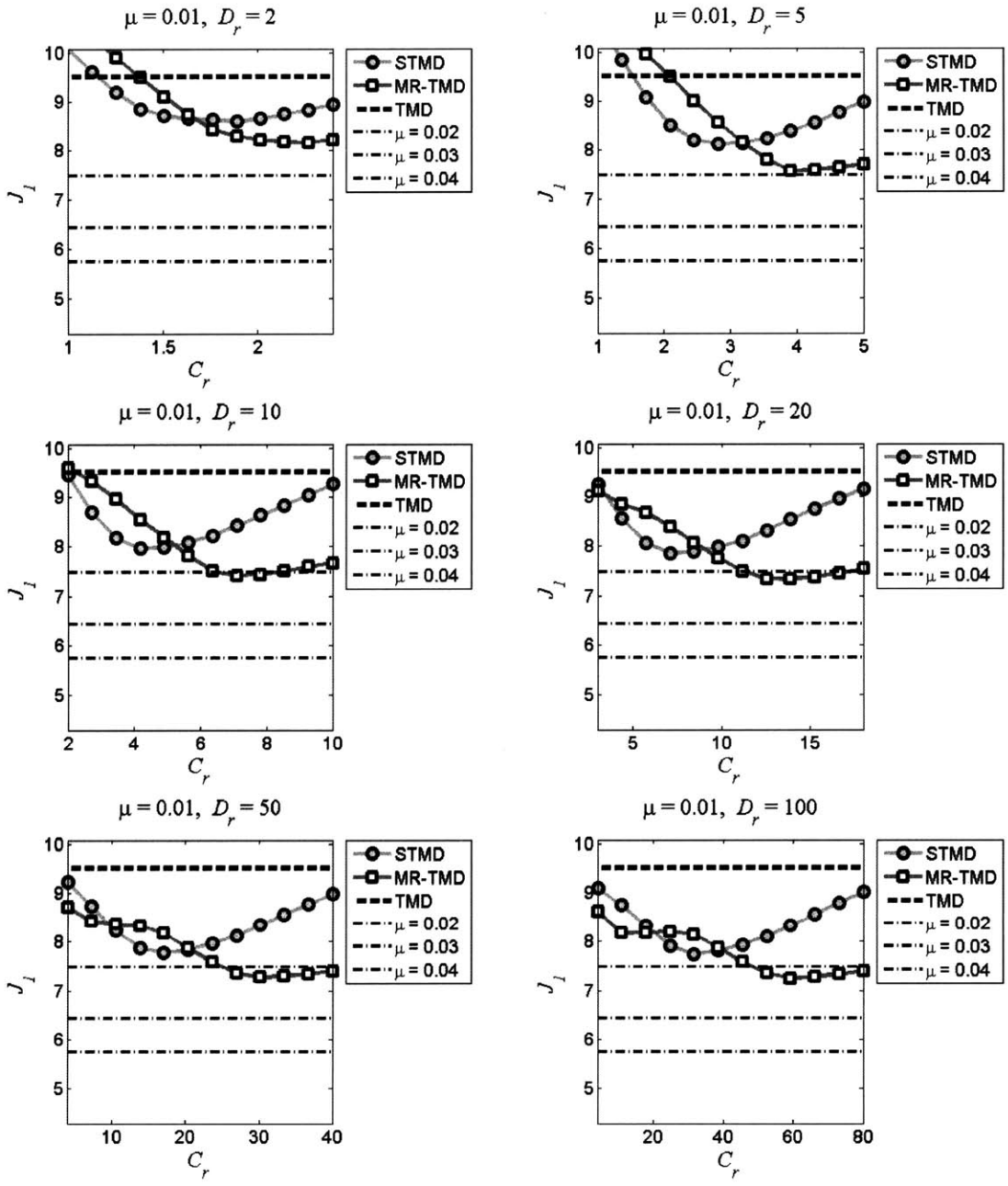

Figure 6-7: $\mu = 0.01$: Finding optimal C_r values for J_1

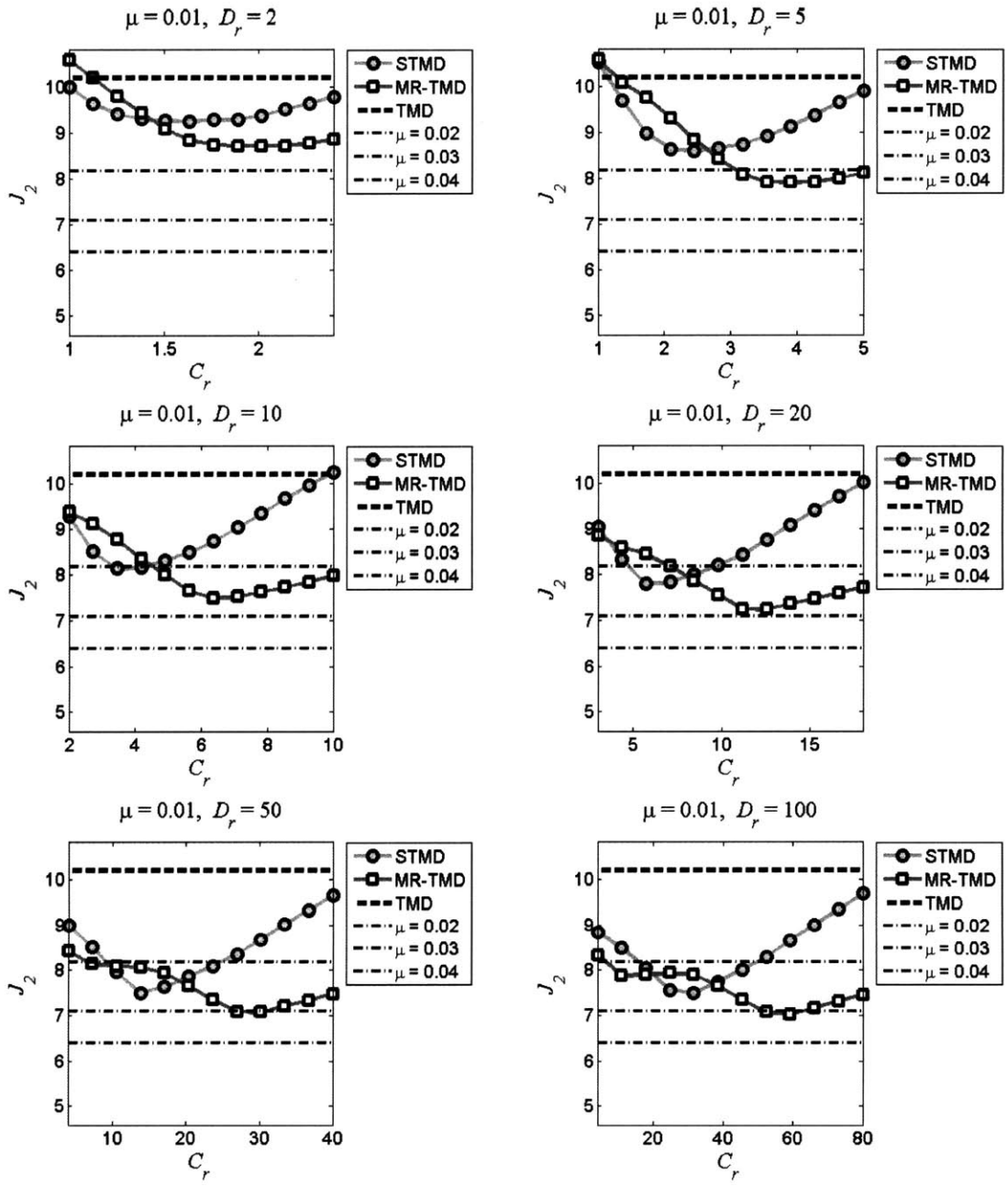

Figure 6-8: $\mu = 0.01$: Finding optimal C_r values for J_2

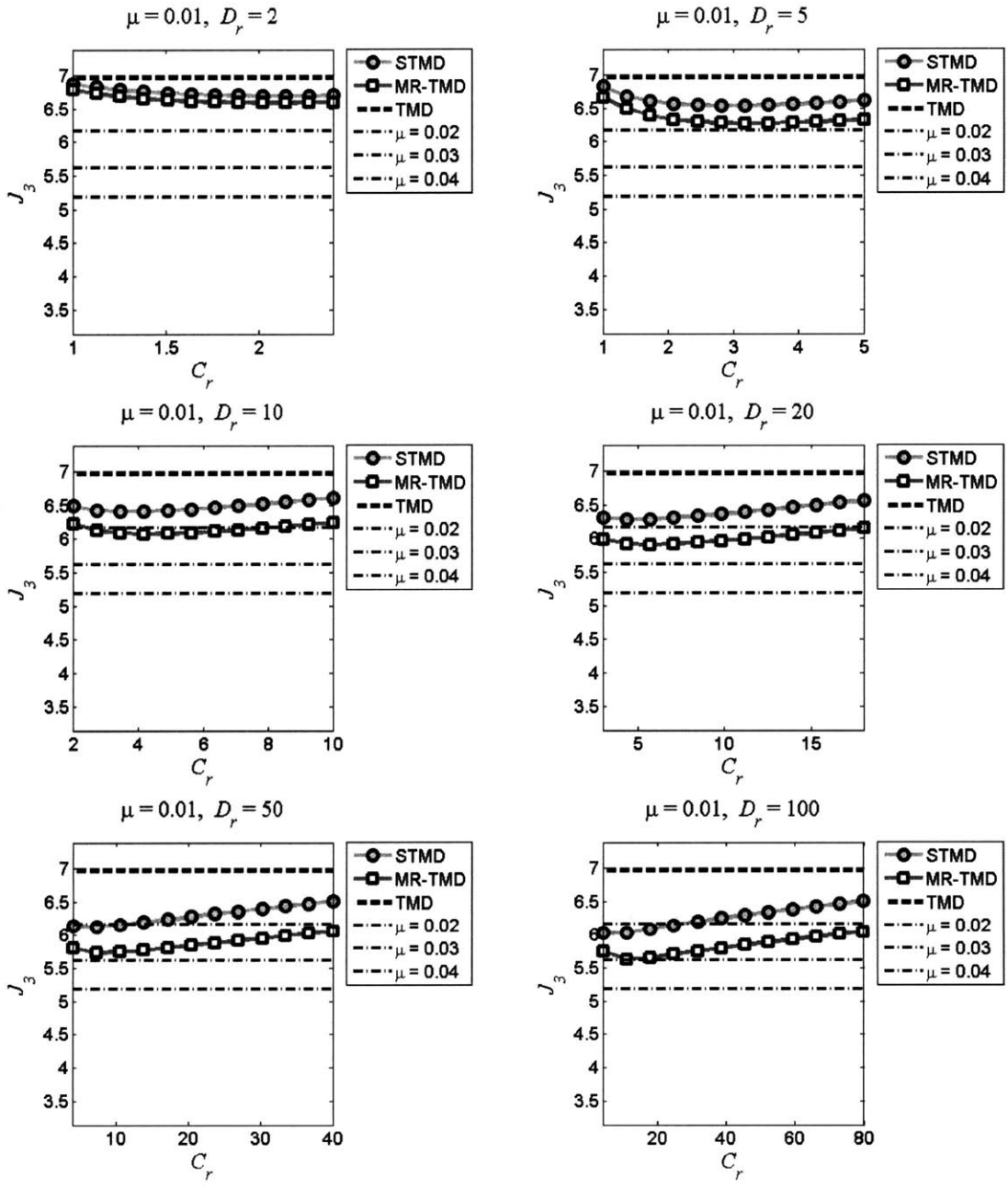

Figure 6-9: $\mu = 0.01$: Finding optimal C_r values for J_3

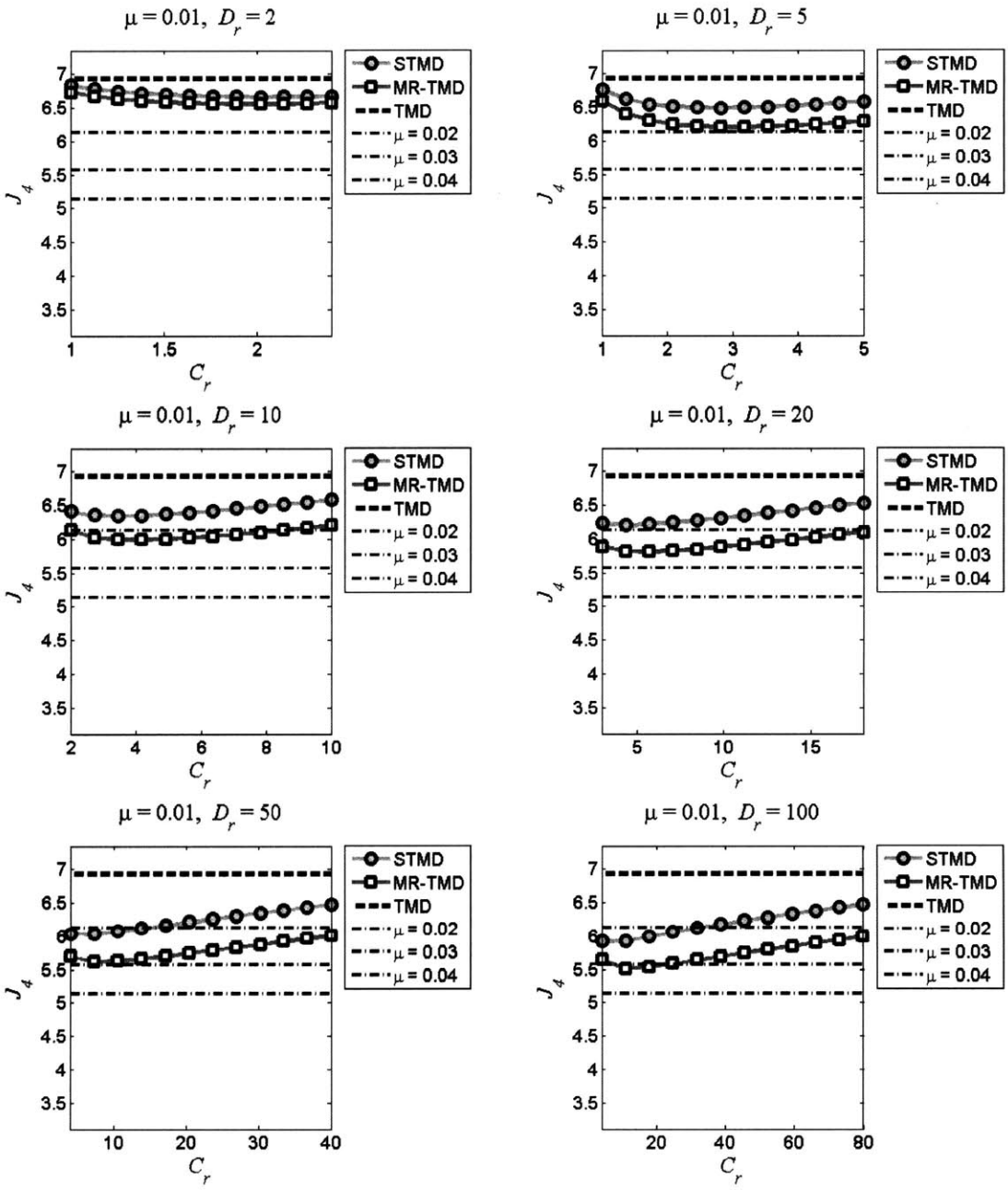

Figure 6-10: $\mu = 0.01$: Finding optimal C_r values for J_4

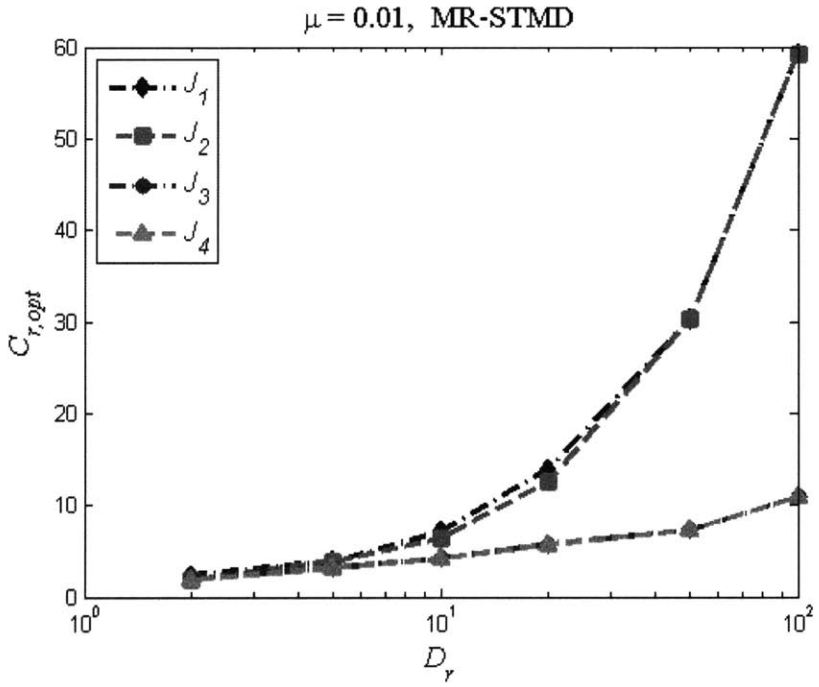

Figure 6-11: Summary of optimal C_r values for $\mu = 0.01$

6.2.2 D_r variability

Based on the values of C_r presented in figure 6-11, the optimized performance of the MR-STMD can be plotted as a function of the damper's dynamic range. The results highlighted for the MR-TMD will again be compared to the previous VO-STMD results:

- Figure 6-12 shows optimized results for all four performance indices, assuming that each may be optimized independently.
- Figure 6-13 shows results for all four performance indices using only C_r values from the optimized J_1 results.
- Figure 6-14 presents $A_d(\omega)$ simulations for minimization of J_1.
- Figure 6-15 presents $A_a(\omega)$ simulations for minimization of J_1.

As before, the C_r values that minimized J_1 have been chosen as the design objective.

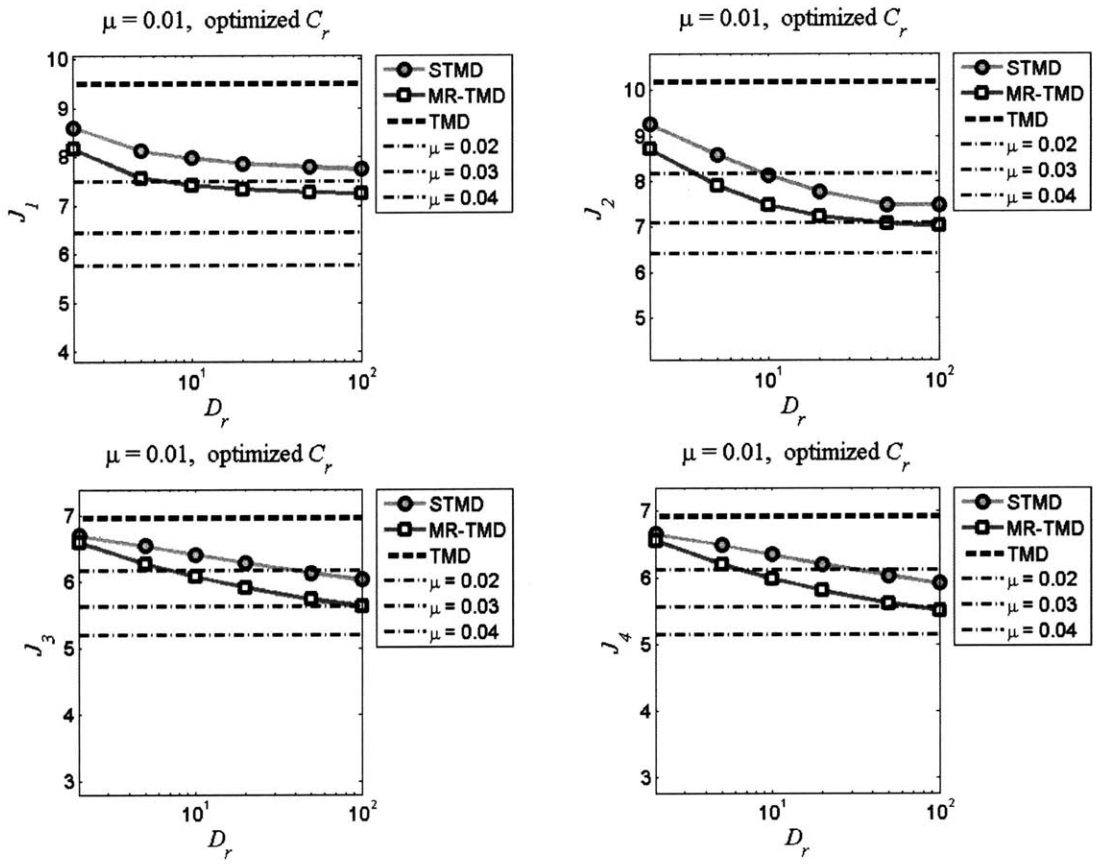

Figure 6-12: $\mu = 0.01$: Independently optimized results as a function of D_r

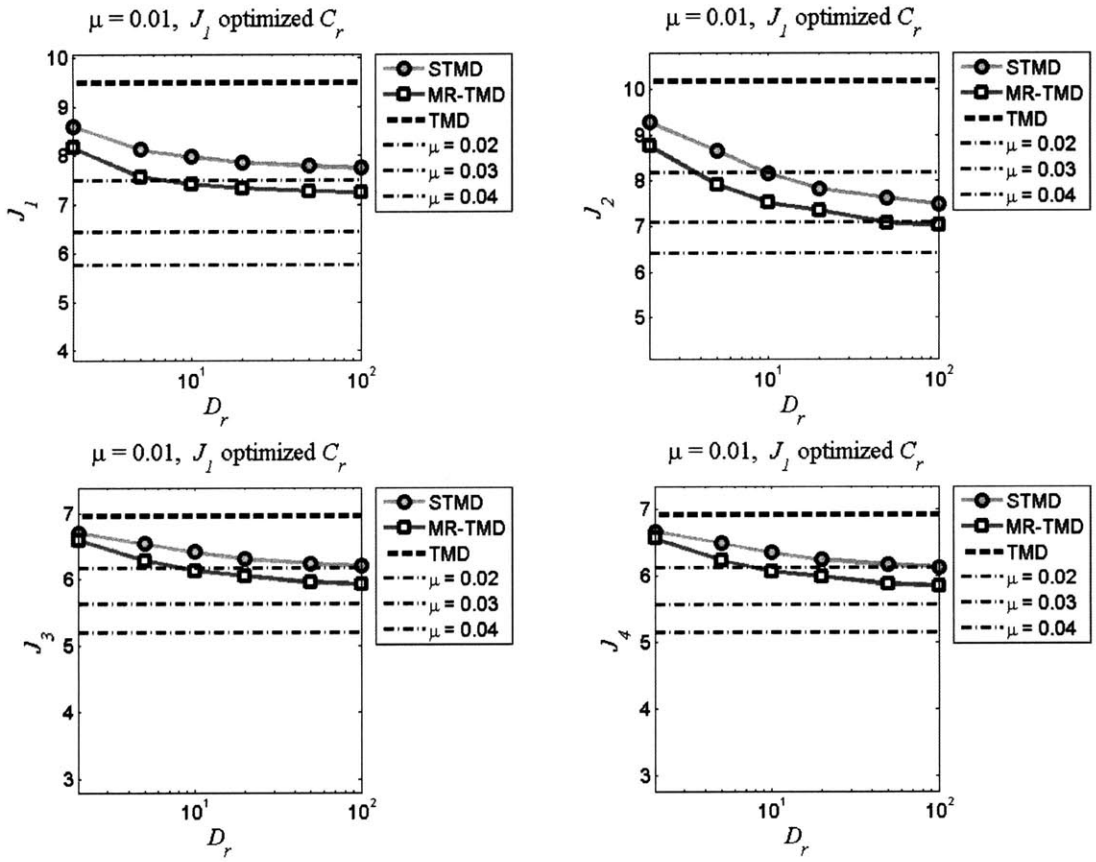

Figure 6-13: $\mu = 0.01$: J_1 optimized results as a function of D_r

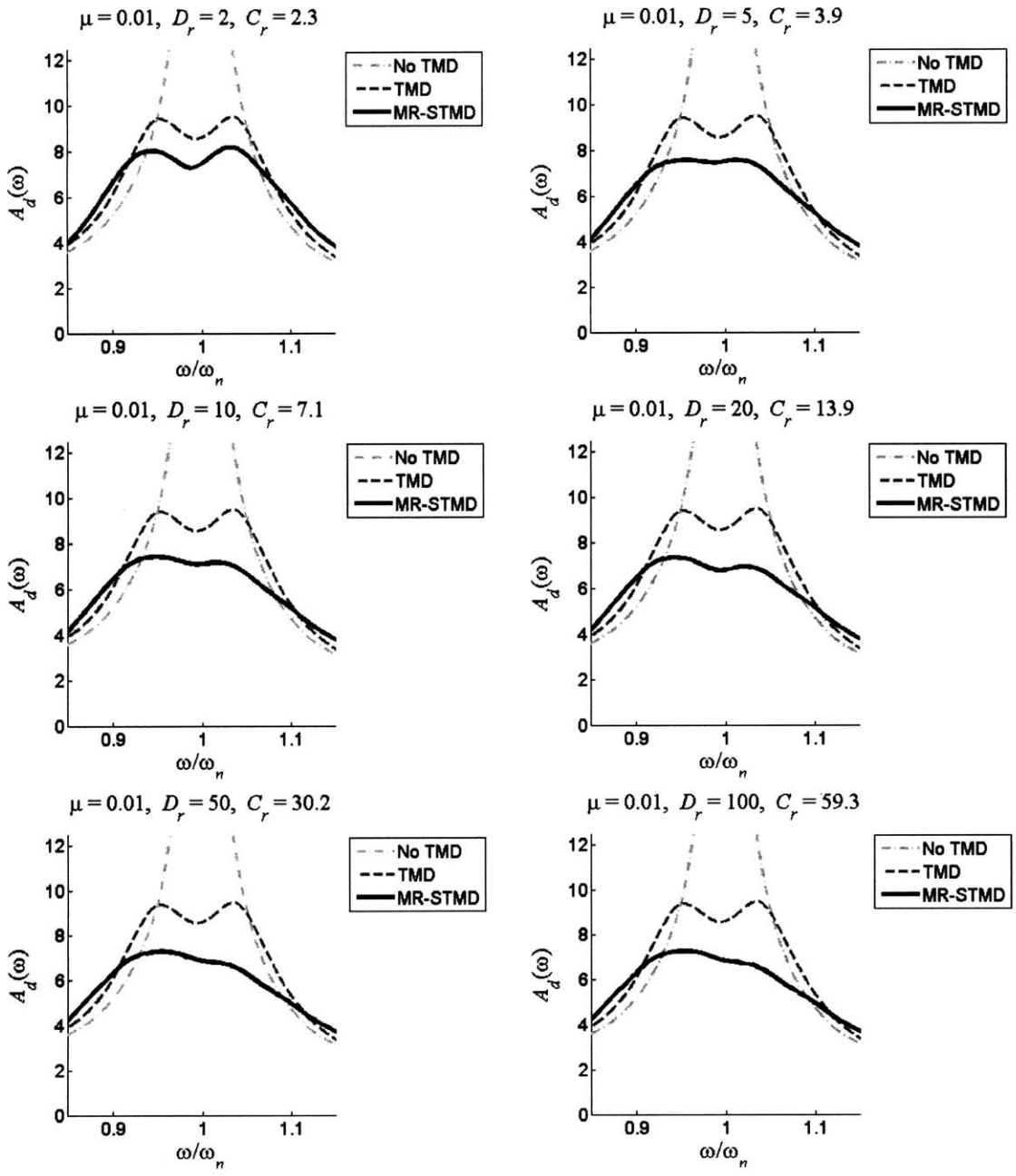

Figure 6-14: $\mu = 0.01 : A_d(\omega)$ simulations for minimized J_1

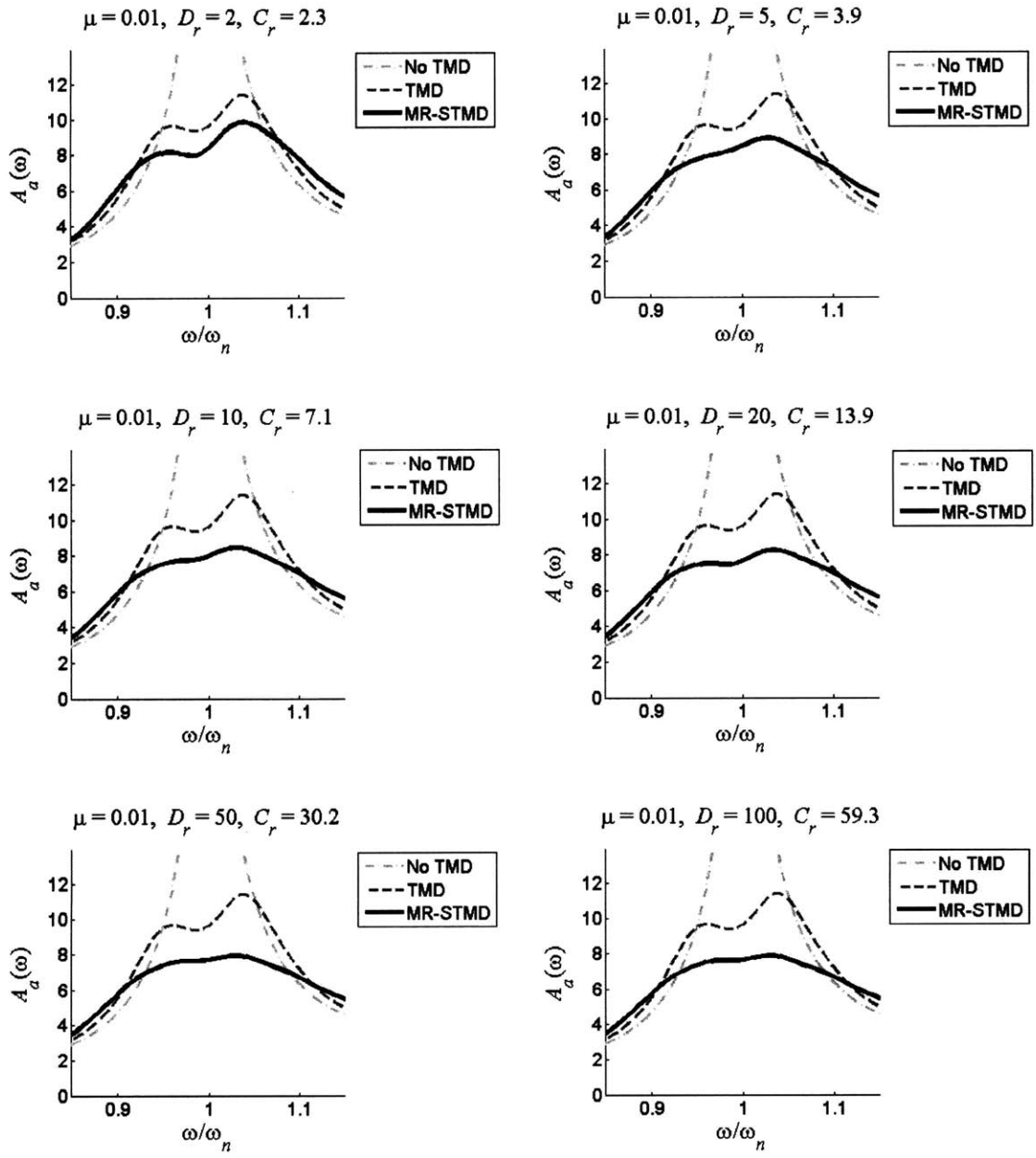

Figure 6-15: $\mu = 0.01 : A_a(\omega)$ simulations for minimized J_1

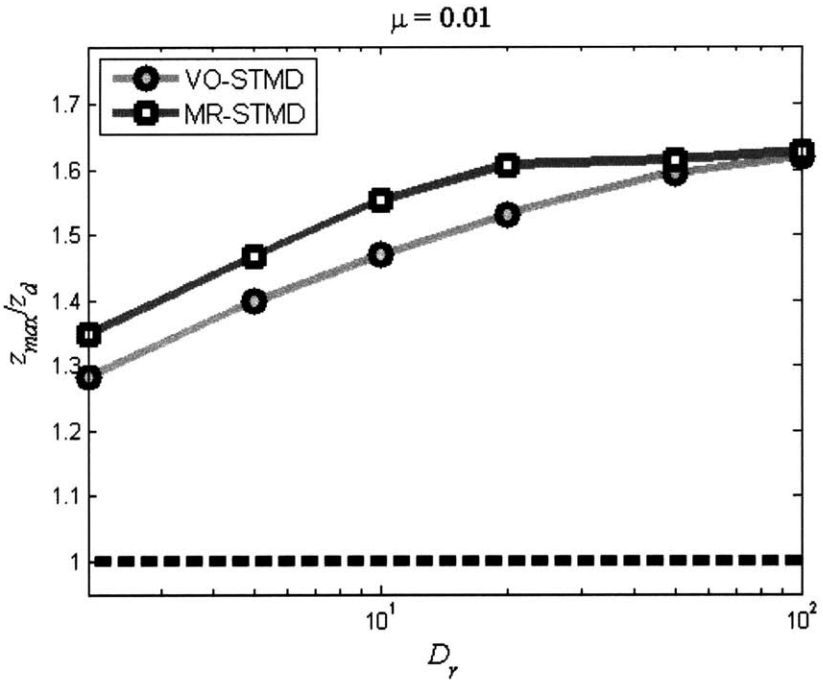

Figure 6-16: $\mu = 0.01$: Relative STMD displacement

6.2.3 Other performance measures

As described in section 5.1.3, each simulation also tracked the maximum relative displacement and the maximum force output of the semi-active damper. Representative results for minimized J_1 simulations are given in figures 6-16 and 6-17.

6.3 Results for $\mu = 0.03$

The second set of results presented are for a mass ratio of 0.03.

6.3.1 C_r optimization

Figures 6-18 and 6-19 present the J_1 and J_2 results, with J_3 and J_4 again excluded due to their lesser importance. The clear trend is that higher values for μ result in lower optimal values for C_r. Design values for C_r based on each of the four performance indices are summarized in figure 6-20.

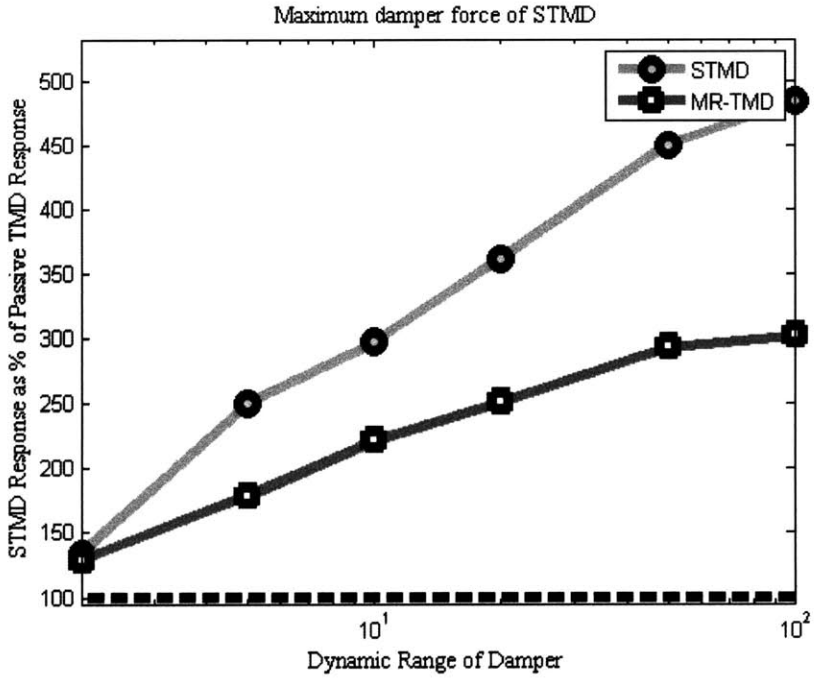

Figure 6-17: $\mu = 0.01$: Maximum damper force

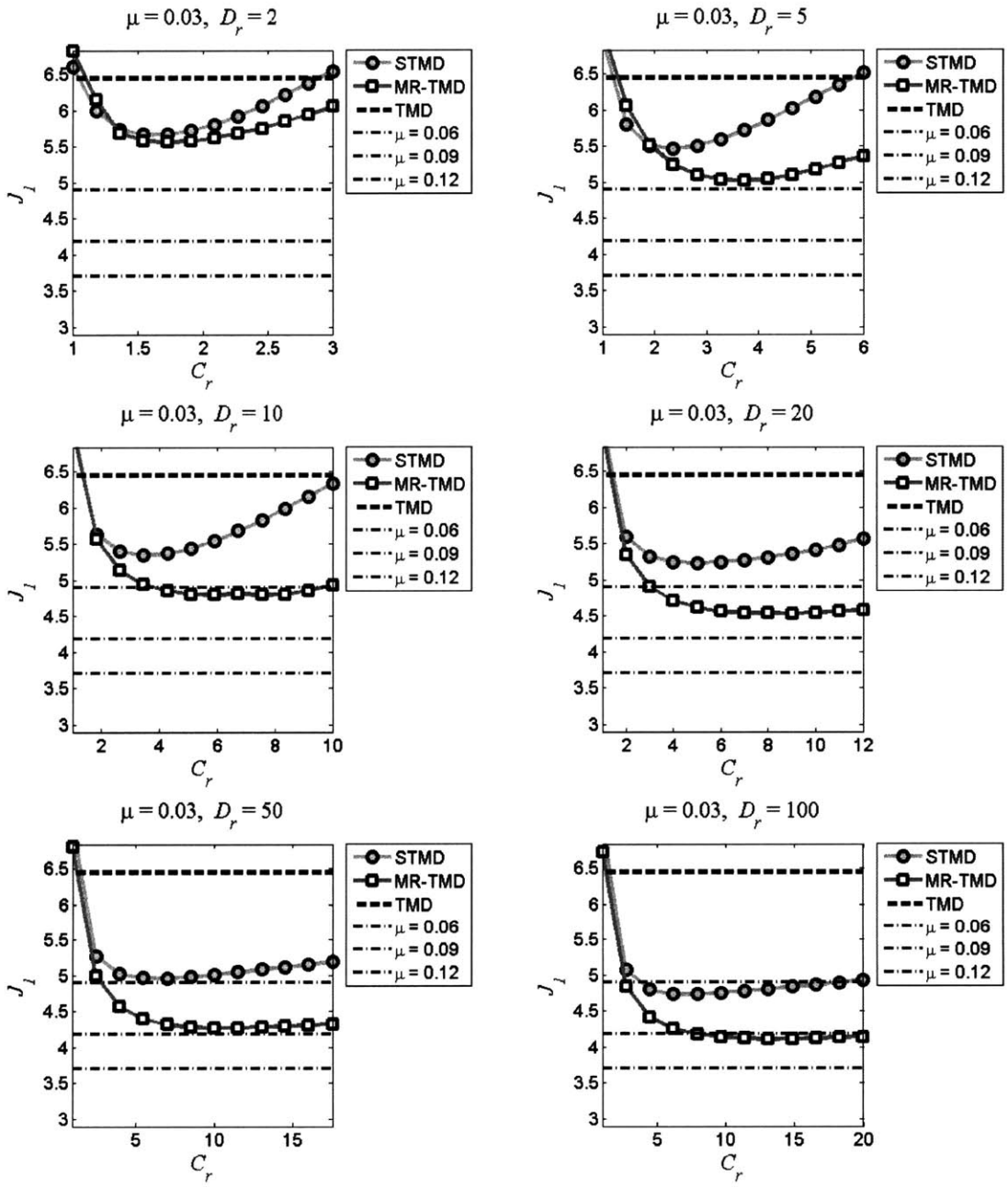

Figure 6-18: $\mu = 0.03$: Finding optimal C_r values for J_1

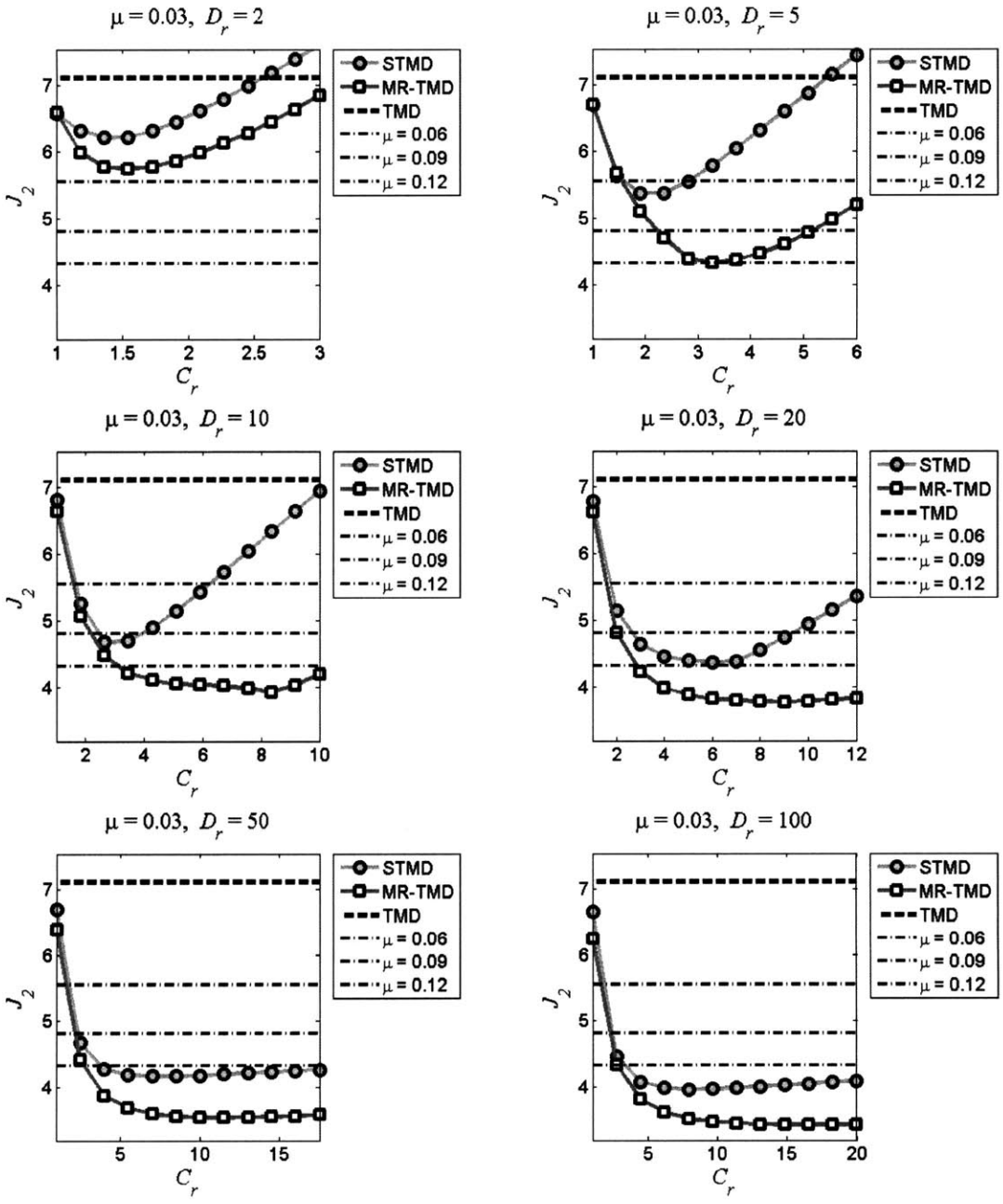

Figure 6-19: $\mu = 0.03$: Finding optimal C_r values for J_2

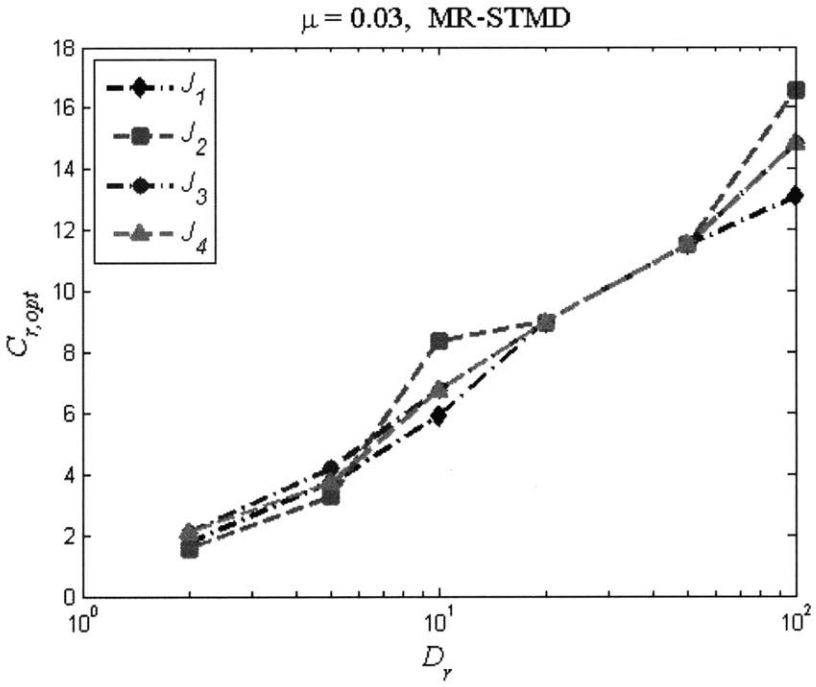

Figure 6-20: Summary of optimal C_r values for $\mu = 0.03$

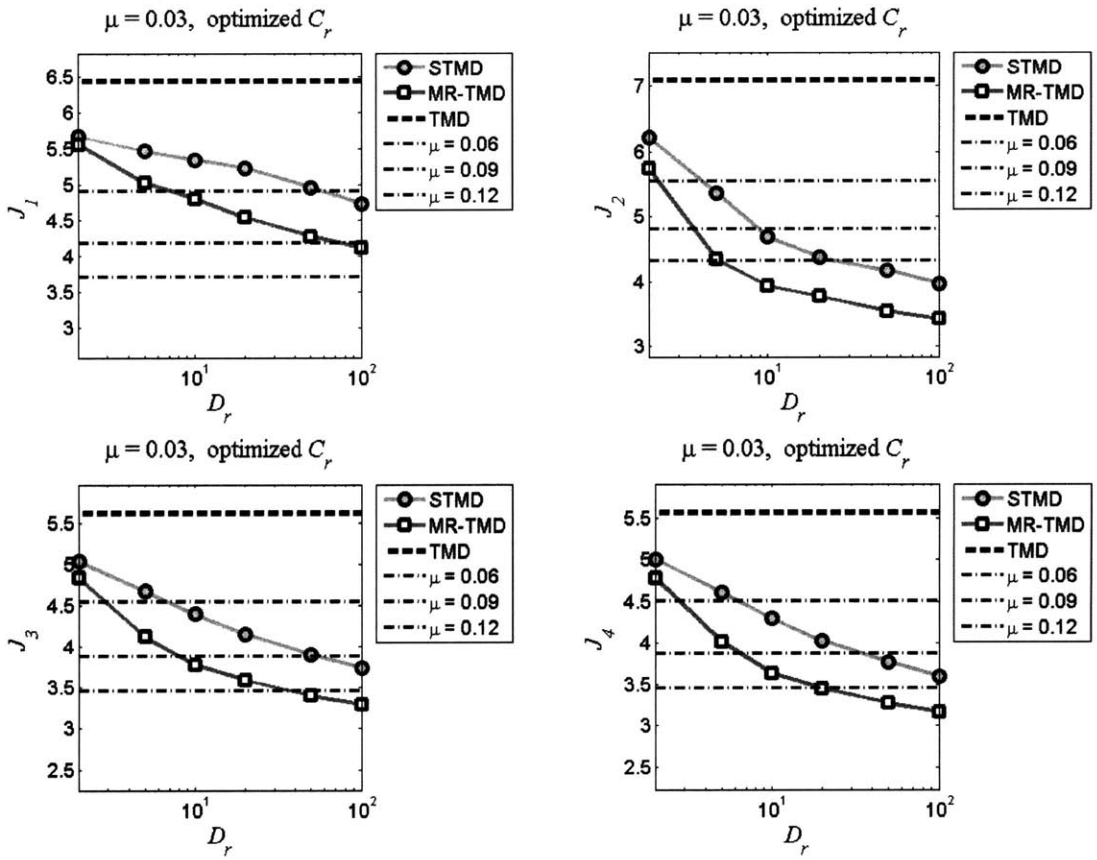

Figure 6-21: $\mu = 0.03$: Independently optimized results as a function of D_r

6.3.2 D_r variability

Based on the values of C_r presented in Figure 6-20, the optimized performance of the MR-STMD can be plotted as a function of the damper's dynamic range. As in the previous section, results will be shown for each performance index optimized individually as well as performance results when J_1 is chosen as the optimization target for C_r selection.

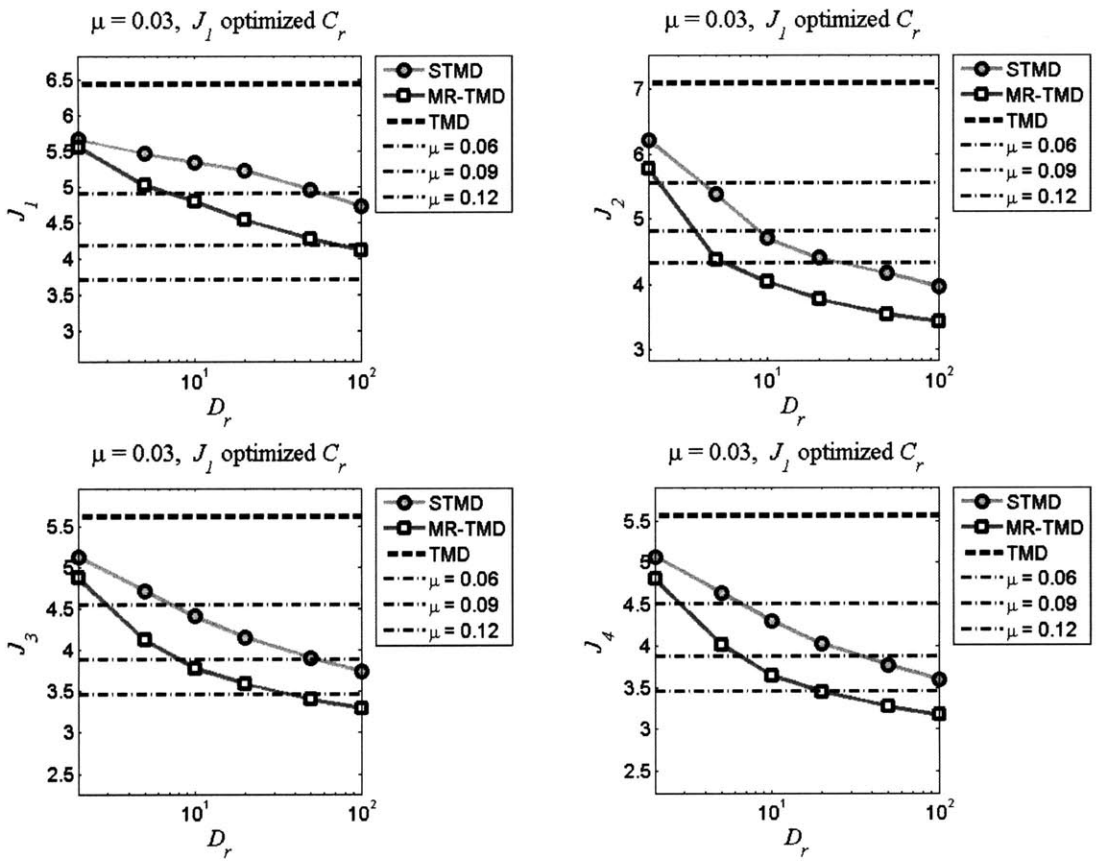

Figure 6-22: $\mu = 0.03 : J_1$ optimized results as a function of D_r

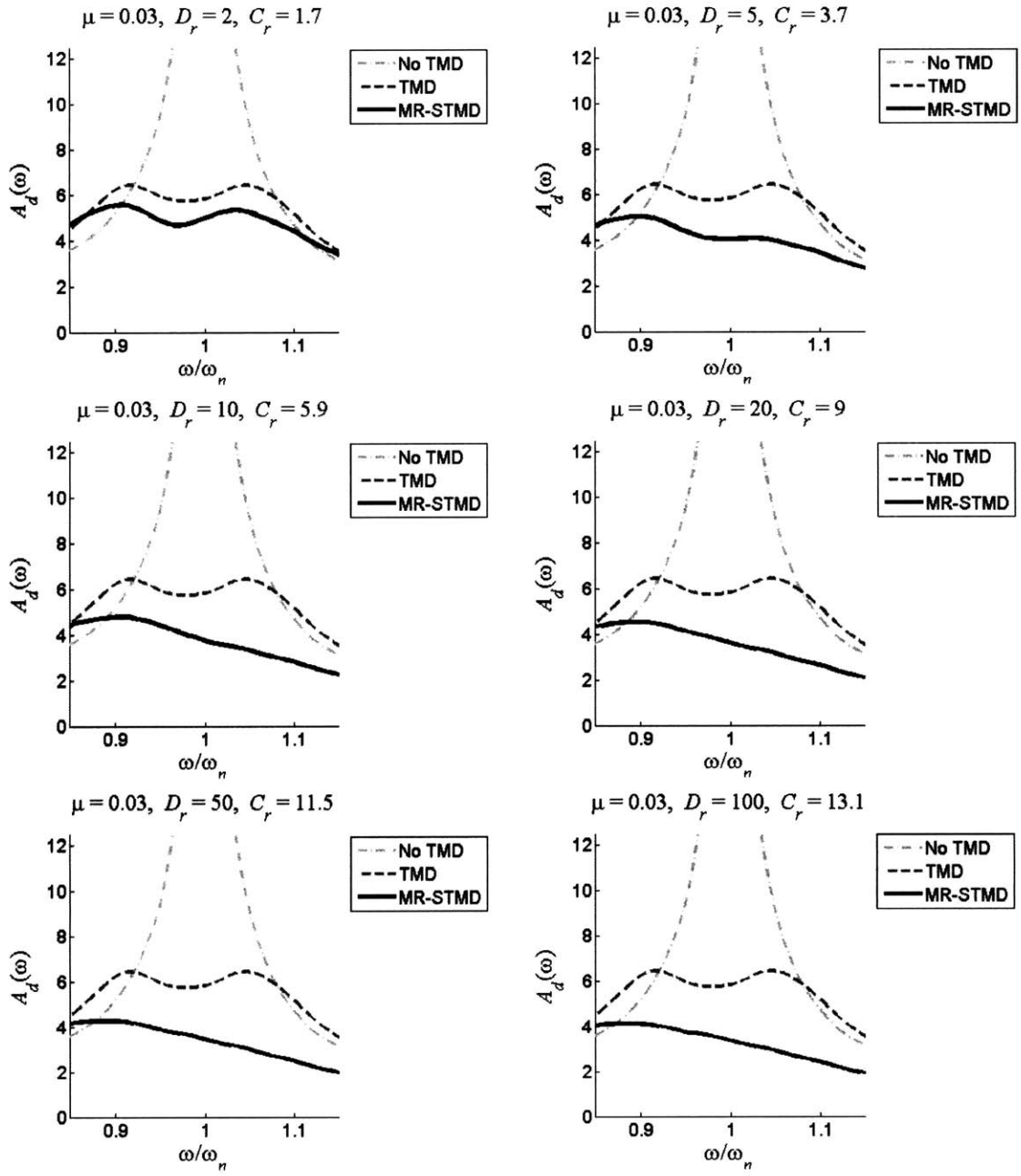

Figure 6-23: $\mu = 0.03 : A_d(\omega)$ simulations for minimized J_1

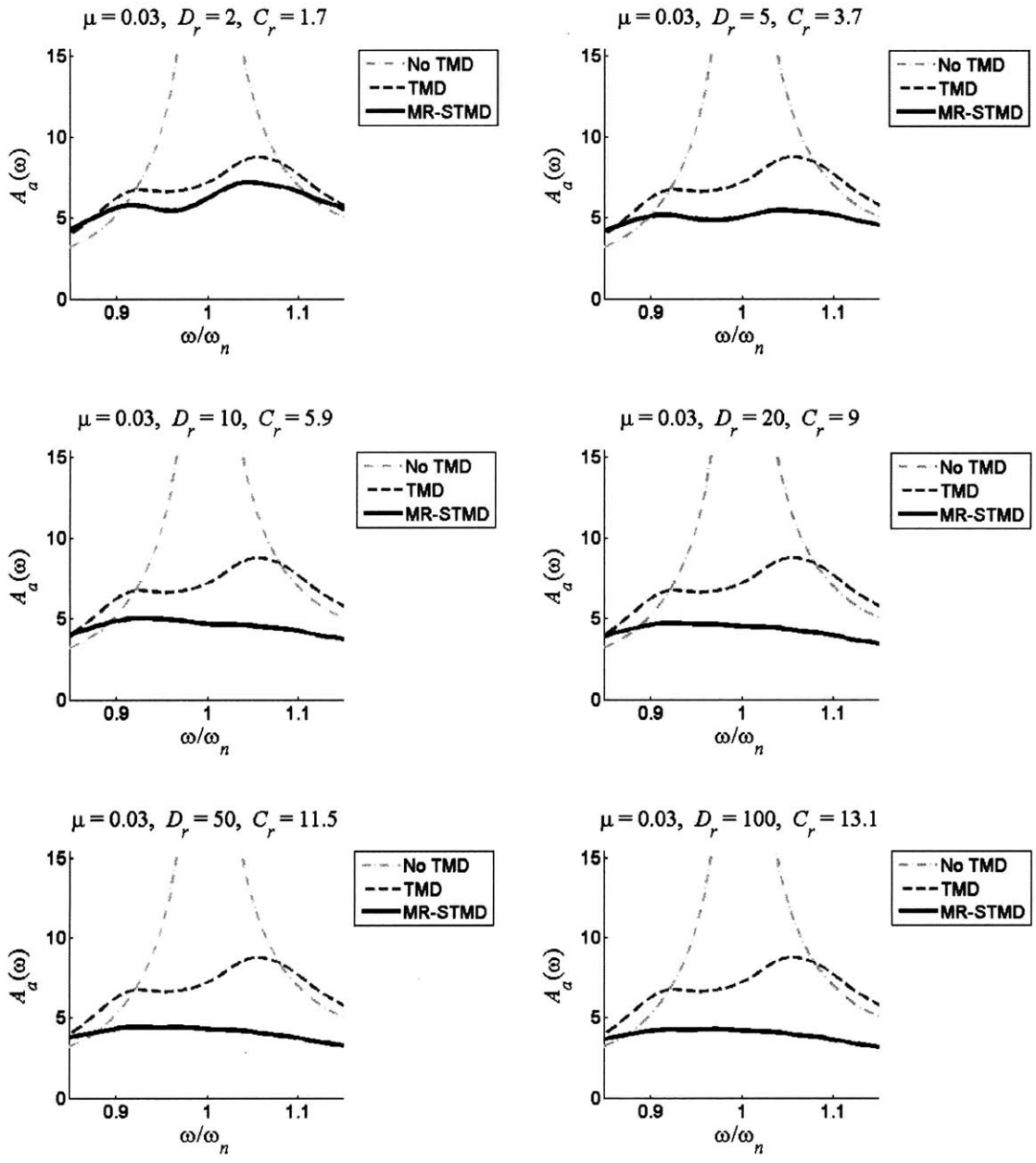

Figure 6-24: $\mu = 0.03 : A_a(\omega)$ simulations for minimized J_1

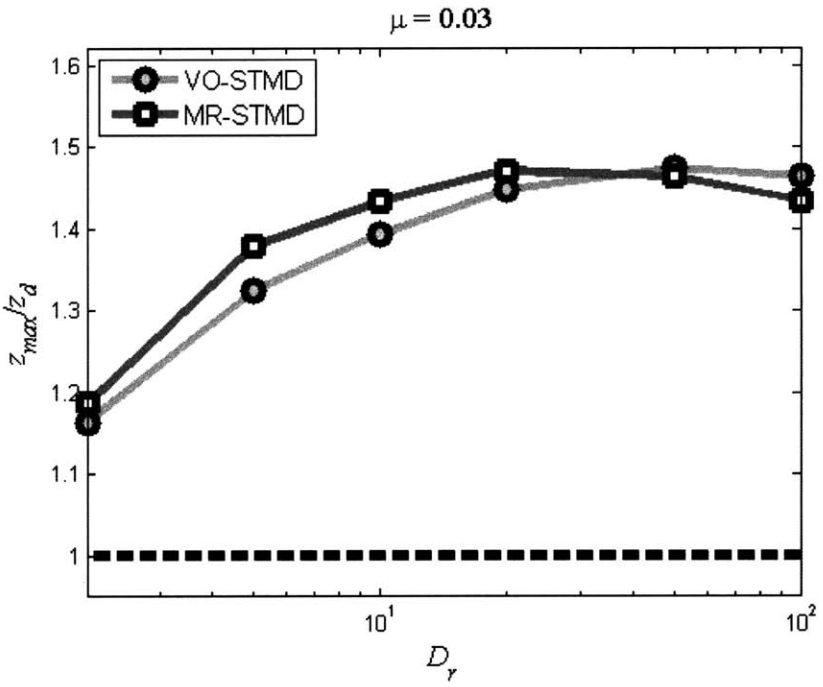

Figure 6-25: $\mu = 0.03$: Relative STMD displacements

6.3.3 Other performance measures

Relative motion and maximum force results for simulations that minimized J_1 are given in figures 6-25 and 6-26. As can be seen, relative displacements are essentially equivalent not only for $\mu = 0.01$ and $\mu = 0.03$ but also for the VO-STMD and MR-STMD. Hence, for a performance-optimized system, there is no trade-off with regards to stroke limitations. However, the maximum damper force output is seen to be significantly lower for the use of an MR damper. This is due largely to the fact that higher C_r values are optimal for the MR-STMD – which leads to a decrease in f_{max} – but is also aided by the accessibility of a greater range of control forces at lower velocities.

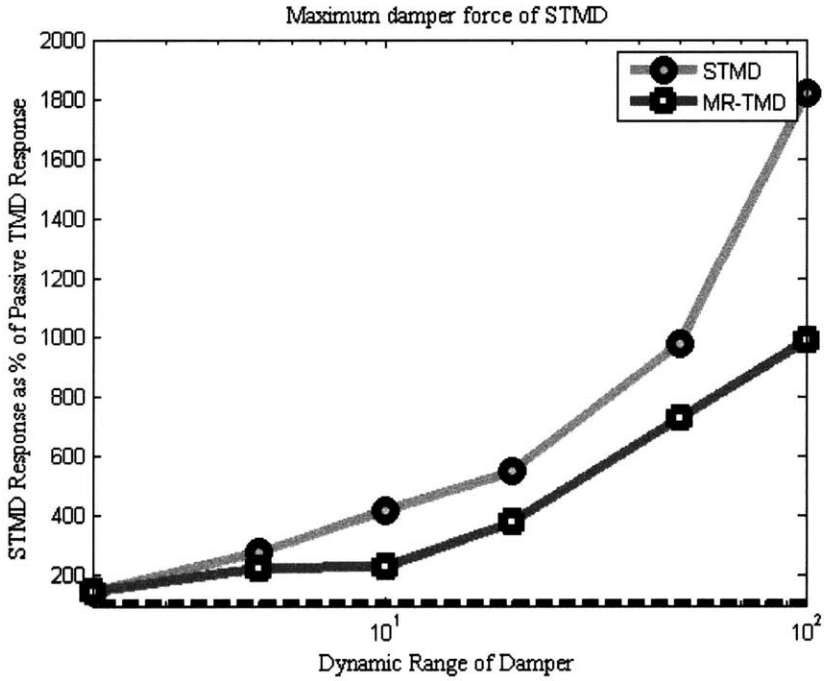

Figure 6-26: $\mu = 0.03$: Maximum damper forces

6.4 Other mass ratios

As with the VO-STMD, the same analysis was also performed for realistic mass ratios of 0.005, 0.0075, 0.015, 0.02, and 0.025. This section compares optimized results of these analyses by presenting only the most relevant outputs:

- Figure 6-27 shows optimized J_1 results.
- Figure 6-28 shows J_2 results using C_r values obtained in the J_1 optimization.
- Figure 6-29 presents representative $A_d(\omega)$ results for $D_r = 10$ and C_r obtained through J_1 optimization.
- Figure 6-30 presents representative $A_a(\omega)$ results for $D_r = 10$ and C_r obtained through J_1 optimization.

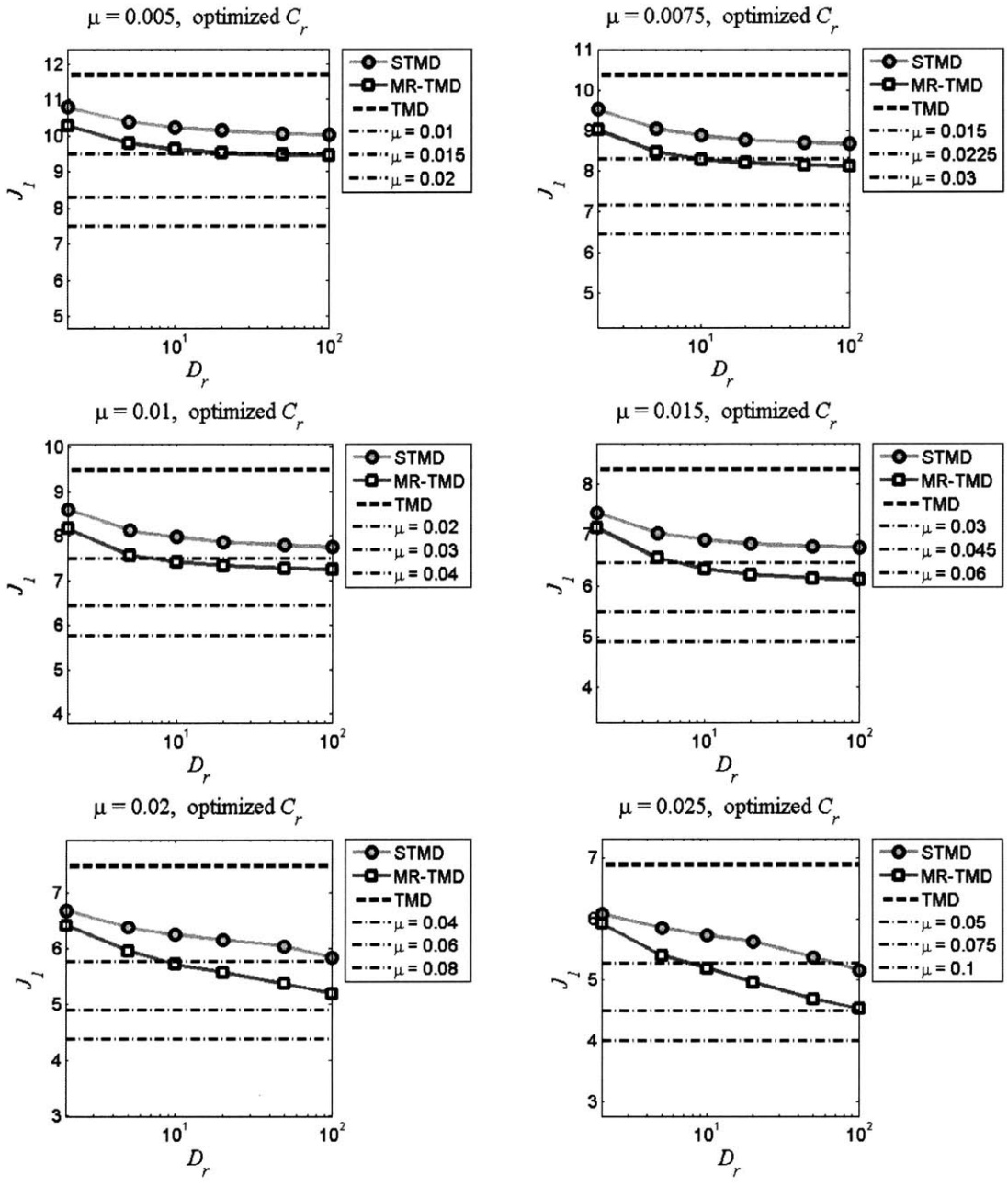

Figure 6-27: Optimized J_1 results for various mass ratios

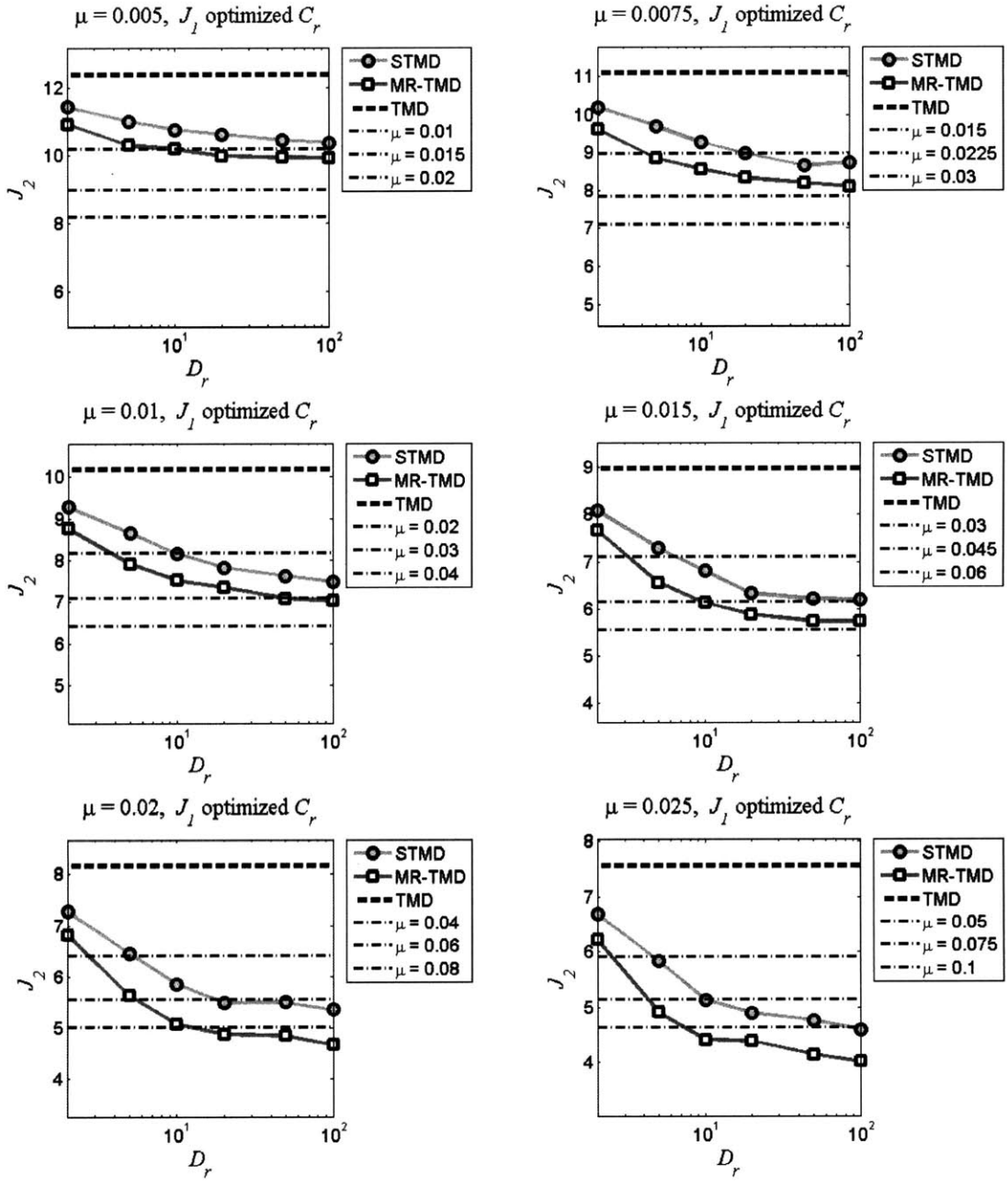

Figure 6-28: J_2 results for optimized J_1 for various mass ratios

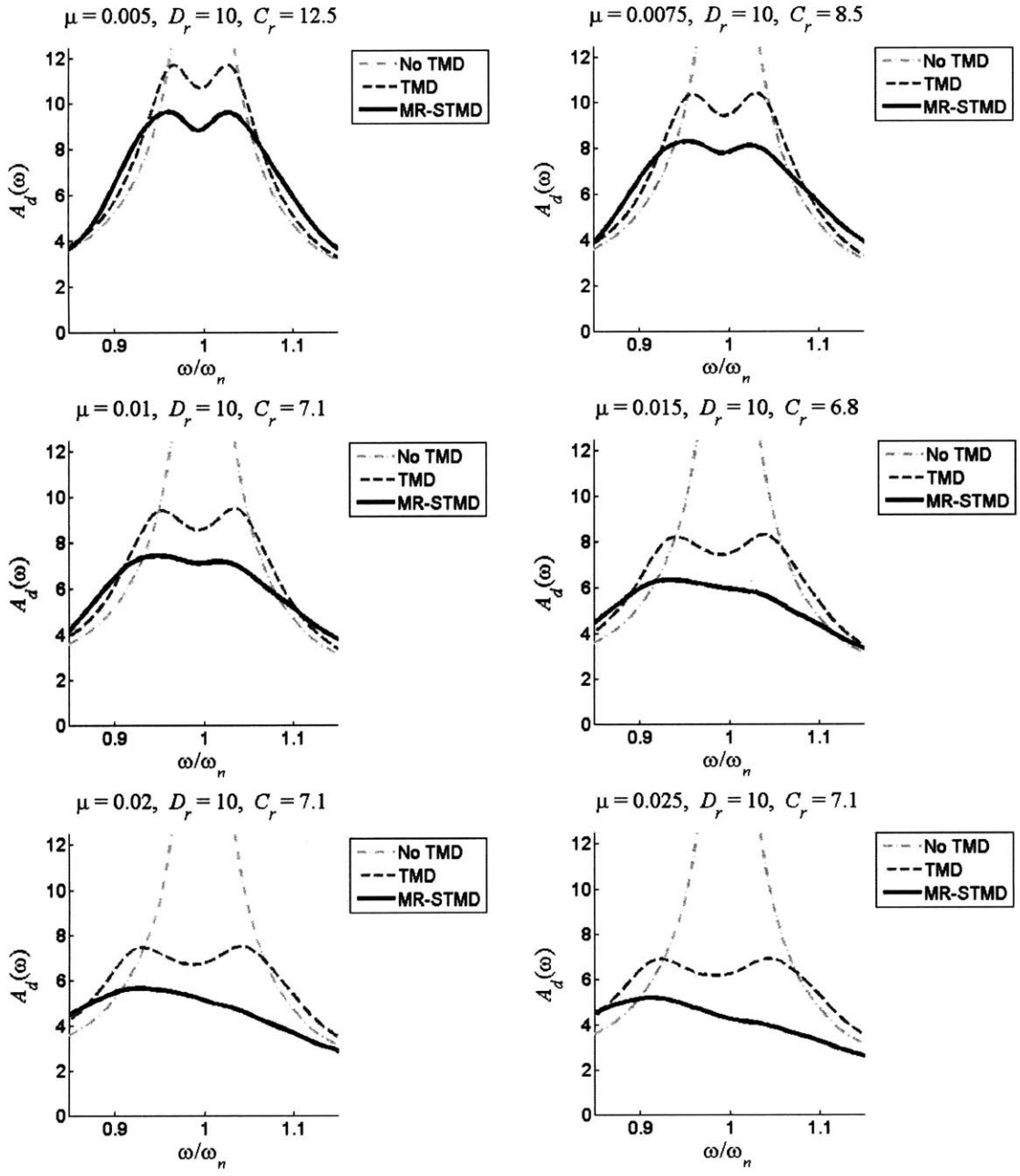

Figure 6-29: $D_r = 10$: $A_d(\omega)$ simulations for minimized J_1

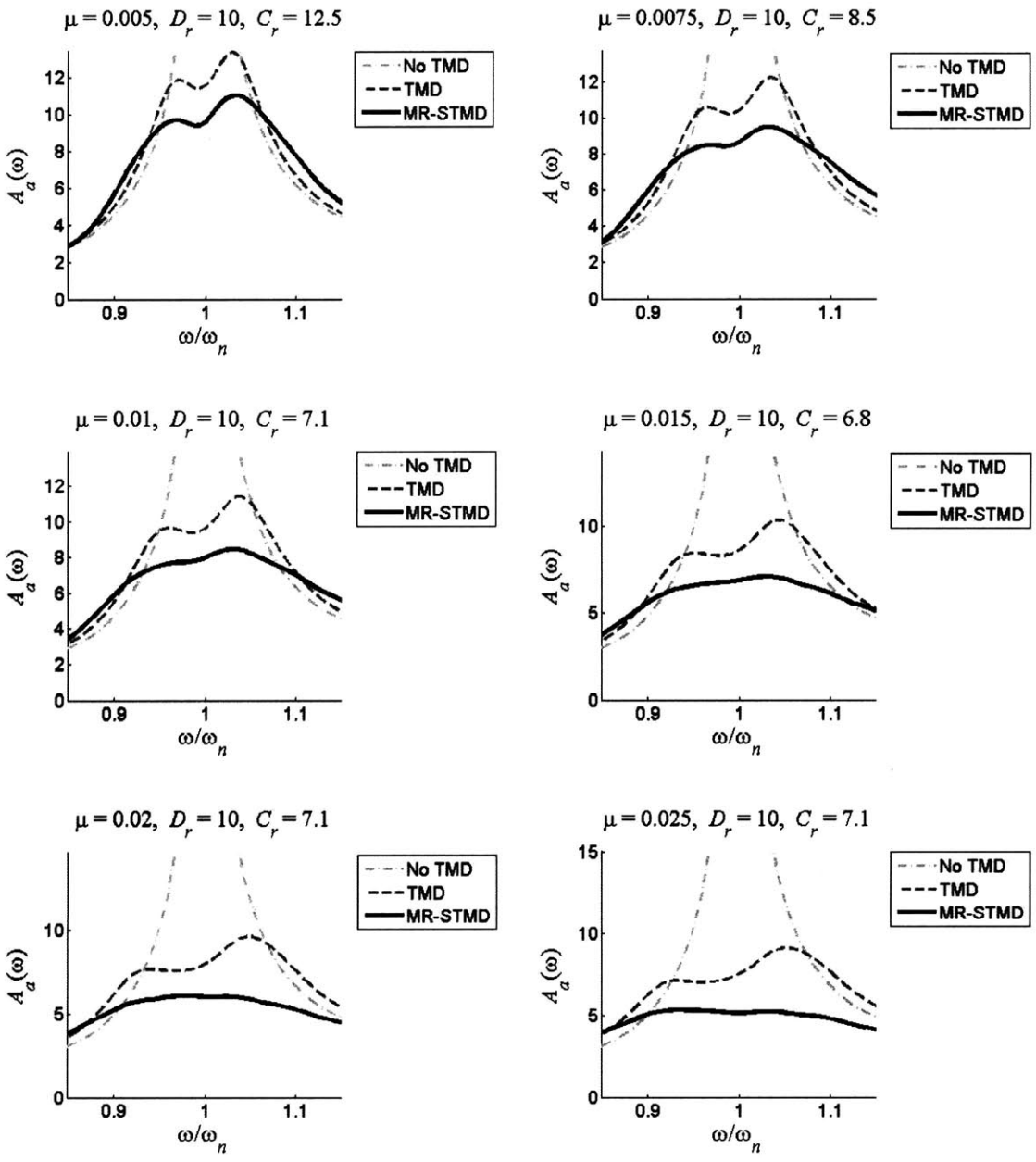

Figure 6-30: $D_r = 10$: $A_a(\omega)$ simulations for minimized J_1

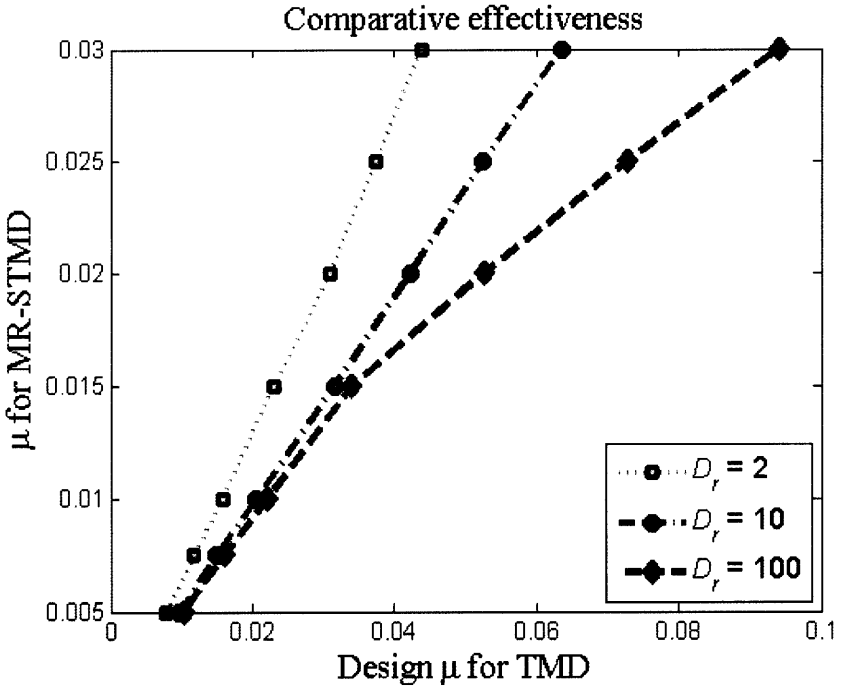

Figure 6-31: Relative effectiveness of MR-STMD systems

6.5 Summary of results

As these analyses have indicated, the performances of MR-STMD systems demonstrate marked improvement as compared to VO-STMD systems with comparable dynamic ranges. For example, using an MR damper with a dynamic range of 10, it is possible to attain performance results equivalent to increasing the mass of a passive system by 100%. This is a significant improvement compared to the 60% increase attainable with a similar VO-STMD system.

Based on the MR-STMD analysis, figure 6-31 summarizes the mass equivalency results for all studies performed, which include full results for several D_r values using the same mass ratios as before:

$$\mu = 0.005,\ 0.0075,\ 0.01,\ 0.015,\ 0.02,\ 0.025,\ \text{and}\ 0.03$$

Figures 6-32 and 6-33 further demonstrate MR-STMD effectiveness in terms of

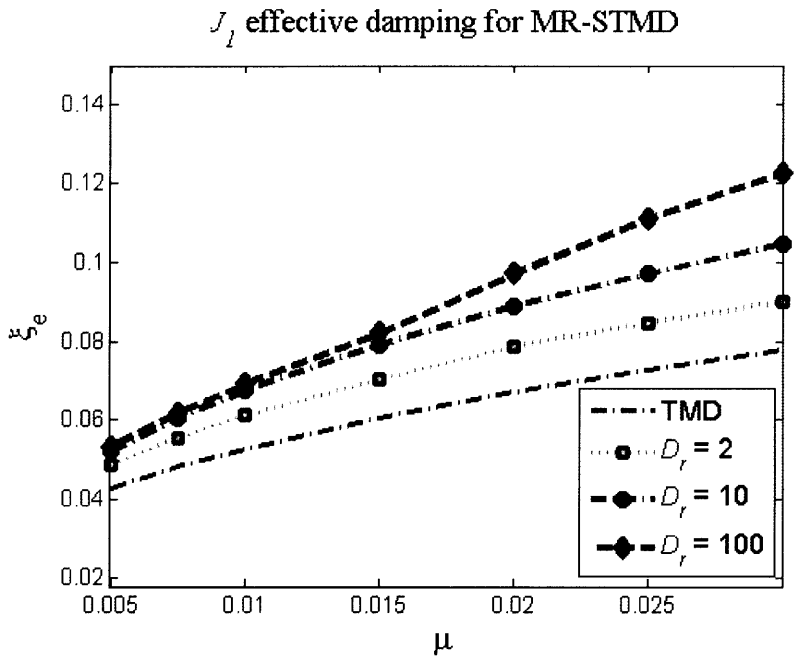

Figure 6-32: Effective damping ratios for peak displacements

the equivalent damping of the controlled system. Even more than for VO-STMDs, the improvement of maximum acceleration values (figure 6-33) is more pronounced than the improvement of maximum displacement values (figure 6-32). This is of great benefit when serviceability considerations dominate the design.

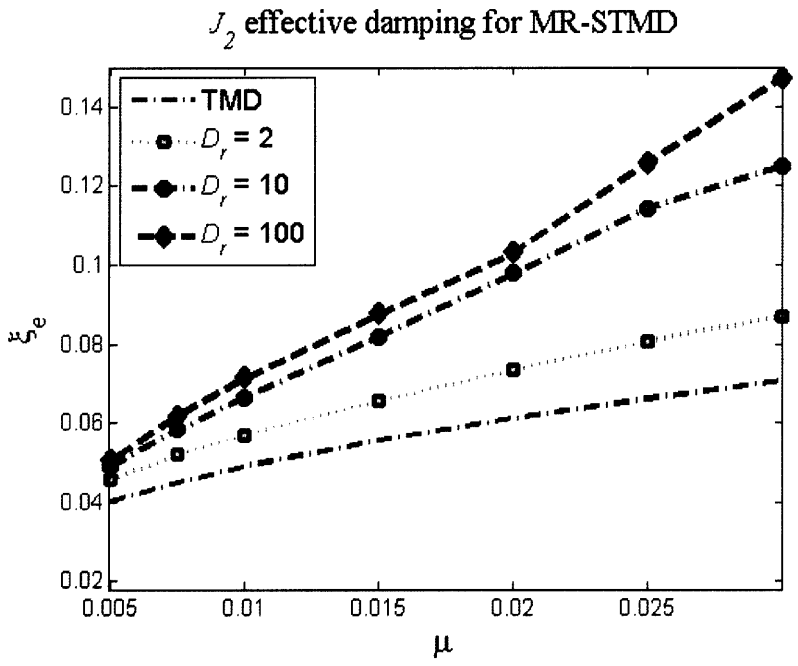

Figure 6-33: Effective damping ratios for peak accelerations

Chapter 7

Conclusions

Based on the analyses presented in chapters 5 and 6, it is possible to make some general conclusions and design recommendations for optimized semi-active tuned mass dampers.

7.1 Summary of motivation

As described in chapter 1, the response of tall buildings subjected to dynamic wind loads has been a subject of much study. For excitations approaching the resonant frequencies of the structure, ensuring structural integrity and serviceability is a significant concern. One traditional solution is the implementation of a tuned mass damper, which acts as a passive damping device in the region of the tuned frequency.

However, TMDs are only efficient within limits of the tuned frequency and depend heavily on the magnitude of their mass. Active systems, such as the active mass driver, have been utilized to improve the effectiveness of the TMD concept, but these systems require significant power and bring the inherent risk of instability. Hybrid semi-active schemes have been proposed, which are stable, require low power, and are controllable, thus providing a broader range of applicability.

Studies have already demonstrated the successful use of magnetorheological dampers for semi-active control of TMD systems. Other semi-active damping devices, such as the variable orifice damper, have also been documented to be effective. Though

semi-active dampers differ widely, with responses ranging from linear (VO) to highly nonlinear (MR), criteria for optimizing a semi-active tuned mass damper based on the limitations of the damping device have not been rigorously developed.

The present analysis addresses this issue be categorizing the effectiveness of STMD systems based on the dynamic range of the damping device (D_r) and a design variable referred to as the damping reduction factor (C_r). Two representative cases, the VO-STMD and MR-STMD, have been analyzed in detail to assess the effect of the dynamic range and of non-linearity in the damping device on the overall performance of the STMD.

7.2 Performance of STMD systems

While semi-active control introduces clear advantages, STMD systems will be preferred to their passive counterparts only if their performance improvements are relevant and do not come with costly complications. This section summarizes the performance benefits of STMD systems and is followed by a discussion of other design design considerations in section 7.2.3.

7.2.1 Reduction in TMD mass

One of the most significant objectives of employing a semi-active TMD may be to reduce the mass ratio, μ, necessary for sufficient vibration mitigation. As the results in chapters 5 and 6 indicated, both the VO-STMD and MR-STMD proved effective at meeting this goal. Figure 7-1 highlights benchmark results for both STMD types and shows the potential of STMD systems to alleviate excessive TMD mass requirements. Even for realistic dynamic range of $_r \approx 10$, the performance improvements of the STMD are equivalent to increasing the mass ratio of the passive system by 60% for VO dampers or 100% for MR dampers.

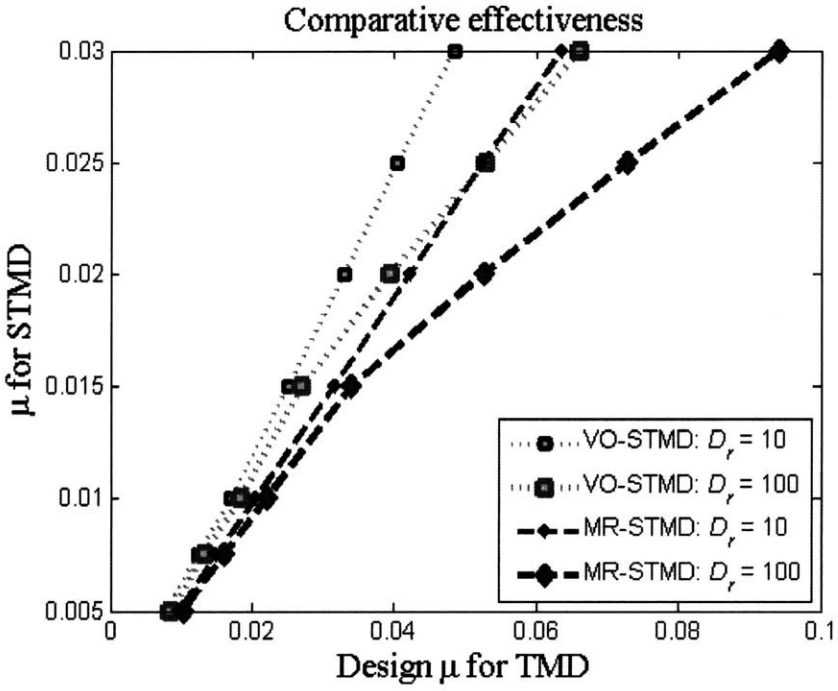

Figure 7-1: Reduction in μ made possible by STMD systems

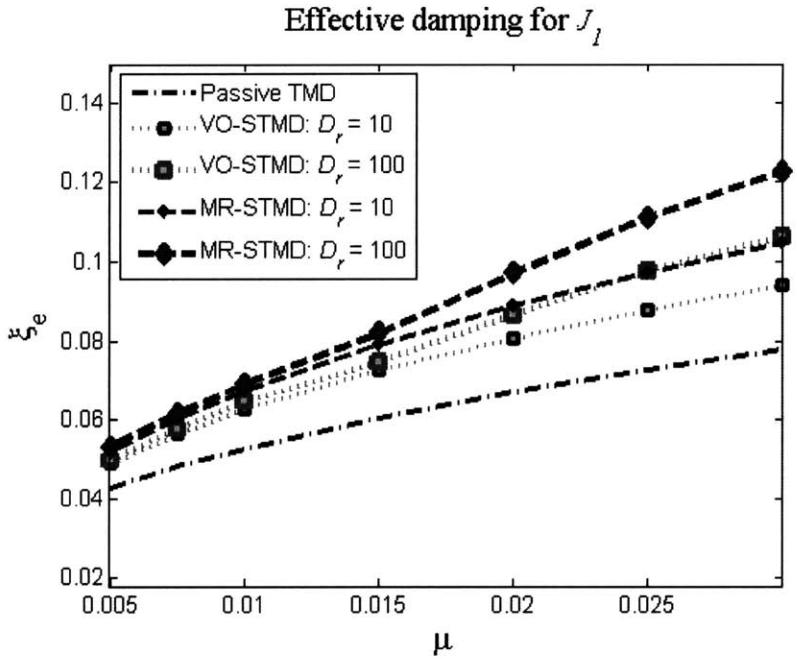

Figure 7-2: Effective damping ratios for peak displacements

7.2.2 Increase in effective damping

Another means of assessing control effectiveness is to compare results based on "effective damping," ξ_e, defined as the damping ratio necessary in a SDOF system to provide equivalent vibration mitigation. Using the performance indices developed in section 5.1.3, ξ_e may describe the damping necessary for equivalent maximum displacement, J_1, or for equivalent maximum acceleration, J_2. Results are given in figures 7-2 and 7-3 and show a marked increase in effective damping for all STMD systems as compared with their passive counterparts.

Based on results for both equivalent mass ratio and effective damping, the MR-STMD produces noticeably better results than the VO-STMD for comparable dynamic ranges. It is observed that an MR-STMD with $D_r = 10$ exhibits nearly equivalent performance benefits to those of a V0-STMD with $D_r = 100$.

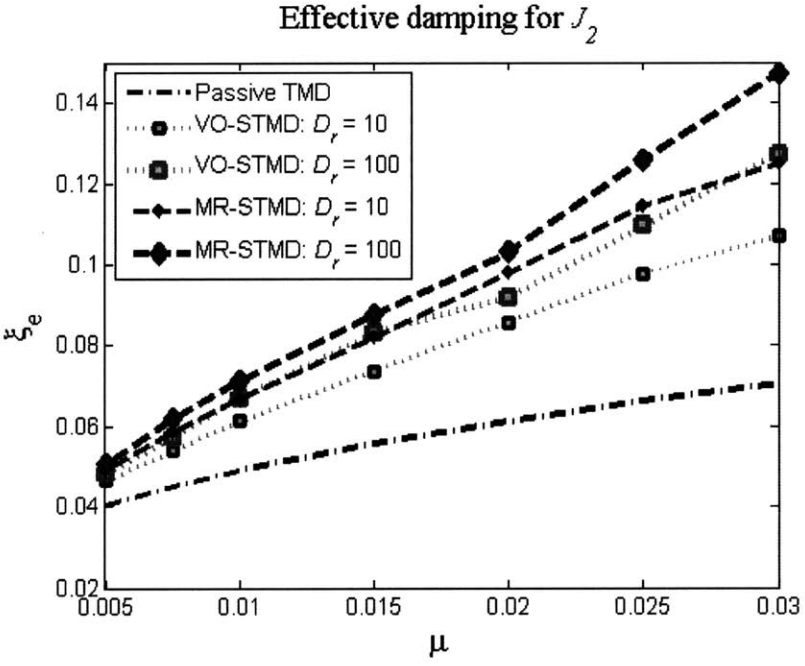

Figure 7-3: Effective damping ratios for peak accelerations

	D_r	C_r	ξ_e	z_{max}/z_d	F_{max}/F_d	Safe Fail
Passive TMD	–	1.0	5.3%	1.0	1.0	–
VO-STMD	10	4.3	6.3%	1.6	2.9	100%
VO-STMD	100	31.1	6.5%	1.8	4.4	100%
MR-STMD	10	6.2	6.7%	1.7	1.9	92%
MR-STMD	100	47.5	7.0%	1.8	2.4	92%

Table 7.1: Comparison of design considerations for $\mu = 0.01$

7.2.3 Other performance metrics

The benchmarks for STMD effectiveness presented in figures 7-1 through 7-3 were obtained by designing each STMD system solely for optimized performance. As explained in section 5.1.3, however, there are other factors to take into account when considering the feasibility of an STMD system. These include the relative displacement of the TMD, the maximum expected damper force, the reliability of the damping device, and the behavior of the system under a control malfunction.

Details for each of these considerations can be found in chapters 5 and 6, but results for representative TMD systems are summarized in tables 7.1 and 7.2. In each of these tables, four STMD systems are compared to a passive system having the same mass ratio. Here, C_r refers to the optimal damping reduction factor for the given system; ξ_e is the effective damping using the J_1 criterion; z_{max}/z_d compares the maximum relative displacement of the STMD with the maximum relative displacement of the passive TMD; F_{max}/F_d compares the maximum semi-active force with the passive TMD damper force; and "safe fail" indicates the optimal effectiveness of the STMD in the event of a control failure[1].

It is readily apparent that an optimized STMD comes at the expense of increased relative displacements and higher required damper forces. While the increase in peak dissipative forces is expected when using a varying damping device, the augmentation of relative motion is generally undesirable. Consequently, if stroke limitations become

[1]This assumes there is a default failure mode as described in sections 5.1.4 and 6.1.4. The percents given are relative to the performance of an optimally-tuned passive TMD: $\% = 100\ (1 - \frac{\xi_{e,p} - \xi_{e,s}}{\xi_{e,p} - \xi}\ )$, where $\xi_{e,p}$ is the equivalent damping of the passive TMD system, $\xi_{e,s}$ is the equivalent damping of the broken STMD system, and ξ is the damping of the primary structure.

	D_r	C_r	ξ_e	z_{max}/z_d	F_{max}/F_d	Safe Fail
Passive TMD	–	1.0	7.8%	1.0	1.0	–
VO-STMD	10	3.5	9.3%	1.4	4.1	100%
VO-STMD	100	7.7	10.6%	1.5	18.1	100%
MR-STMD	10	6.6	10.4%	1.5	2.1	72%
MR-STMD	100	14	12.3%	1.5	10.0	72%

Table 7.2: Comparison of design considerations for $\mu = 0.03$

a design concern, the specifics of the controller may have to be adjusted to reduce relative displacements rather than optimize only the performance.

7.3 Implications

Discussion thus far has focused on specific STMD systems using either a variable-orifice or magnetorheological damper to supply the semi-active reactive forces. Based on the data obtained, however, it is possible to make some useful generalizations about the design of STMDs and the selection of semi-active damping devices.

7.3.1 Linear vs. non-linear damping devices

The models used for the VO and MR damper in this study were selected partially for their ability to represent broader categorizations of semi-active devices, namely linear (VO) and non-linear (MR) dampers. As demonstrated graphically in section 4.5, non-linear devices such as the MR damper provide a larger range of accessible control forces, including vastly improved responses for low velocities.

Preferrability of non-linear devices

Based on the results of this study, it is clear that this expanded range of control forces directly influences the efficacy of an STMD. For example, for a given dynamic range, the MR-STMD out-performed the VO-STMD in all measures of control effectiveness; in order to produce similar results, the VO-STMD required a dynamic range an order of magnitude larger than that of the MR-STMD. Additionally, the maximum force

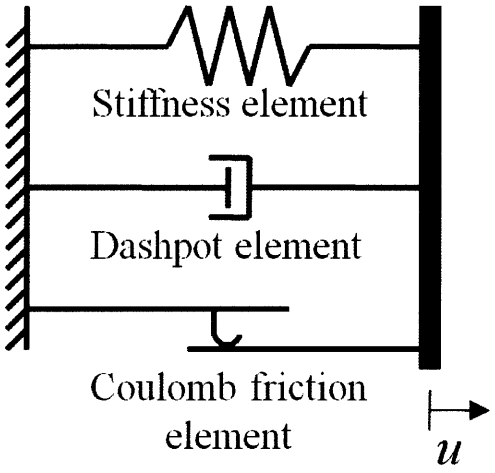

Figure 7-4: Alternative non-linear damping device

requirements for the damper are substantially less for the MR-STMD than for the VO-STMD, as evidenced in tables 7.1 and 7.2. Hence, a non-linear damping device need not be as robust as a linear one to accomplish the same performance objectives.

Since the relative displacements of the VO-STMD and MR-STMD are very comparable, the only observed shortcoming of utilizing a non-linear damping device is the absence of an optimum failure mode. That is, as described in section 5.1.4, a linear semi-active damper may default to the optimal level of passive damping in the event of a control malfunction. Non-linear dampers, however, do not afford this flexibility; even if a failure mode is programmed, its control will be sub-optimal as compared to a passive TMD. Consequently, system reliability must be taken into consideration.

Extension to other non-linear damping devices

Apart from a system failure, these observations suggest that any semi-active damping device with significant non-linearity will provide the best results for a variable-damper based STMD. While MR-dampers have been the focus of this analysis, other damping devices may be preferred due to the uncertainties associated with the MR fluid and limitations imposed by manufacturers. For example, a controllable Coulomb friction element in parallel with a traditional viscous damper would maintain the benefits

of non-linearity while providing higher reliability and increased design flexibility. A schematic of such a device is shown in figure 7-4, which also includes a stiffness element to mimic the hysteresis exhibited by rheological dampers.

To verify these conclusions, simulations were performed using this hybrid damping device instead of an MR-damper. With dynamic range and damping reduction factor defined as in section 6.1.1, the same optimization process was undertaken. Representative results for J_1 optimization with $\mu = 0.01$ and $D_r = 2, 10$ are compared with those of the MR-damper in figure 7-5, as well as summary optimization plots. Slight differences in system behavior are evident, but overall effectiveness is relatively indistinguishable. Accordingly, it is confirmed that semi-acvie damper non-linearity supersedes other device details in importance, leaving it as a matter of engineering judgment to determine the most suitable components for a given STMD.

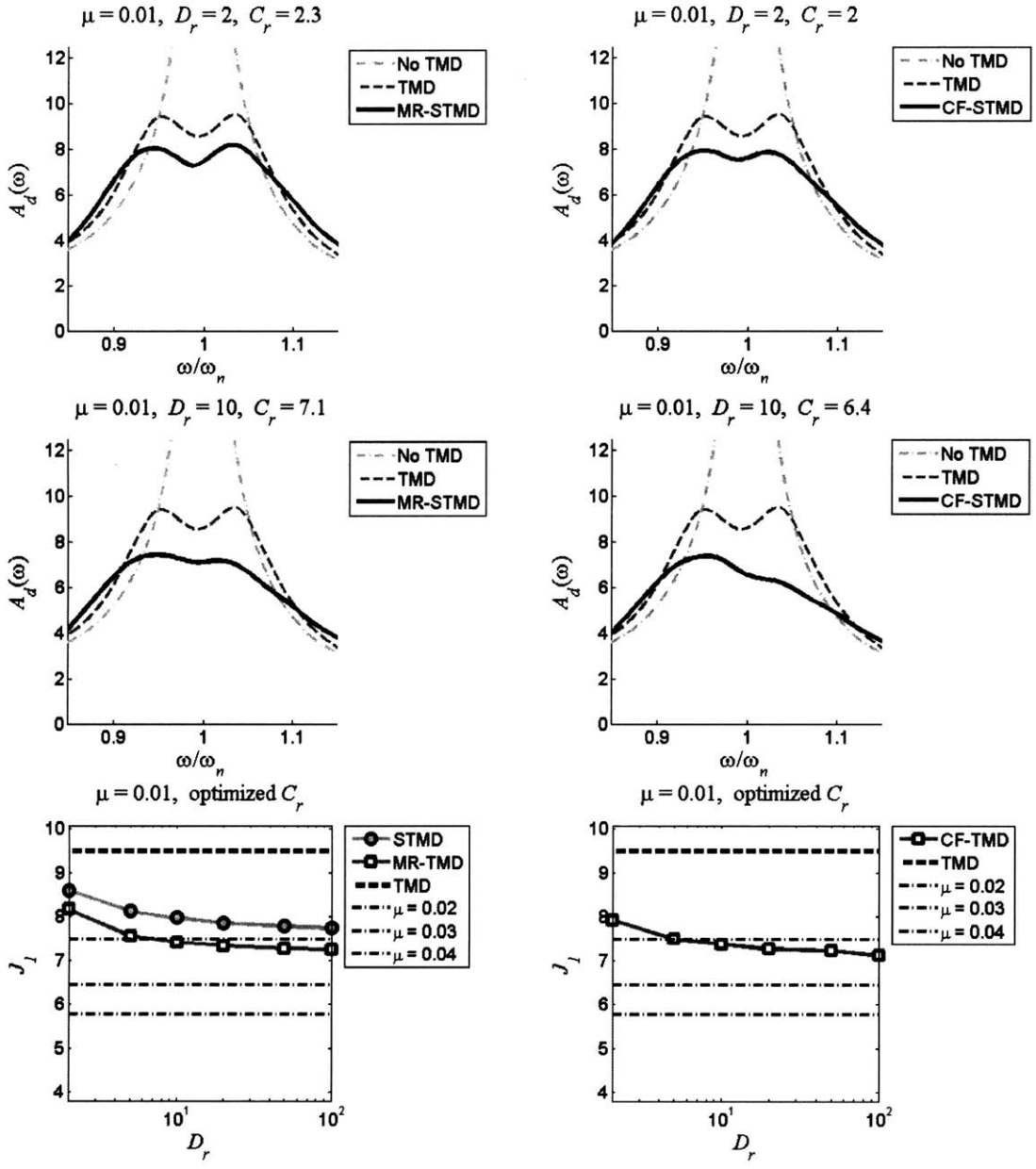

Figure 7-5: Non-linear device comparison: MR damper (left) and Coulomb friction damper (right)

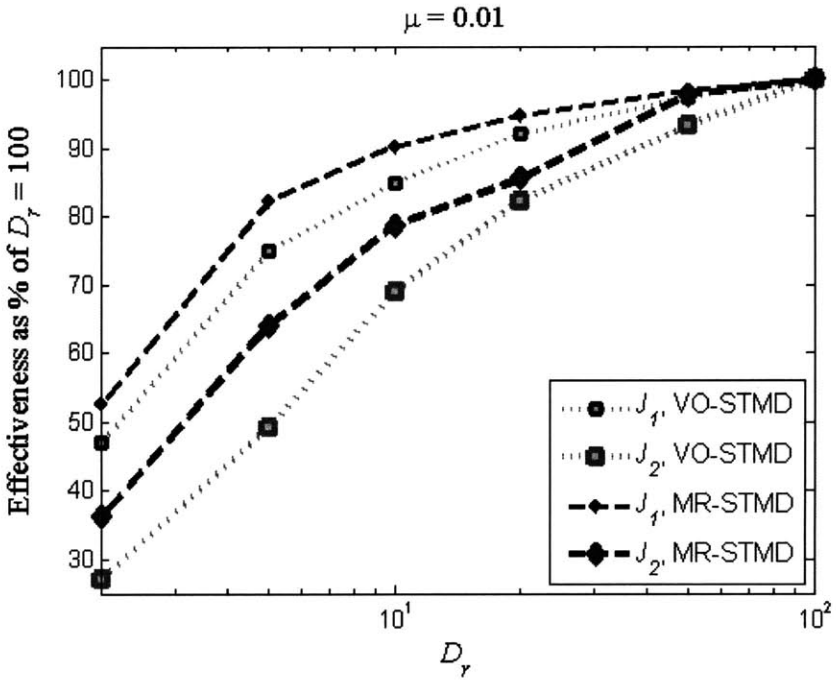

Figure 7-6: Influence of damper dynamic range, $\mu = 0.01$

7.3.2 Impact of dynamic range

Regardless of which damping device is selected for an STMD, its potential impact is further limited by its dynamic range (see sections 5.1.1 and 6.1.1). While this is an inherent limitation of virtually all semi-active damping devices, its influence on STMD performance results had not yet been documented.

The influence of the dynamic range is shown in figures 7-6 and 7-7 for both the J_1 and J_2 performance criteria. All results are presented as percents calibrated such that 0% corresponds to the effective damping of a passive TMD and 100% corresponds to the effective damping of the STMD with a dynamic range of 100.

As can be seen, the importance of the dynamic range increases for higher mass ratios. However, for realistic mass ratios such as $\mu \approx 0.01$, most of the benefit of an STMD can still be gained even with a relatively low dynamic range. For example, for $\mu = 0.01$ and an MR damper with $_r = 10$, displacement mitigation has already surpassed 90% the effectiveness of an MR-STMD with a dynamic range of 100.

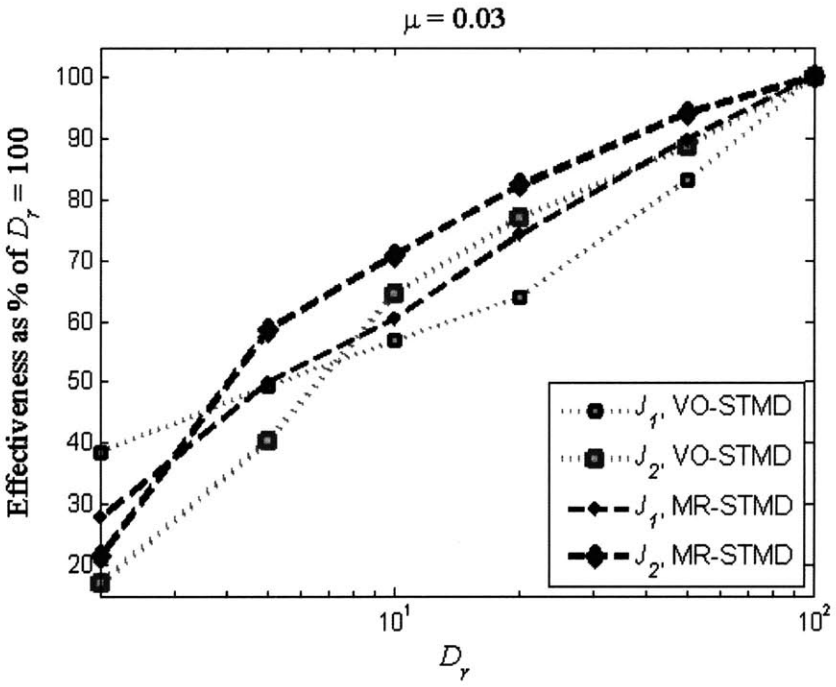

Figure 7-7: Influence of damper dynamic range, $\mu = 0.03$

These are encouraging results for the practicality of STMD systems, for $D_r \geq 10$ has become relatively standard for industrial-sized semi-active dampers. Hence, demonstrating control success with $D_r = 10$ is a critical step in validiting STMD feasibiliy.

7.3.3 Closing remarks

The analysis presented here has elucidated the potential of semi-active damping devices to significantly improve passive tuned mass damper performance. Results have shown the superiority of non-linear damping devices, have demonstrated effective results for realistic dynamic ranges, and have suggested that the prescribed TMD mass may be reduced by a factor of up to two when semi-active control is implemented. These findings give particular promise to STMD implementation in both retrofit situations – in which space constraints may be significant – and in design situations where extraordinarily large masses would otherwise be required.

Bibliography

[1] M. Abdel-Rohman. Optimal design of active tmd for building control. *Building and Environment*, 19(3):191–195, 1984.

[2] M. Abdel-Rohman and M. Al-Zanaidi. Design of appendages for tall building control. *Journal of structural engineering*, 113(2):397–408, February 1987.

[3] M. Abé and T. Igusa. Semi-active dynamic vibration absorbers for controlling transient response. *Journal of Sound and Vibration*, 198(5):547–569, 1996.

[4] S. Ankiraddi and H.T.Y. Yang. Simple atmd control methodology for tall buildings subject to wind loads. *Journal of Structural Engineering*, 122(1):83–91, January 1996.

[5] T. Asami, O. Nishihara, and A.M. Baz. Analytical solutions to h_∞ and h_2 optimization of dynamic vibration absorbers attached to damped linear systems. *Transactions of the ASME*, 124, 2002.

[6] K.-J. Bathe. *Finite Element Procedures.* Prentice Hall, Upper Saddle River, New Jersey, 2003.

[7] Y. Bingkang and L. Chunxiang. Seismic response of controlled structures with active multiple tuned mass dampers. *Earthquake Engineering and Engineering Vibration*, 5(2):205–213, December 2006.

[8] J.E. Brock. A note on the damped vibration absorber. *Journal of Applied Mechanics*, 13, 1946.

[9] L.-L. Chung C.-L. Lee, Y.-T. Chen and Y.-P. Wang. Optimal design theories and applications of tuned mass dampers. *Engineering Structures*, 28:43–53, 2006.

[10] H. Cao and Q.S. Li. New control strategies for active tuned mass damper systems. *Computers and Structures*, 82, 2004.

[11] C.C. Chang and H.T.Y. Yang. Control of buildings using active tuned mass dampers. *Journal of Engineering Mechanics*, 121(3):355–366, March 1995.

[12] F.-K. Chang. Human response to motions in tall buildings. *Journal of the Structural Division*, 99, 1973.

[13] J.J. Connor. *Introduction to Structural Motion Control.* Prentice Hall, Upper Saddle River, New Jersey, 1996.

[14] S.H. Crandall and W.D. Mark. *Random Vibration in Mechanical Systems.* Academic Press, New York, 1963.

[15] S.J. Dyke et al. Modeling and control of magnetorheological dampers for seismic response reduction. *Smart Materials and Structure*, 5:565–575, 1996.

[16] H. Frahm. Device for damping vibrations of bodies. U.S. Patent No. 989,958, 1909.

[17] R.J. Hansen, J.W. Reed, and E.H. Vanmarcke. Human response to wind-induced motion of buildings. *Engineering Journal*, 16, 1979.

[18] J.P. Den Hartog. *Mechanical Vibrations.* McGraw-Hill, New York, fourth edition, 1997.

[19] S. Hidaka, Y.K. Ahn, and S. Morishita. Acaptive vibration control by a variable-damping dynamic absorber using er fluid. *Journal of Vibration and Acoustics*, 121, 1999.

[20] G.W. Housner et al. Structural control: past, present, and future. *Journal of Engineering Mechanics*, 123(9):897–971, September 1997.

[21] D. Hrovat, P. Barak, and M. Rabins. Semi-active versus passive or active tuned mass dampers for structural control. *Journal of Engineering Mechanics*, 109(3):691–705, June 1983.

[22] Y. Ikeda. Effect of weighting a stroke of an active mass damper in the linear quadratic regulator problem. *Earthquake Engineering and Structural Dynamics*, 26, 1997.

[23] L.M. Jansen and S.J. Dyke. Semi-active control strategies for mr dampers: a comparative study. *Journal of Engineering Mechanics*, 126(8):795–803, August 2000.

[24] H.-R. Ji, Y.-J. Moon, C.-H. Kim, and I.-W. Lee. Structural vibration control using semiactive tuned mass damper. In *KKCNN Symposium on Civil Engineering*, volume 18, Korea, December 2005.

[25] E. Kausel. *Advanced Structural Dynamics.* Unpublished, Massachusetts Institute of Technology, 2009.

[26] H. Kim and H. Adeli. Wind-induced motion control of 76-story benchmark building using the hybrid damper-tlcd system. *Journal of Structural Engineering*, 131(12):1794–1802, 2005.

[27] J.-H. Koo, M. Ahmadian, and M. Elahinia. Semi-active controller dynamics in a magneto-rheological tuned vibration absorber. In *Smart Structures and Materials - Proceedings of SPIE*, volume 5760, pages 69–76, March 2005.

[28] J.-H. Koo et al. In search of suitable control methods for semi-active tuned vibration absorbers. *Journal of Vibration and Control*, 10, 2004.

[29] N. Kurata et al. Actual seismic response controlled building with semiactive damper system. *Earthquake Engineering and Structural Dynamics*, 28, 1999.

[30] C.H. Loh, P.Y. Lin, and L.L. Chang. Semiactive control of building structures with semiactive tuned mass damper. *Computer-Aided Civil and Infrastructure Engineering*, 20, 2005.

[31] L.-Y. Lu. Predictive control of seismic structures with semi-active friction dampers. *Earthquake Engineering and Structural Dynamics*, 33, 2004.

[32] R.A. Lund. Active damping of large structures in winds. In *ASCE Convention and Exposition*, Boston, April 1979.

[33] L.E. Mackriell, K.C.S. Kwok, and B. Samali. Critical mode control of a wind-loaded tall building using an active tuned mass damper. *Engineering Structures*, 19(10):834–842, October 1997.

[34] S.F. Masri, R. Kumar, and R.C. Ehrgott. Modeling and control of an electrorheological device for structural control applications. *Smart Materials and Structures*, 4, 1995.

[35] Y. Matsunaga, T. Mizuno, and T. Kobori. Dynamic loading test on actual size variable hydraulic damper. *Seismic Engineering*, 364, 1998.

[36] N.H. McClamroch and H.P. Gavin. Closed loop structural control using electrorheological dampers. In *Procedings of the National Control Conference*, pages 4173 – 4177, Seattle, June 1995.

[37] R.J. McNamara. Tuned mass dampers for buildings. *Journal of the Structural Division*, 103:1785–1798, 1977.

[38] O.B. Mekki et al. Damping and stiffness semi-active control of a tuned mass damper by using a novel semi-active control device. 2006.

[39] R.K. Miller et al. Active vibration control of large civil structures. *Journal of Engineering Mechanics*, 114(9):1542–1570, September 1988.

[40] S. Nagarajaiah and N. Varadarajan. Novel semiactive variable stiffness tuned mass damper with real time tuning capability. In *Proceedings of the 13th Engineering Mechanics Conference*, Reston, Virginia, 2000. CD-ROM.

[41] O. Nishihara and H. Matsuhisa. Design of a dynamic vibration absorber for minimization of maximum amplitude magnification factor (derivation of algebraic exact solution). *Japanese Society of Mechanical Engineers*, 63, 1997.

[42] N. Niwa et al. Dynamic loading test and simulation analysis of full-scale semi-active hydraulic damper for structural control. *Earthquake Engineering and Structural Dynamics*, 29, 2000.

[43] K. Ogata. *Modern Control Engineering.* Prentice Hall, Upper Saddle River, New Jersey, third edition, 1997.

[44] J. Ormondroyd and J.P. Den Hartog. The theory of the damped vibration absorber. *Transactions of the ASME*, 50, 1928.

[45] W.N. Patten and R.L. Sack. Semiactive control of civil engineering structures. In *Procedings of the American Control Conference*, pages 1078–1082, Baltimore, June 1994.

[46] T. Pinkaew and Y. Fujino. Effectiveness of semi-active tuned mass dampers under harmonic excitation. *Engineering Structures*, 23:850–856, 2001.

[47] S.E. Randall, III D.M Halsted, and D.L. Taylor. Optimum vibration absorbers for linear damped systems. *Journal of Mechanical Design*, 103, 1981.

[48] P. Reina. Giant damper doubles as building's interior adornment. *Engineering News Record*, 2003.

[49] A.M. Reinhorn et al. Full-scale implementation of active control ii: installation and performance. *Journal of Structural Engineering*, 119, 1993.

[50] F. Ricciardelli, A. Occhiuzzi, and P. Clemente. Semi-active tuned mass damper control strategy for wind-excited structures. *Journal of Wind Engineering and Industrial Aerodynamics*, 88, 2000.

[51] M. Sakamoto et al. Practical applications of active and hybrid response control systems and their verifications by earthquake and strong wind observations. In *Proceedings of First World Conference on Structural Control.*

[52] F.M. Sauer and C.F. Garland. Performance of the viscously damped vibration absorber applied to systems having frequency squared excitation. *Journal of Applied Mechanics*, 16, 1949.

[53] T.T. Soong and J.C.H. Chang. Structural control using active tuned mass damper. *Journal of the Engineering Mechanics Division*, 106, 1980.

[54] B.F. Spencer et al. Phenomenological model for magnetorheological dampers. *Journal of Engineering Mechanics*, 123(3):230–238, March 1997.

[55] B.F. Spencer and Michael K. Sain. Controlling buildings: a new frontier in feedback. *IEEE Control Systems Magazine on Emerging Technology*, 17, 1997.

[56] G. Strang. *Computational Science and Engineering.* Wellesley-Cambridge Press, Wellesley, Massachusetts, 2007.

[57] A.G. Thompson. Optimum tuning and damping of a dynamic vibration absorber applied to a force excited and damped primary system. *Journal of Sound and Vibration*, 77(3):403–415, 1981.

[58] H.-C. Tsai and G.-C. Lin. Optimum tuned-mass dampers for minimizing steady-state response of support-excited and damped structures. *Earthquake Engineering and Structural Dynamics*, 22:957–973, 1993.

[59] N. Varadarajan and S. Nagarajaiah. Wind response control of building with variable stiffness tuned mass damper using emperical mode decomposition/ hilbert transform. *Journal of Engineering Mechanics*, 130(4):451–458, April 2004.

[60] J.Y. Wang et al. Magneto-rheological tuned liquid column dampers (mr-tlcds) for vibration mitigation of tall buildings: modelling and analysis of open-loop control. *Computers and Structures*, 83, 2005.

[61] G.B. Warburton. Optimum absorber parameters for various combinations of response and excitation parameters. *Earthquake Engineering and Structural Dynamics*, 10, 1982.

[62] J.C. Wu, W.C. Lu, and Hsu. Implementation of a feasible control design process incorporating robustness criteria for wind-excited high-rise buildings. *Journal of Structural Engineering*, 132:89–101, 2006.

[63] Y.L. Xu, W.L. Qu, and Z.H. Chen. Control of wind-excited truss tower using semiactive friction damper. *Journal of Structural Engineering*, 127(8):861–868, 2001.

[64] H. Yamaguchi. Damping of transient vibration by a dynamic absorber. *Japanese Society of Mechanical Engineers*, 54, 1988.

[65] N. Yan, C.M. Wang, and T. Balendra. Optimal damper characteristics of atmd for buildings under wind loads. *Journal of Structural Engineering*, 125(12):1376–1383, December 1999.

[66] G. Yang et al. Large-scale mr fluid dampers: modeling and dynamic performance considerations. *Engineering Structures*, 24, 2002.

[67] G. Yang et al. Dynamic modeling of large-scale magnetorheological damper systems for civil engineering applications. *Journal of Engineering Mechanics*, 130(9):1107–1114, September 2004.

[68] J.N. Yang. Application of optimal control theory to civil engineering structures. *Journal of Engineering Mechanics*, 101, 1975.

[69] J.N. Yang and A.K. Agrawal. Semi-active hybrid control systems for nonlinear buildings against near-field earthquakes. *Engineering Structures*, 24, 2002.

[70] J.N. Yang, S. Lin, and F. Jabbari. h_∞-based control strategies for civil engineering structures. *Structural Control and Health Monitoring*, 11:223–237, 2004.